Tampereen teknillinen yliopisto, Julkaisu
Tampere University of Technology, Publication

Dan Pada

Steel Skeleton Behaviour in Decaying Fire

Licentiate thesis submitted for the grading as part of the degree of Licentiate of Science in Technology
Tampere, April 17, 2011

Tampereen teknillinen yliopisto – Tampere University of Technology
Tampere 2011

Tampere University of Technology
PO Box 600, FI-33101 TAMPERE
http://www.tut.fi

ABSTRACT OF LICENTIATE THESIS

Author:
Dan Pada

Name of thesis:
Steel Skeleton Behaviour in Decaying Fire

Date
April 17, 2011

Faculty:	Faculty of Built Environment
Department:	Department of Civil Engineering Research Centre of Metal Structures
Opponent:	D.Sc. (Tech.) Jyri Outinen
Supervisor:	Prof. D. Sc. (Tech.) Markku Heinisuo
Instructor:	D.Sc. (Tech.) Jyrki Kesti

The purpose of this licentiate thesis was to study the behaviour of a typical all steel industrial hall, the CEE-hall by Ruukki, with roof trusses exposed to fire, taking into account all the phases of the fire, focusing especially on the decay phase. Based on the results from the analyses, general rules on how to consider the decay phase in the design of the structure were sought. In order to perform the analyses it was necessary to take both material and geometrical non-linearity into account.

In order to complete the study it was necessary to use an advanced non-linear FEA-software, Vulcan, which is specially developed for studying structures exposed to fire. The utilization of this program included a short visit to the University of Sheffield, UK, where the software has been developed, in order to study its usage and possibilities. The software proved very useful and valuable throughout the whole course of the study.

Extensive testing and several analyses with different configurations were performed to develop the final analysis models. In order to simplify the model and save calculation time the final model was made up of only three of the middle frames of the CEE-hall. The parts of the building omitted from the model were considered in the boundary conditions with the help of springs. A local fire reaching a maximum gas temperature of 800 °C, situated first at mid-span and then at quarter-span, was chosen as the scenario to be studied.

The structure was able to endure the exposure to the elevated temperatures even though the top chords underwent substantial permanent deformations, which in turn led to a change in the behaviour of the structure and a redistribution of the internal forces. The structure essentially started behaving as a three-pin portal frame, relying heavily on the bottom chords being able to sustain the large compressive forces developed in them.

One of the most important observations made during the analyses was that the largest internal forces were developed in the decay phase, proving the importance of taking all the phases of the fire into account when designing a structure for the case of fire. For this type of structure exposed to local fire scenarios, this study furthermore showed that in the structural fire safety design it is necessary to consider the large compressive forces that may develop in the bottom chords normally designed for tensile forces. The study also showed the importance of considering the stiffness of the structure in the design, as it greatly influences the magnitude of the internal forces developed in the structure during the fire exposure.

Keywords	Language	Number of pages
steel, decaying fire, Vulcan, non-linear analysis, roof-truss, Ramberg-Osgood	English	99 + appendixes

Tampereen teknillinen yliopisto
PL 600, 33101 TAMPERE
http://www.tut.fi

LISENSIAATINTYÖN TIIVISTELMÄ

Tekijä:
Dan Pada

Lisensiaatintyön nimi:
Teräsrungon käyttäytyminen hiipuvassa palossa

Päivämäärä:
27. huhtikuuta 2011

Tiedekunta:	Rakennetun ympäristön tiedekunta
Laitos:	Rakennustekniikan laitos
	Metallirakentamisen tutkimuskeskus
Vastaväittelijä:	TkT Jyri Outinen
Työn valvoja:	Prof. TkT Markku Heinisuo
Työn ohjaaja:	TkT Jyrki Kesti

Tämän lisensiaatintyön tarkoituksena oli tutkia tyypillisen teräksisen kattoristikoilla varustetun teollisuushallin, Ruukin CEE-halli, käyttäytymistä palotilanteessa, ottaen huomioon kaikki palon vaiheet, keskittyen erityisesti hiipuvaan vaiheeseen. Analyysien tulosten perusteella etsittiin yleisiä sääntöjä hiipuvan vaiheen huomioon ottamiseksi suunnittelussa. Analyysiä varten piti huomioida sekä materiaalin että geometrian epälineaarisuus.

Tutkielman suorittamiseksi tarvittiin edistyksellinen epälineaarinen FEA-ohjelma, Vulcan, joka on erityisesti palolle altistettujen rakenteiden tutkimiseen kehitetty ohjelma. Vulcanin käyttöön liittyi lyhyt vierailu ohjelman kehittäneeseen University of Sheffieldiin Iso-Britanniaan, jossa tutustuttiin sen käyttöön ja mahdollisuuksiin. Ohjelma osoittautui erittäin käyttökelpoiseksi ja arvokkaaksi koko tutkielman ajan.

Laajamittainen testaus ja useat analyysit eri asetuksilla suoritettiin lopullisen analyysimallin kehittämiseksi. Mallin yksinkertaistamiseksi ja laskenta-ajan säästämiseksi lopulliseen malliin sisällytettiin ainoastaan kolme CEE-hallin keskikehää. Ne rakennuksen osat, jotka jätettiin mallin ulkopuolelle, otettiin huomioon reunaehdoissa jousien avulla. Paikallinen palo, jossa kaasujen maksimilämpötila oli 800 °C ja joka sijoitettiin ensiksi jännevälin keskelle ja sitten jännevälin neljännekseen, valittiin tutkimustilanteeksi.

Rakenne kesti kohonneista lämpötiloista syntyneet rasitukset vaikka yläpaarteet kärsivät huomattavista muodonmuutoksista. Tämä aiheutti rakenteen toimintatavan muutoksen ja sisäisten voimien uudelleenjakaantumisen. Rakenne toimi itse asiassa kolminivelkehänä, turvautuen voimakkaasti alapaarteiden kykyyn kestää niissä kehittyneet suuret puristusvoimat.

Tärkeimpiä analyysien aikana tehtyjä havaintoja oli, että suurimmat sisäiset voimat kehittyivät hiipuvassa vaiheessa, mikä osoittaa palon kaikkien vaiheiden huomioon ottamisen paloturvallisuussuunnittelussa erittäin tärkeäksi. Lisäksi tutkimus osoitti suurten puristusvoimien huomioon ottamisen välttämättömyyden tämän tyyppisen paikalliselle palolle altistetun rakennuksen palotilanteen suunnittelussa, koska ne voivat kehittyä normaaliin tapaan vetovoimille mitoitetuissa alapaarteissa. Sen lisäksi tutkimus osoitti rakenteen jäykkyyden huomioon ottamisen tärkeyden suunnittelussa, koska se vaikuttaa merkittävästi palon aikana rakenteessa kehittyvien sisäisten voimien suuruuteen.

Avainsanat	Kieli	Sivumäärä
teräs, hiipuva palo, Vulcan, epälineaarinen analyysi, kattoristikko, Ramberg-Osgood	Englanti	99 + liitteet

PREFACE

Only half a year after graduating as Master of Science from the Helsinki University of Technology, I found myself working on yet another thesis, this time my Licentiate Thesis. What lead me to that point can perhaps be described as a series of coincidences, such as the so called financial crisis that struck the world in 2008, combined with my personal interest in structural fire engineering. Now, almost two years later, putting the finishing touches on this Licentiate Thesis and looking back on the work done, I have to admit it's often been a challenging time, but it has also been a meaningful and rewarding time, giving me the opportunity to gain a great deal of new insights and strengthen my interest in the subject even more.

First of all I would like to thank my supervisor, Professor Markku Heinisuo at Tampere University of Technology, for always being supportive and coming up with ideas and solutions for various problems throughout the research work. I'm also very thankful to D.Sc. (Tech.) Jyri Outinen and D.Sc. (Tech.) Jyrki Kesti at Rautaruukki Oyj for following my work and giving me valuable help and advice.

My work also included a short, but intensive visit at the University of Sheffield, UK, and for my time there and for helping me with the use of Vulcan, I would like to thank Professor Ian Burgess and D.Sc. (Tech.) Florian Block.

For the financial support of this study I would especially like to thank Rautaruukki Oyj, but also Tampere University of Technology, Tekniikan Edistämissäätiö, SNIL-stipendirahasto, Aaro Kohonen Oy and COST, European Cooperation in Science and Technology.

My final and very special thanks go to my parents and brother, as well as my beloved fiancée, Silvia.

Helsinki, March, 2011

Dan Pada

Table of Contents

1 Introduction 1
1.1 Background of research 1
1.2 Objective of research 2
1.3 Scope of research 2
2 Literature review 3
2.1 Material properties of steel during fire 3
2.1.1 Eurocode model 3
2.1.2 Smoothed Ramberg-Osgood model 4
2.2 Mechanical properties of steel after fire exposure 5
2.2.1 Outinen 5
2.2.2 Kirby 7
2.3 Strain reversal during cooling phase 8
2.4 Fire tests 10
2.4.1 Li 10
2.4.2 Wang, Y.C. and Ding, J. 11
2.4.3 Wang, Y.C. 15
2.5 Numerical studies 15
2.5.1 Iu 15
2.5.2 Bailey 16
2.5.3 Santiago 16
2.5.4 Moss & Bong 19
2.5.5 Lu, Mäkeläinen and Outinen 21
2.6 Tie forces 23
2.6.1 Tie forces according to Eurocode 23
2.6.2 Wald 23
2.6.3 Horizontal forces according to "Fire Safety of Industrial Hall" 24
2.7 Conclusions on literature review 26
3 Software 28
3.1 SAFIR 29
3.1.1 Background 29
3.1.2 Experience of usage 29
3.1.3 SAFIR in literature 30
3.2 Vulcan 30

3.2.1 Background 30
3.2.2 Learning process 31
3.2.2.1 Visit at the University of Sheffield 31
3.2.2.2 Completion of visit 31
3.2.2.3 Accomplishments during the visit 32
3.2.2.4 Future advantages and co-operation 33
3.2.3 Analysis test 33
4 Case Study – CEE hall 34
4.1 Tie forces according to Eurocode 36
4.2 Development of analysis model 36
4.2.1 2D main frame analysis at ambient temperature 36
4.2.2 3D main frame analysis at ambient temperature 37
4.2.3 2D main frame analysis at elevated temperature 37
4.2.4 2D main frame analysis at elevated temperature, fixed supports 39
4.2.5 3D main frame analysis at elevated temperature 41
4.2.6 3D main frame analysis at elevated temperature, fixed supports 42
4.2.7 3D main frame analysis at elevated temperature, Eurocode temperature pattern 44
4.2.8 Local fire 1: mid-span fire 47
4.2.9 Local fire 2: mid-span fire, fixed base connections 52
4.2.10 Local fire 3: mid-span fire, temperature groups 53
4.2.11 Local fire 4: fire at column 57
4.2.12 Local fire 5: three frames, mid-span fire 59
4.2.13 Local fire 5, comparison of material models 63
4.3 Final analyses 64
4.3.1 Mid-span local fire 66
4.3.2 Mid-span local fire, strengthened truss 77
4.3.3 Mid-span local fire, Eurocode temperature development 79
4.3.4 Quarter span local fire 84
4.3.5 Quarter span local fire, strengthened model 85
5 CONCLUSIONS 94
5.1 Results 94
5.2 Design aspects 95
5.3 Limitations 96

5.4 Suggestions for future research 97
6 Bibliography 98
APPENDIX A VULCAN INSTRUCTIONS 100
APPENDIX B Eurocode Formulas 116

NOTATION

Abbreviations

FEA	Finite Element Analysis
FEM	Finite Element Method
CFRHS	Cold-Formed Rectangular Hollow Section

Symbols

Latin upper case letters

A	cross sectional area [mm^2]
A_m/V	section factor [1/m]
A_t, B_t, N_t	temperature-dependent parameters for the Ramberg-Osgood stress-strain model for steel at elevated temperatures [N/mm^2, N/mm^2, -]
E	modulus of elasticity [N/mm^2]
$E_{a,\vartheta}$	slope of the linear elastic range [N/mm^2]
F	tensile lateral force [kN]
I	second moment of area [mm^4]
K	column effective length factor [-]
L	span of the tie [m]
L_c	unsupported length of column [mm]
L_{cr}	buckling length in the buckling plane considered [mm]
$M_{y,fi,Ed}$	design bending moment about y-axis [Nmm]
$M_{z,fi,Ed}$	design bending moment about z-axis [Nmm]
N_{cr}	Euler critical buckling load [N]
$N_{fi,Ed}$	design axial compressive load [N]
$N_{fi,\vartheta,Rd}$	design tensile resistance [N]
N_{Rd}	design resistance of the cross-section $N_{pl,Rd}$ at ambient temperature according to SFS-EN 1993-1-1 [N]
Q_{tot}	total vertical load acting on frame [kN]
T	temperature [°C]
T_i	tie force, internal ties [kN]
T_p	tie force, perimeter ties [kN]
V	volume of the member per unit length [m^3/m]
$W_{pl,y}$	plastic bending moment resistance about y-axis [mm^3]
$W_{pl,z}$	plastic bending moment resistance about z-axis [mm^3]

Latin lower case letters

c_a	specific heat of steel [J/kgK]
c_p	coefficient related to the slope of the roof [-]
$f_{p,\vartheta}$	proportional limit [N/mm^2]
f_y	yield strength [N/mm^2]
$f_{y,\vartheta}$	effective yield strength [N/mm^2]
g_k	characteristic self-weight [kN/m^2]

h_{net}	design value of the net heat flux per unit area [W/m^2]
$h_{net,c}$	heat transfer by convection [W/m^2]
$h_{net,r}$	heat transfer by radiation [W/m^2]
i	radius of gyration about the relevant axis [mm]
k_{sh}	correction factor for shadow effect [-]
k_y	interaction factor for y-axis [-]
$k_{y,\vartheta}$	reduction factor for the yield strength at temperature ϑ_a reached at time t [-]
$k_{y,E}$	reduction factor for the slope of the linear elastic range at temperature ϑ_a reached at time t [-]
k_z	interaction factor for z-axis [-]
l	span of heated bay [m]
n_{eff}	coefficient related to the number of heated bays [-]
q_k	characteristic variable load [kN/m^2]
q_{tot}	total vertical load for frame [kN/m]
s	spacing of ties [m]
t	time [min]

Greek upper case letters

Φ	configuration factor [-]
$\Delta\vartheta_{a,t}$	increase of temperature [°C]
Δt	time interval [s]
Θ_g	gas temperature in the vicinity of the exposed member [°C]
Θ_m	surface temperature of the member [°C]
Θ_r	effective radiation temperature of the fire environment [°C]
Φ	configuration factor (often taken as 1) [-]

Greek lower case letters

α_c	coefficient of heat transfer [W/m^{2}K]
$\beta_{M,y}$	equivalent uniform moment factors for the y-axis [-]
$\beta_{M,z}$	equivalent uniform moment factors for the z-axis [-]
$\gamma_{M,0}$	partial factor at normal temperature [-]
$\gamma_{M,fi}$	partial factor at elevated temperature [-]
ε_f	emissivity of fire [-]
ε_m	emissivity of member [-]
ε_t	strain at temperature T [-]
$\varepsilon_{p,\vartheta}$	strain at the proportional limit [-]
$\varepsilon_{y,\vartheta}$	yield strain [-]
$\varepsilon_{t,\vartheta}$	limiting strain for yield strength [-]
$\varepsilon_{u,\vartheta}$	ultimate strain [-]
ϑ_a	steel temperature [°C]
$\bar{\lambda}$	non dimensional slenderness for the relevant axis at ambient temperature [-]
ρ_a	unit mass of steel (can be taken as 7850 kg/m^3) [kg/m^3]
σ	Stephan Boltzmann constant, 5,67*10^{-8} W/m^{2}K^4

σ_t	stress at temperature T [N/mm^2]
$\chi_{min,fi}$	minimum value of reduction factors for flexural buckling $\chi_{y,fi}$ and $\chi_{z,fi}$ [-]
ψ	relevant factor in the expression for combination of action effects for the accidental design situation (i.e. ψ_1 or ψ_2 in accordance with expression (6.11b) of EN 1990) [-]

1 INTRODUCTION

1.1 Background of research

In the natural fire safety concept, the structures are exposed to a natural fire curve or model, representing a real life fire source. These natural fires can often be described with the help of a heat release rate curve as a function of time. This curve is generally made up of three phases; the growth phase, the stationary or flashover phase and the decay phase, as seen in Figure 1. The fire curve does however not necessarily always contain the stationary phase, but can be made up of only the growth and decay phases.

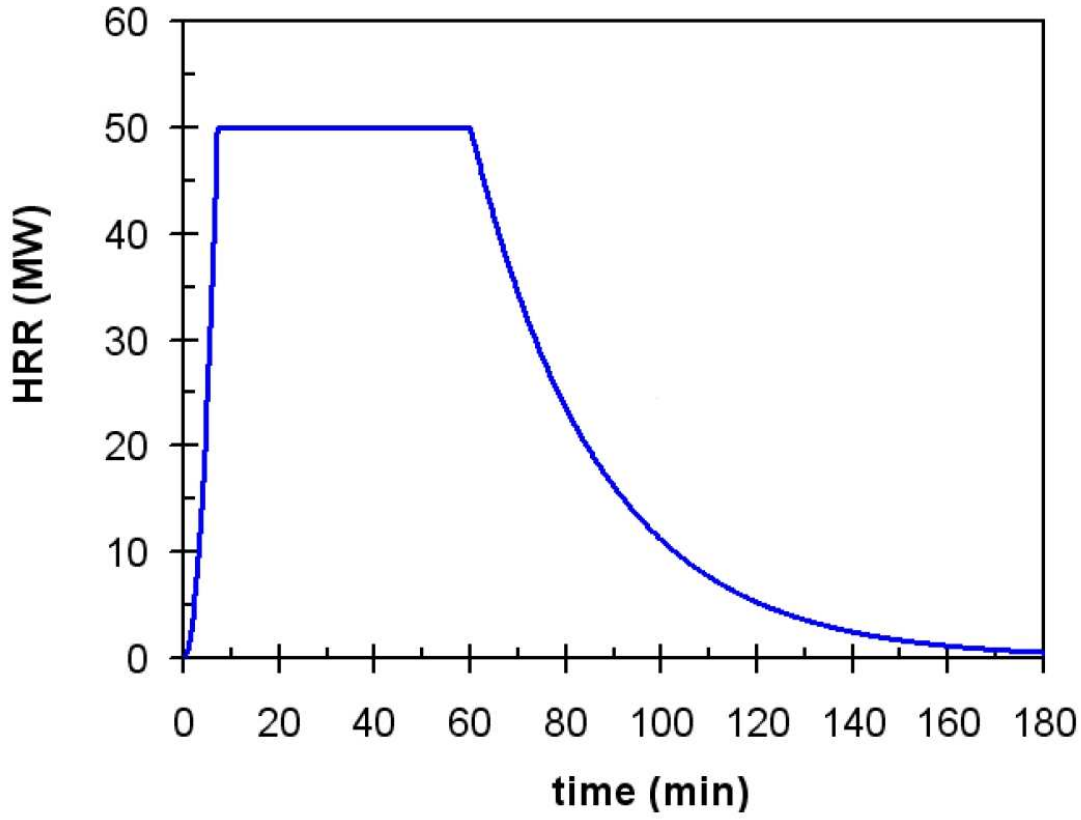

Figure 1 Example fire curve

Traditionally buildings have been designed according to the ISO 834 standard fire curve, developed in the 1930s originally with the intention to represent most common fires in rather small fire compartments (1). In a more advanced structural fire design using the natural fire safety concept, usually only the stationary phase of the fire, when the temperature is the highest, has been considered. However, full-scale fire tests and real fires have shown that the decay phase of the fire can be very severe, sometimes even critical, for steel skeletons in buildings (2). Hence, in some cases it may be necessary to complete the structural fire safety design not only for the stationary phase, but the whole fire curve. This almost inevitably leads to a non-linear, both geometrical and material, analysis.

1.2 Objective of research

The objective of this research is to study a typical industrial steel skeleton building with I-profile columns and roof trusses made up of rectangular hollow sections exposed to natural fires taking into account all three phases of the fire. This type of structure with column-truss frames has previously not been studied in the decay phase of the fire, so there is hardly any information available on the general behaviour of the structure and the forces developed in it during the decay phase. Bearing this in mind and the fact that previous studies on other types of structures have shown the importance of the decay phase, there is a great need to study the behaviour of this type of structure exposed to a natural fire including the decay phase. In more detail, the target is to evaluate whether the unprotected steel skeleton is able to withstand the complete fire or not, and especially how it performs in the decay phase of the fire. Based on the results from the analyses general conclusions will be drawn on how to take the decay phase of the fire into account in the design of this type of structure, as no such information has been available up to this date.

1.3 Scope of research

The scope of the research is to study the structural behaviour of a typical steel skeleton industrial hall, i.e. the CEE-hall by Ruukki, exposed to local natural fire scenarios including the decay phase. Focus will be put especially on the behaviour of the unprotected steel roof-truss during the decay phase of the fire. The study will also only deal with static non-linear analyses, no dynamical studies will be performed.

Due to the great deal of complexity involved in non-linear analyses on structures exposed to fires, this research is to a large extent performed with the help of advanced non-linear FEM-software, mainly Vulcan. As the usage of non-linear FEM-software is almost inevitable when dealing with structures exposed to fire, part of the scope also is to study the actual usage and implementation of the software in the design process of the structure, one possible future implementation being in the Ruukki NFD-system. This in turn means looking into different software available and studying their possibilities for implementation in structural fire safety design, as well as studying how the input of the software is made up; possibly making use of already existing models made for ambient temperature analyses.

2 LITERATURE REVIEW

According to C.G. Bailey et al. the full-scale fire tests conducted by the Building Research Establishment at Cardington demonstrated the importance of studying the behaviour of the complete building throughout the full duration of the fire, including the cooling phase. This was also supported by analytical studies. Furthermore, even though a structure may be able to resist the fire up to its maximum temperature, failure can occur during the cooling phase, due to the high axial tensile forces developed during cooling. (2)

Generally, residual effects in members affected by fire take place as a result of the thermal effects on the affected members and the restraints from the surrounding cooler structure. When steel is heated the material softens and undergoes thermal expansion, which in the case of a beam leads to bending and extension. Both of these phenomena are however resisted by the adjacent cooler structure, leading to permanent deformations, often including shortening of the heated members. When the steel members then cool down, they regain their strength and contract, resulting in residual forces, often in the shape of axial tension. (3)

2.1 Material properties of steel during fire

Both the Eurocode 3 Part 1-2 (4) and the smoothed Ramberg-Osgood stress-strain material models for structural steel at elevated temperatures will be used in the study and are here presented briefly.

2.1.1 Eurocode model

The Eurocode stress-strain model for steel at elevated temperatures is given in Eurocode 3 Part 1-2 (4). The model is defined stepwise by the equations described in Figure 2.

Strain range	Stress σ	Tangent modulus
$\varepsilon \le \varepsilon_{p,\theta}$	$\varepsilon E_{a,\theta}$	$E_{a,\theta}$
$\varepsilon_{p,\theta} < \varepsilon < \varepsilon_{y,\theta}$	$f_{p,\theta} - c + (b/a)\left[a^2 - (\varepsilon_{y,\theta} - \varepsilon)^2\right]^{0,5}$	$\frac{b(\varepsilon_{y,\theta} - \varepsilon)}{a\left[a^2 - (\varepsilon_{y,\theta} - \varepsilon)^2\right]^{0,5}}$
$\varepsilon_{y,\theta} \le \varepsilon \le \varepsilon_{t,\theta}$	$f_{y,\theta}$	0
$\varepsilon_{t,\theta} < \varepsilon < \varepsilon_{u,\theta}$	$f_{y,\theta}\left[1 - (\varepsilon - \varepsilon_{t,\theta})/(\varepsilon_{u,\theta} - \varepsilon_{t,\theta})\right]$	-
$\varepsilon = \varepsilon_{u,\theta}$	0,00	-
Parameters	$\varepsilon_{p,\theta} = f_{p,\theta}/E_{a,\theta}$ $\varepsilon_{y,\theta} = 0,02$	$\varepsilon_{t,\theta} = 0,15$ $\varepsilon_{u,\theta} = 0,20$
Functions	$a^2 = (\varepsilon_{y,\theta} - \varepsilon_{p,\theta})(\varepsilon_{y,\theta} - \varepsilon_{p,\theta} + c/E_{a,\theta})$ $b^2 = c(\varepsilon_{y,\theta} - \varepsilon_{p,\theta})E_{a,\theta} + c^2$ $c = \frac{(f_{y,\theta} - f_{p,\theta})^2}{(\varepsilon_{y,\theta} - \varepsilon_{p,\theta})E_{a,\theta} - 2(f_{y,\theta} - f_{p,\theta})}$	

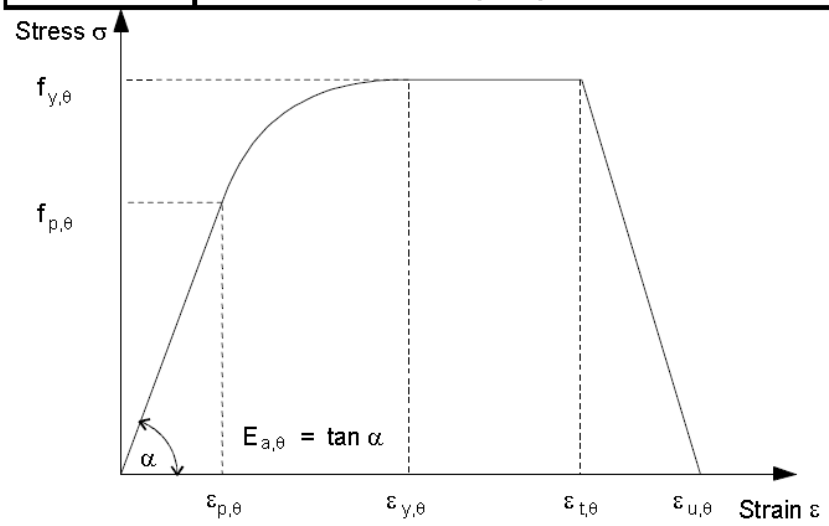

Figure 2 Eurocode stress-strain model for steel at elevated temperatures

where

$f_{y,\vartheta}$	effective yield strength [N/mm^2]
$f_{p,\vartheta}$	proportional limit [N/mm^2]
$E_{a,\vartheta}$	slope of the linear elastic range [N/mm^2]
$\varepsilon_{p,\vartheta}$	strain at the proportional limit [-]
$\varepsilon_{y,\vartheta}$	yield strain [-]
$\varepsilon_{t,\vartheta}$	limiting strain for yield strength [-]
$\varepsilon_{u,\vartheta}$	ultimate strain [-]

2.1.2 Smoothed Ramberg-Osgood model

The smoothed Ramberg-Osgood stress-strain model was developed from the original Ramberg-Osgood model by PhD Paul Shepherd (5) in order to avoid discontinuous results for buckling of heated columns. The main equation of the smoothed model, the same as in the original Ramberg-Osgood model, is

$$\varepsilon_t = \left(\frac{\sigma_t}{A_t}\right) + \frac{1}{100}\left(\frac{\sigma_t}{B_t}\right)^{N_t}$$

where

ε_t	strain at temperature T [-]
σ_t	stress at temperature T [N/mm^2]
T	temperature [°C]
A_t, B_t, N_t	temperature-dependent parameters given in Figure 3 [N/mm^2, N/mm^2, -]

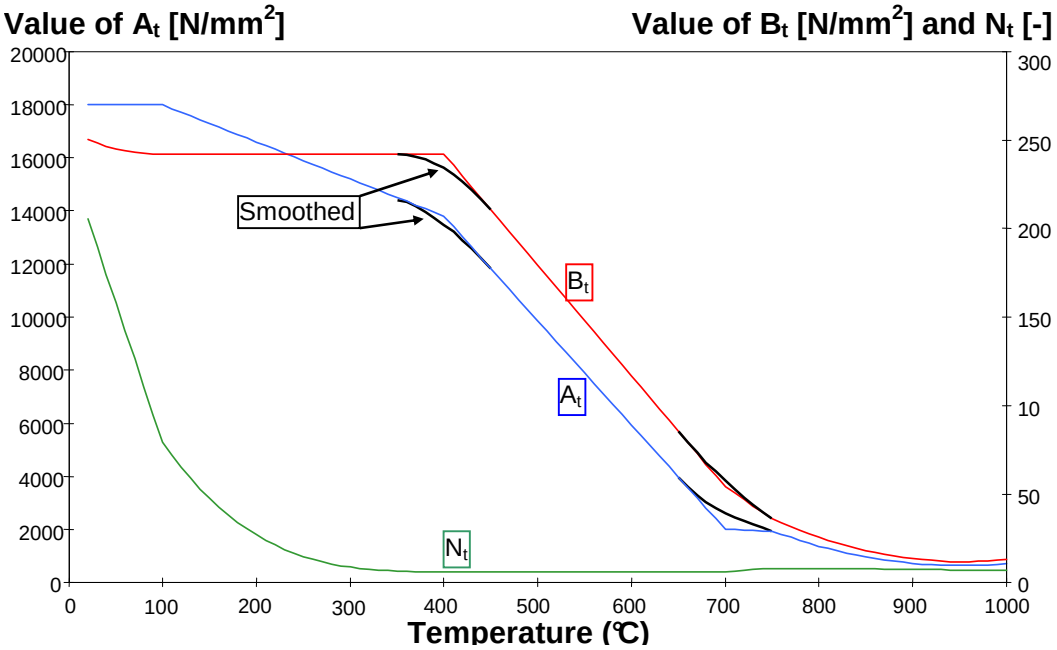

Figure 3 Ramberg-Osgood parameters

2.2 Mechanical properties of steel after fire exposure

There is quite a lot of information available from tests on the mechanical properties of steel during the heating phase of a fire, whereas only a few studies have focused on the mechanical properties of steel after fire exposure, i.e. when the steel has cooled down.

2.2.1 Outinen

J. Outinen studied and tested the mechanical properties of structural steel, mainly at high temperatures, in his doctoral dissertation (6). He however also performed tensile tests at ambient temperature on structural steel materials from samples tested at elevated temperatures in order to evaluate the residual strength of the fire exposed materials. The two steel grades tested for residual strengths were S355J2H, a steel grade commonly used in hollow steel sections, and S350GD+Z, which is a hot-dip galvanized steel commonly used in cold-formed steel structures.

The actual yield strength of the S355J2H steel measured before fire exposure was much higher than the nominal yield strength of 355 N/mm^2, reaching 529 N/mm^2. Tensile tests were carried out at ambient temperature on the specimens that had been subjected to elevated temperatures with a maximum of 710 °C. The tests showed that the strength was quite well preserved with only a small drop, still remaining above the nominal value. For this steel material Outinen

concluded that "if the distortions of a steel structure are within the tolerance limits, the strength of the material is still adequate". He however also added that a safer approach could be to limit the utilization after fire to 90 % of the nominal yield strength. The results from the tests can be seen in Figure 4, where the black lines mark the results after heating.

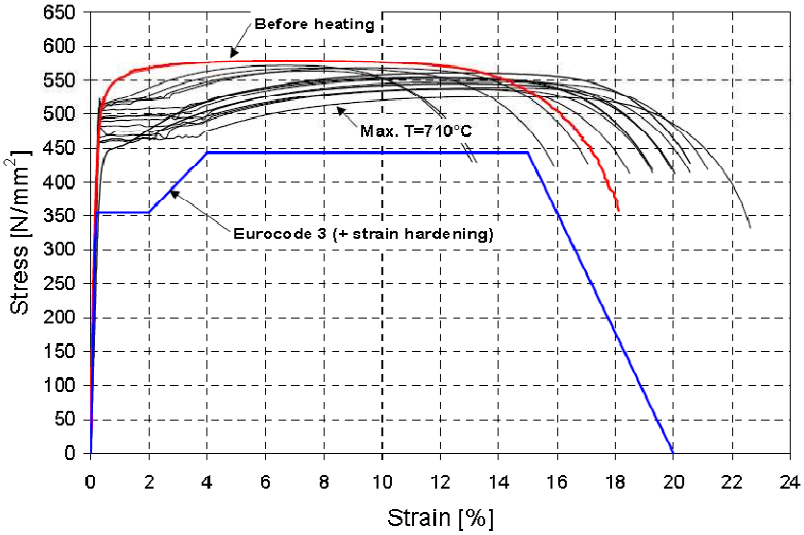

Figure 4 Tensile test results of structural steel S355J2H (6)

The measured yield strength of the S350GD+Z steel was quite near the nominal value of 350 N/mm^2, even though the exact value is not presented other than graphically. The tested specimens had been exposed to temperatures as high as 950 °C. According to the tests, the material suffered only a small drop in strength, indicating that the same post-fire limit of utilization can be used for this material as for S355J2H, i.e. 90 % of the nominal yield strength, provided that the distortions are within the shape and straightness tolerances of the structure. It's also worth mentioning that even though the tested thin-gauge steel members were quite distorted after fire exposure, the strength of the steel had not decreased much below the nominal value. The results from the test can be seen in Figure 5.

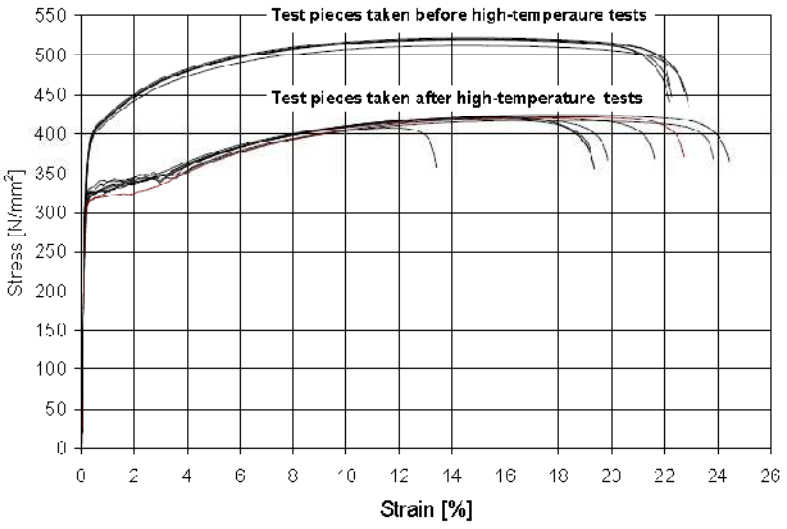

Figure 5 Tensile test results of structural steel S350GD+Z (6)

The zinc coating melts already at 419,6 °C, which can work as an indicator of the temperatures reached during a fire. If the coating is unaffected, the temperatures have not been high enough to cause any drop in the strength level. If the coating however is affected, it's often preferable to change the member after fire exposure, rather than repairing the coating, which seldom is worth the effort.

2.2.2 Kirby

B.R. Kirby et al. (7) studied the possibilities of reinstatement of fire damaged steel and iron framed structures in the mid 1980's. They studied structural steels, cast- and wrought iron, bolts, reinforcing- and prestressing steels and cold formed galvanized steel products. Only the testing and results of the structural steels will be presented here. Two mild steels and three microalloyed steels were tested.

The tests were carried out by heating the material in a furnace at temperatures between 100 °C and 1000 °C for 1 h and 4 h periods. After the heat treatment, the material was cooled in air and the tested according to BS18 Part 2. The tests measured yield strength or 0,2 % proof stress, tensile strength, elongation at fracture and for round specimens reduction in area. 2 mm V-notch Charpy impact test were also carried out on all grades of steel. Furthermore, the metallurgy of the materials was examined.

Two Grade 43A, which largely corresponds to S275, mild steels were studied; one with a high room temperature yield and tensile strength (335 N/mm^2 and 472 N/mm^2, Charpy 27 J ITT -35 °C), and one low strength (238 N/mm^2 yield, 408 N/mm^2 tensile strength, Charpy 27 J ITT -5 °C). The tests showed that exposure to temperatures up to 600 °C had virtually no effect on the strength of the steel, regardless of exposure time. With higher temperatures the strength started to decrease and also the exposure time had an effect on the strength; the longer the exposure, the more the strength decreased. The high strength mild steel was also more affected than the low strength mild steel.

The authors however concluded that regardless of exposure temperature and time, the strength properties are unlikely to fall more than 10 % of the specified value. The ductility tests showed that the materials were not seriously embrittled when heated up to 600-700 °C, still being far from brittle at room temperature even after being heated to higher temperatures. The microstructural examinations showed substantial changes to the microstructure, especially after longer fire exposures at higher temperatures, which however did not seem to affect the strength too much.

The first microalloyed steel to be tested, grade 50 steel, was of American specification, alloyed with vanadium, corresponding to BS4360: Grade 50B steel, or today S355 steel. Up to 600 °C the material showed no loss in strength. With higher temperatures the material started to degrade, and after 800 °C the material properties were 27 % below specification. However, above 800 °C the material started to regain its properties. The ductility tests showed quite similar type of results as the strength tests and the microstructural tests showed quite similar changes as for mild steels, apart from having a smaller grain size.

The second microalloyed steel was BS4360: Grade 50D modified, which was a quality steel for rolling premium notch though sections, developed for offshore industry. Up to 600 °C the

properties of the steel were almost unaffected, however after heat treatments above that temperature the strength was gradually reduced. The strength was still at no point less than 6 % below specifications, but it must be remembered that this was due to the fact that the original strength was well above requirements. The ductility suffered a small reduction at 250 °C and also a bigger reduction above 600 °C but returned at even higher temperatures. The microstructure changed in a similar manner to mild steels, apart from that no Widmanstätten[1] structures were present at any point and that it had a very fine grain size.

The third and last microalloyed steel was COR-TEN B, which is a quality resistant to weather exposure, as it forms a thin rust layer which works as protection against further exposure. For this steel, no changes in the properties were observed below 650 °C. First the tensile strength started to deteriorate, then also the yield stress. However, at higher temperature exposures the strength properties did not deteriorate. The notch toughness of the material did not drop until the steel had been heated to 750 °C for 1 h. After tests at 800 and 900 °C, the toughness was at as-received value. Metallurgical changes were also observed.

The results from Kirby are hence quite in line with Outinen's results, in most cases the strength is largely unaffected, and very seldom the loss in strength is more than 10 % of the minimum specification. The toughness of the material may though in some cases need special attention and study after the fire.

2.3 Strain reversal during cooling phase

In the traditional analytical approaches to study the performance and safety of steel structures exposed to fire, focus has been on the growing and fully developed fire, i.e. exposure to increasing temperatures. This has generally been based on unique stress-strain curves defined for specific temperatures. However, when studying the decay phase of the fire, i.e. cooling of the structures, a proper model for the strain reversal, taking into account the effect of permanent strains for members stressed above the elastic limit, is needed. (3)

J.A. El-Rimawi et al. (3) presented a simple model for describing the unloading path of structural members by making assumptions based on the effect of cyclic loading at ambient temperature. This is legitimated as an effect similar to that of unloading at ambient temperature may develop during the decay phase of a fire, due to the fact that the load-deformation characteristics are dependent of the temperature. The method assumes that the load in a member is first reduced to zero, after which the permanent deformation is calculated. After this the load-deformation path is approximated by a bi-linear representation. The first line is assumed to be parallel to the tangent to the original curve at the origin, and this is also the unloading path. The second line is the tangent to the original curve at a point where the load is equal, but opposite in sign, to the actual load in the member. The procedure was also implemented in a computer program, NARR2.

C.G. Bailey et al. (2) employed the Massing Rule and developed a strain reversal model based on the work by El-Rimawi et al. (3) using a curvilinear unloading path where El-Rimawi et al. used a bi-linear path. Furthermore C.G. Bailey et al. assumed that cyclic loading of steel members in fire does not occur, allowing for the definition of a unique and reversible unloading

[1] Widmanstätten patterns, or Thomson structures, are unique figures of long nickel-iron crystals.

path. According to this model the loading and unloading paths are coincident as long as the strain values remain in the elastic region, whereas the loading and unloading paths separate if the unloading starts from the inelastic ranges, resulting in an unloading path in the shape of a hysteresis loop. The comparison between El-Rimawi's and Bailey's models can be seen in Figure 6. As steel has no well-defined yield plateau at elevated temperatures, Bailey et al. defined the upper bound of the elastic limit at 0,1 % proof stress.

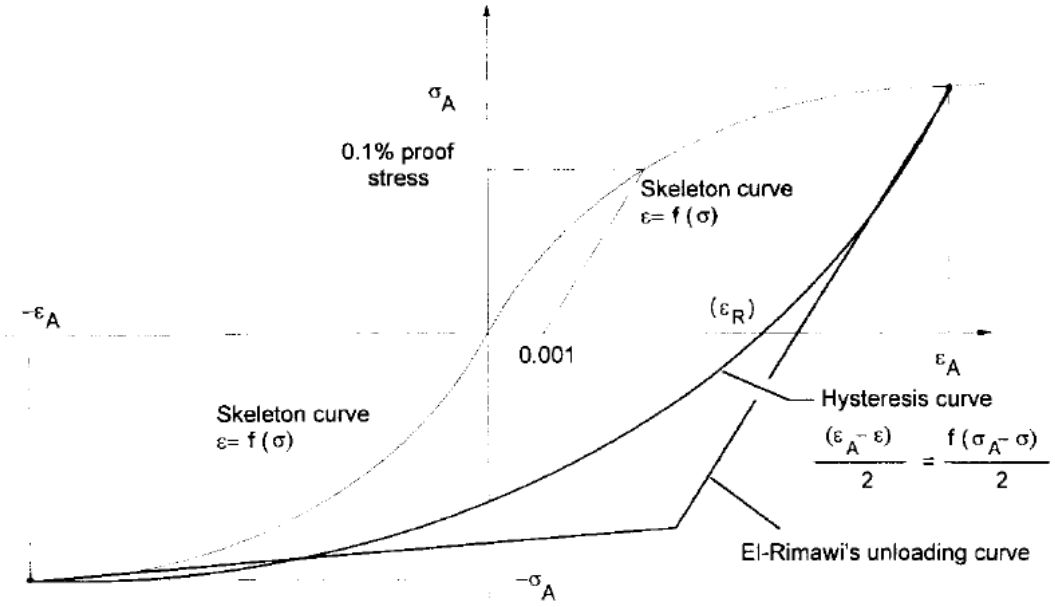

Figure 6 Definition of loading and unloading curves. The hysteresis curve represents the curve by Bailey et al. (2)

Using the plastic hinge method C.K. Iu et al. (8) developed a fire analysis method including the cooling effect by modification from the nonlinear inelastic finite element program GMNAF (Geometric and material nonlinear analysis of frames, The Hong Kong Polytechnic University) and previous fire analysis by themselves. The cooling effect is taken into account through an "incremental-iterative procedure for searching for the path of unloading consequent upon strain reversal during cooling". The plastic strains of the members are determined and incorporated into the method in order to model the strain reversal effect on cooling material behaviour. Opposed to previous models by Franssen (included in SAFIR), El-Rimawi and Bailey, where the reference point of nonlinear solution procedures refers to the original configuration for all temperature levels, the reference point in the method by Iu et al. is updated during cooling. According to Iu et al., this method should be more efficient in tracing the equilibrium paths during cooling.

P. Wang et al. (9) pointed out that there are a couple of disadvantages with using the Massing Rule used in the methods by Bailey and Franssen in a computer analysis, making it difficult and heavy to run. According to Wang, also the method described by El-Rimawi has some difficulties. Therefore Wang presented a new unloading path that should be easier to implement in design and in computer programs. The presented unloading path can be seen in Figure 7 and consists of a linear part and a curved part. The unloading path for temperature T_2 in Figure 7 is constructed by the line EO_2, which is parallel to the tangent to the original curve at the origin, and the curve O_2E', which is a shift of a half of the original curve O_1B' at the temperature T_2.

The linear part down to zero stress level is hence the same as for El-Rimawi. This way the problems with Bailey's and El-Rimawi's should be avoided, hence providing a more easily solved method.

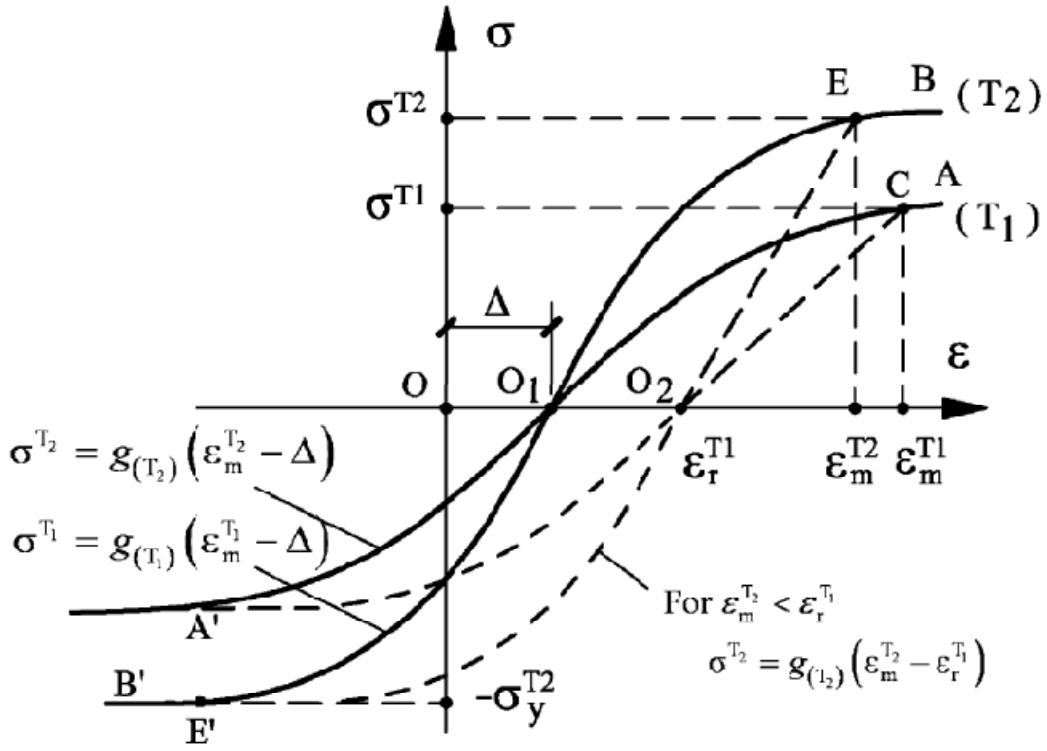

Figure 7 Unloading path defined by a line and a half of the original stress-strain curve (9)

2.4 Fire tests

2.4.1 Li

G-Q Li et al. (10) conducted experiments on restrained steel beams subjected to both heating and cooling at the Fire Laboratory of Tongji University in Shanghai, China. Two specimens of beams, with different degree of restraint, were tested in a furnace. The steel quality of the beams exposed to fire was Q235B whereas the rest of the test rig was made up of Q345 steel. The top flange of the tested beams was wrapped with ceramic fibre blanket, in order to simulate the effect of a concrete slab on top of the beam. The load was applied through two hydraulic jacks with a load ratio of 70 % of the ambient temperature load resistance, corresponding to 130 kN. The temperature was increased until the deflection of the beam reached about 1/16 of its span, after which the fire was turned off and the specimens started to cool down. The test setup can be seen in Figure 8.

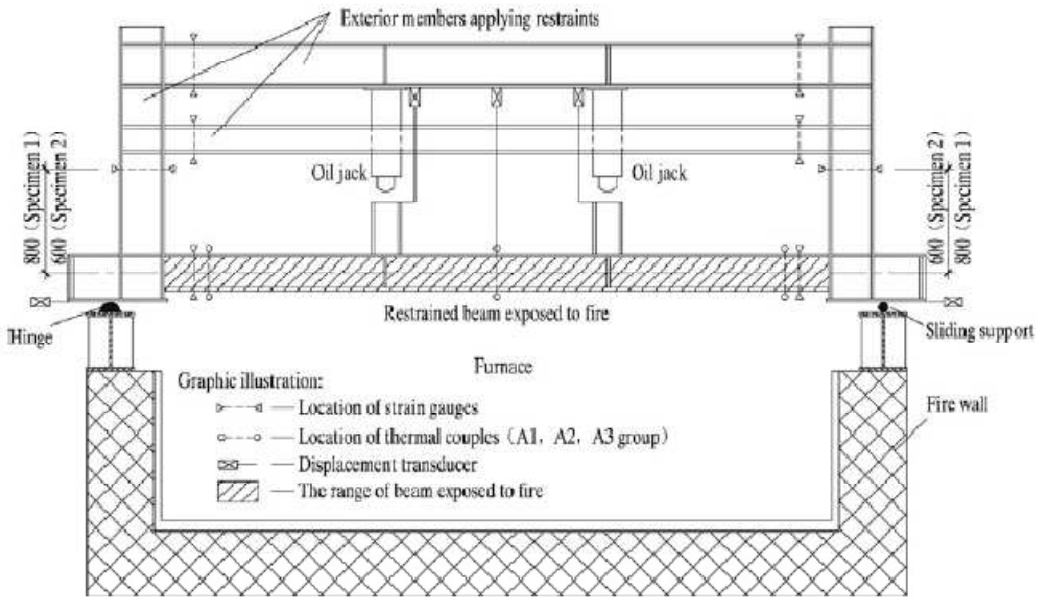

Figure 8 Test setup (10)

The specimens suffered from large deflections, which also remained after cooling down, indicating that plastic deformations had taken place. The columns of the test rig were also bent, showing that large axial forces had been developed in the restrained beams during the test. Local buckling of the bottom flange of the restrained beams also occurred near the beam ends. No "runaway" displacement, which is typical for isolated steel beams during fire tests, was observed for the restrained beams. This is due to the catenary action that occurred at a deflection of about 1/20 of the span, enhancing the load-bearing capacity of the restrained beam. (10)

The beam ends were at the beginning of the test pushed outward due to thermal expansion, but after some time began moving inwards because of the large deflection. After the fire had gone out, the beam ends kept moving inwards as the beam started to contract due to cooling.

For the first minutes of the tests axial compression was developed in the tested beams due to thermal expansion. However, after about 14 minutes the compression changed to tension, due to the catenary action. When the fire had gone out at 19 min and 21 min respectively for the two tests, the tension was first quickly increased, as the contraction was restrained, but the increase in tension force slowed down after only a few minutes. Axial compression as high as close to 400 kN and axial tension close to 1200 kN was measured during the test. Hardly any deflection reversal during the cooling was however observed.

2.4.2 Wang, Y.C. and Ding, J.

Y.C. Wang and J. Ding performed fire tests on sub-frames consisting of a steel beam connected to concrete filled tubular columns with different types of joints at the Fire Testing Laboratory of the University of Manchester, UK. The main area of interest of the tests was the behaviour of the joints under heating, however, two tests were also performed where the decay phase was included. Even though the tests focused on the joints, the forces and deflections of the beam are also presented. Only the tests inclusive of the decay phase will be presented hereafter. (11)

The test rig can be seen in Figure 9. The span of the beam was 2 m, the steel grade S275 and the profile 178x102x19UB. The beam was not laterally restrained, and could hence experience lateral torsional buckling. The upper flange of the beam was covered with a 15 mm thick ceramic fibre blanket in order to simulate the heat-sink effect of a concrete slab on top of the beam. Otherwise the beam and columns were unprotected. The columns were restrained from lateral movement at the ends but free to move in the longitudinal direction. The beam was loaded by two transverse point loads imposed by two hydraulic jacks to a nominal load ratio of 50 % of the ambient temperature load resistance (taking lateral torsional buckling of the beam into account but assuming that there was no bending moment resistance of the joints at the ends). The temperature of the furnace was intended to follow the ISO 834 standard fire, but this was not entirely possible due to the thermal mass of the test assembly. (11)

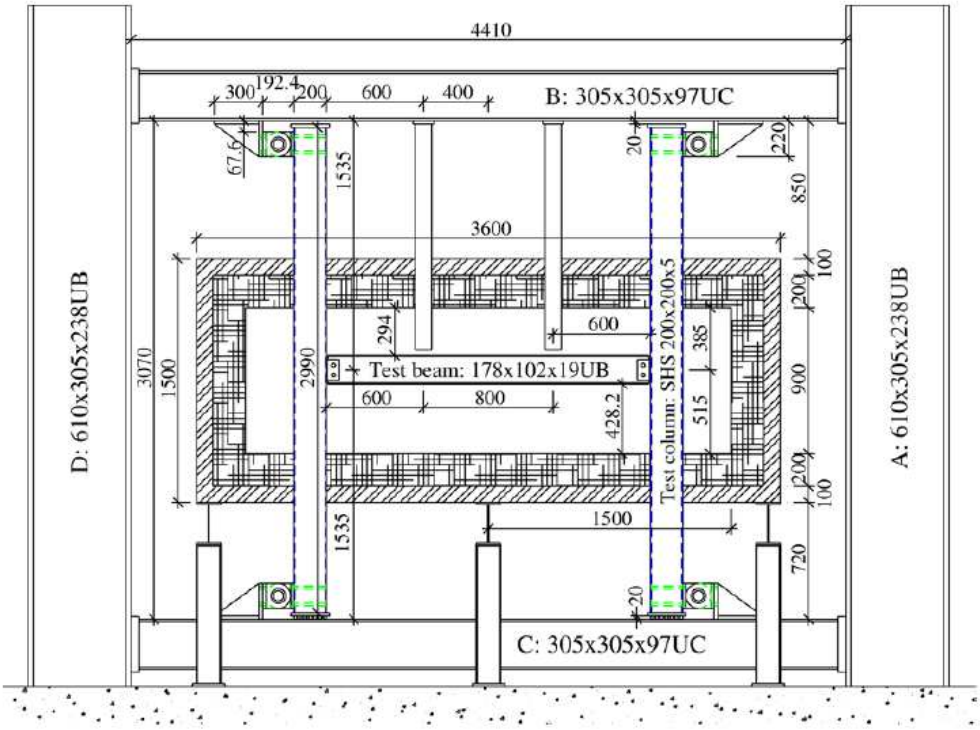

Figure 9 Test rig (11)

In test 9, which was the first test including the decay phase, the beam was connected to the columns through fin plates according to Figure 10. The loads were applied gradually before the furnace was ignited without any visible deformation. 26 minutes after the fire ignition the beam started to deflect rapidly as the beam reached the maximum temperature resisted by a corresponding axially unrestrained beam failing by lateral torsional buckling, and the beam started to twist. The furnace was stopped at 26,6 minutes and a fan was turned on to provide cooling. The deflection did however not stop to increase immediately and continued to grow until 36,3 minutes when it started to decrease. At 106,7 minutes the furnace door was opened and the test was ended at 331 minutes without fraction of failure of the sub-frame. The beam suffered from large twisting and as the beam span was quite short, the tension force developed in the beam during the catenary action was not high enough to cause failure of the joints. (11)

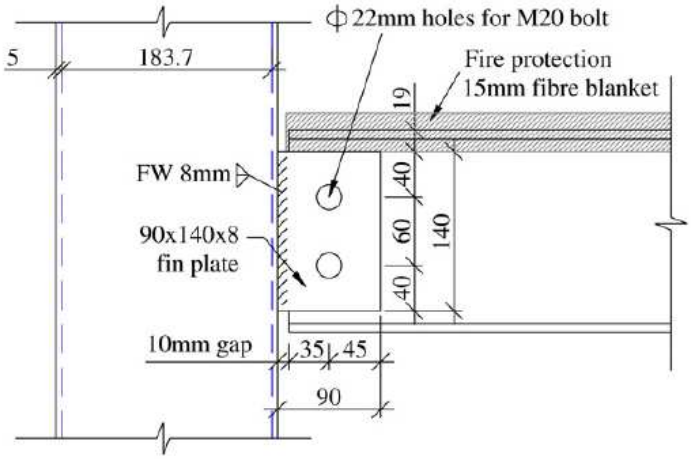

Figure 10 Test 9 joint (11)

In test 10, which also included the decay phase, the connections were made with a reverse channel as in Figure 11. The loads were applied in the same way as in test 9. The furnace was stopped at 23,1 minutes into the test in order to prevent lateral torsional buckling and before large deflection occurred and a fan was turned on to provide cooling. At 29,7 minutes the deflection started to decrease slowly but started to increase again at 56 minutes. The furnace door was opened at 158 minutes and the test was ended at 320 minutes without fracture or failure. The beam suffered from slight bending. (11)

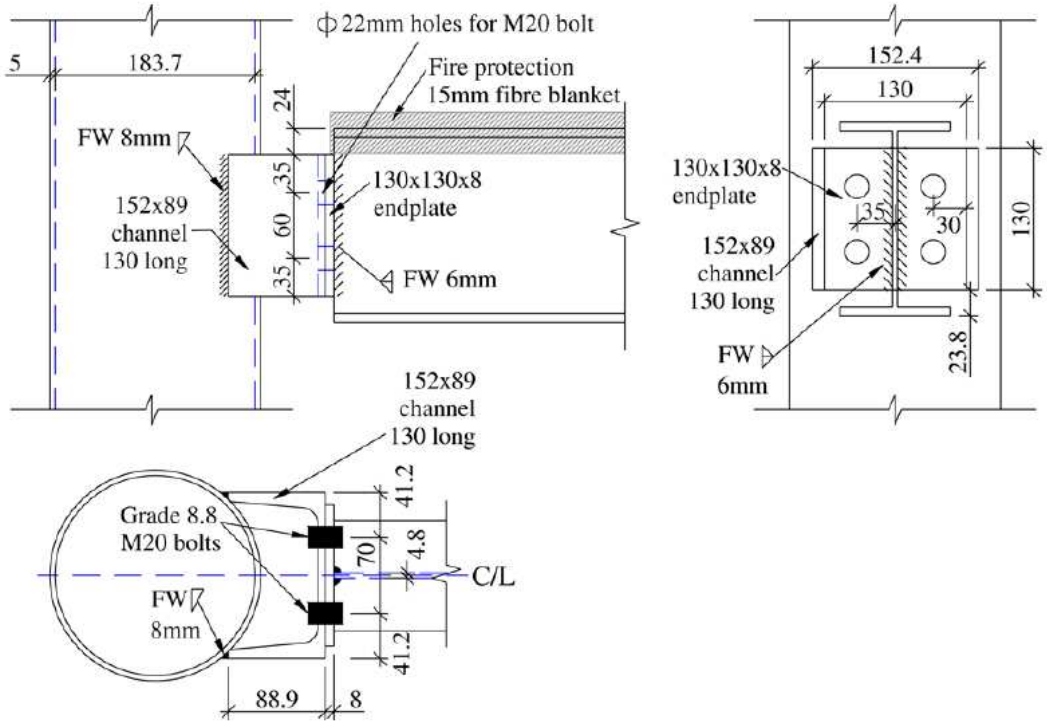

Figure 11 Test 10 joint (11)

The relationships between the temperature and the deflection for tests 9 and 10 are presented in Figure 12. The curves for the axial force - temperature relationships for tests 9 and 10 are shown in Figure 13.

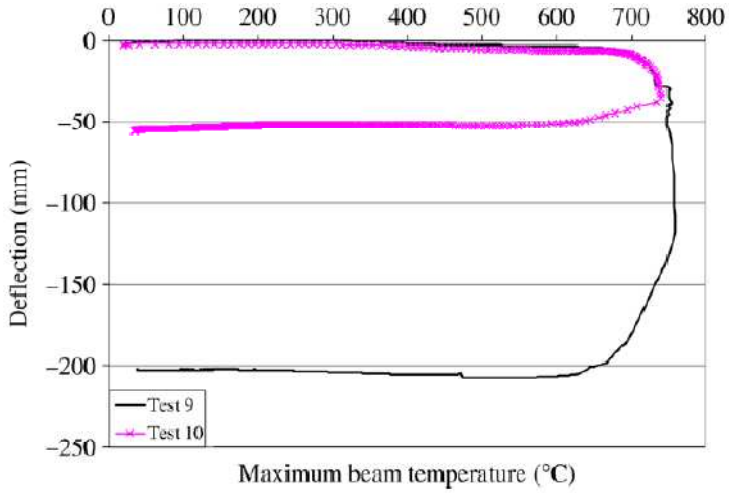

Figure 12 Beam vertical deflection - temperature curves for tests 9 and 10 (11)

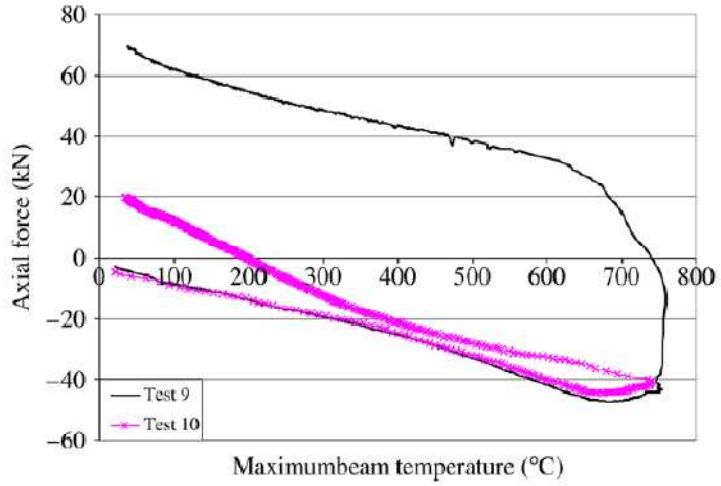

Figure 13 Beam axial force - temperature relationships for tests 9 and 10 (11)

From the pictures it can be seen that the deflections first increased slowly due to thermal bowing and the axial compression forces grew due to thermal expansion. When the beams then were heated to the limiting temperature for bending they started to lose their strength and stiffness and the deflections started to increase rapidly whereas the compressive forces decreased. In test 9 the beam went into catenary action and the deflection grew quite big and a tensile force was developed, also leaving a significant residual tensile force. This did not happen in test 10 for the simple reason that the cooling phase started a bit earlier and the maximum temperature was a bit lower than in test 9, still being in compression when the cooling started. Hence the residual tensile force was much lower after the test than in test 9. (11)

Even though the findings of the study are quite interesting, it seems as a too small number of tests were performed and as the joints were different in tests 9 and 10 the results are not directly comparable. Furthermore as the span of the beam was so small, the catenary forces were quite small.

2.4.3 Wang, Y.C.

Y.C. Wang et al. at the University of Manchester, UK, also performed a series of both real fire tests and numerical simulations in cooperation with the University of Sheffield, UK. The test rig of the real fire tests was pretty much the same as in the test described above by Y.C. Wang and J. Ding, the main difference being different profile sizes used. The tests were performed in order to study the effects of joints on steel structural behaviour in fire. Several different types of joints were used; fin plate, flexible endplate, flush endplate, extended endplate and web cleat. As the focus lied so heavily on the joints, the results will only be presented in a more general manner here. (12)

The overall behaviour of the structure was very much the same as in the previous work by Y.C. Wang and J. Ding. As the temperature of the test rig started to increase, a large compressive force was developed in the beam due to the axial restraint. As the temperature was further increased, the strength of the steel started to degrade and the compressive force decreased. In the next stage the deflection started to grow rapidly as the bending resistance limit was reached. In the final stage of the heating the beam went into catenary action and a tensile force was developed. In order of the structure not to collapse, not only the beam had to withstand the compressive and tensile forces, but also the joints had to sustain the forces and have sufficient ductility. The magnitude of the axial forces developed in the beam relied heavily on the stiffness of the restraining columns rather than on the joint type.(12)

The fire tests were also simulated and analysed with ABAQUS. In order of the ABAQUS model to overcome the temporary instabilities before complete failure, it was necessary to use an artificial damping that dissipated the energy released during these temporary instabilities, involving great computational efforts. In general the results from the FE models simulated the real fire tests very well, except for weld fracture and bolt thread stripping as they were not included in the ABAQUS models. (12)

2.5 Numerical studies

2.5.1 Iu

Iu et al. (8) presented a verification and comparison between the different strain reversal models, based on a numerical analysis of a simply supported beam. The span of the beam was 6 m with the cross-section 356x171x51 UB, subjected to a uniform load of 30,6 kN/m. It was heated non-uniformly to 650 °C and then cooled to ambient temperature. Figure 14 shows a comparison of the results of the different methods by El-Rimawi (shown as NARR2), Bailey (hysteresis curve) and Iu's own method (present analysis). It can be seen that Iu's method gives the smallest permanent deformation, whereas El-Rimawi's method gives the largest. Iu also presented comparisons under a smaller uniform loading, which resulted in much smaller differences in the permanent deformations.

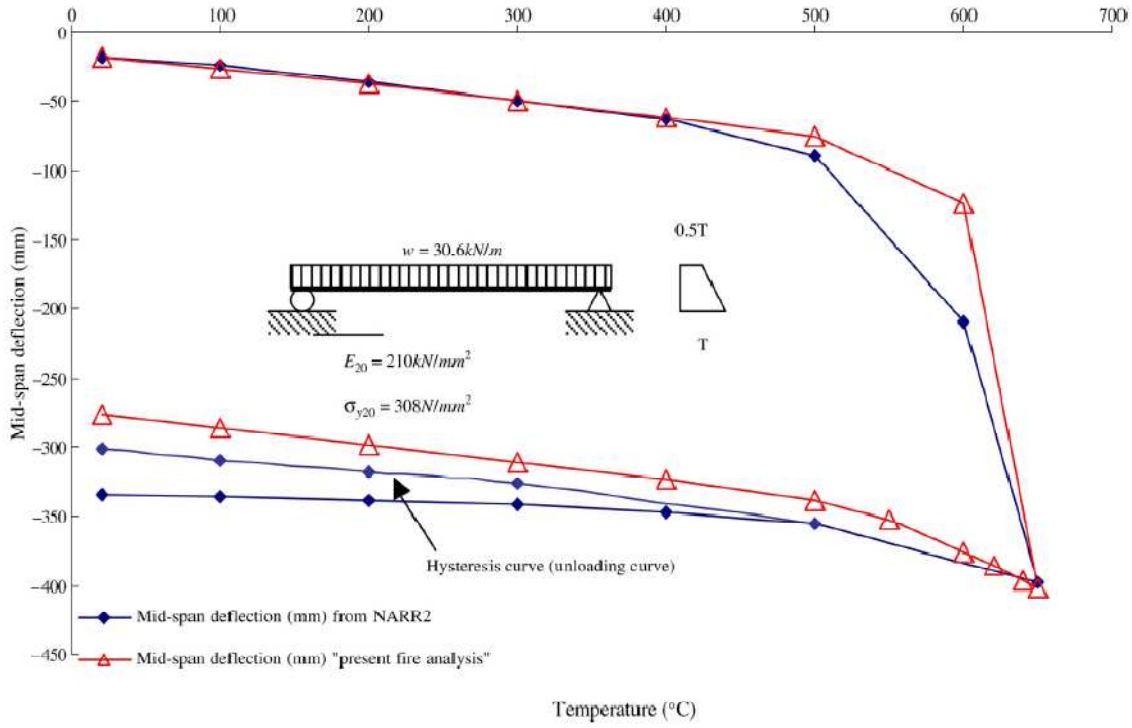

Figure 14 Temperature-deflection curve of a non-uniformly heated beam under uniform loading (8)

2.5.2 Bailey

In (2) C.G. Bailey et al. performed a numerical study on the effects of progressive spread of fire in a building, resulting in both cooling and heating taking place at the same time in different areas of the building. Based on their results, they concluded that for the studied two-dimensional bare steel frames, a spreading fire produces larger beam displacements in the bays where the fire begins, than for the case when there is simultaneous heating of all bays. This is due to the fact that when a beam starts to cool and its adjacent beams are heated, the compression in the cooling beam grows, which increases its vertical displacement.

2.5.3 Santiago

A. Santiago et al. (13) performed a nonlinear numerical study of a sub-frame consisting of an exposed steel beam restrained between a pair of fire protected steel columns. In the model the beam supported a steel-concrete composite slab and was welded to the columns. The material was assumed to be S355 according to Eurocode 3. The beam carried a load corresponding to self-weight and a uniform load of 10 kN/m, which corresponds to about 20 % of the beam resistance at room temperature. The thermal load, which is presented in Figure 15, was assumed to be almost the same as a fire curve including both heating and cooling observed at the 7th Cardington fire test, the only difference being a slightly lower maximum temperature. The sub-frame was modelled in both LUSAS and SAFIR using 3D shell elements and can be seen in Figure 16.

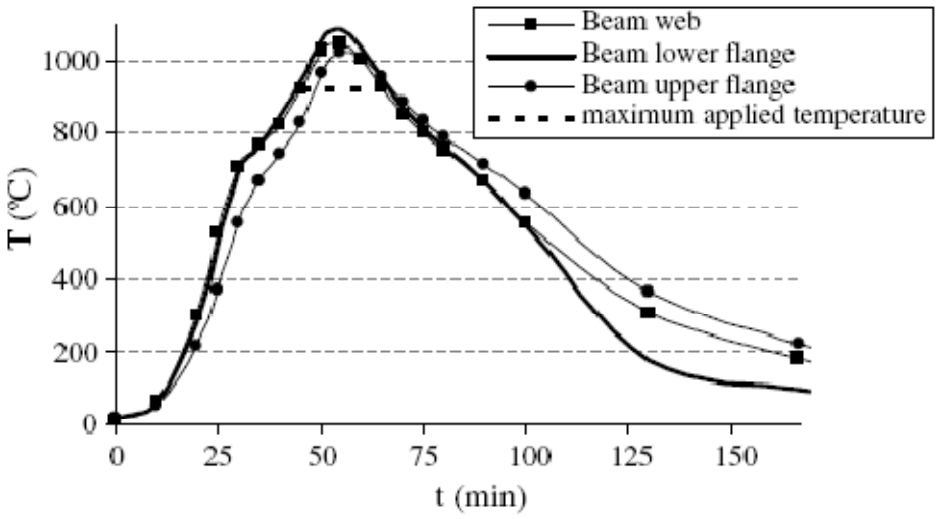

Figure 15 Thermal load (13)

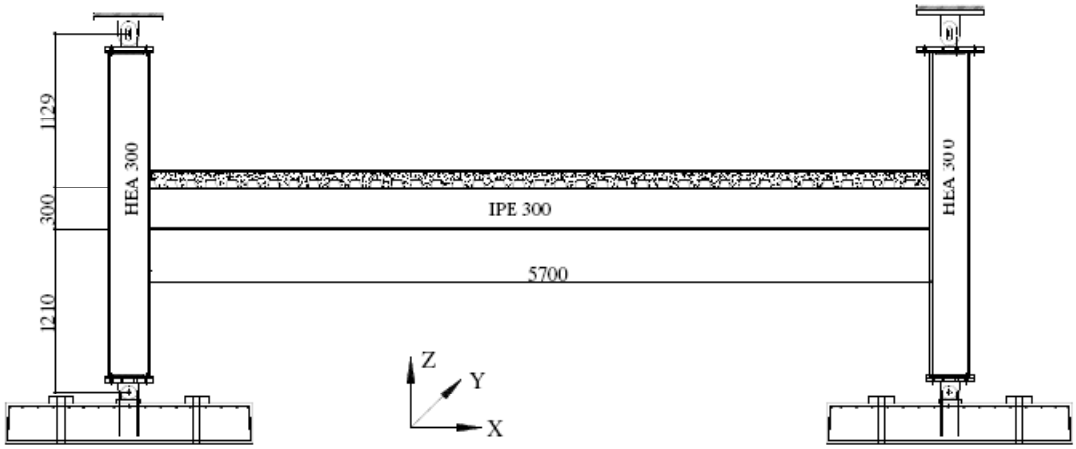

Figure 16 Sub-structure model (13)

The development of the mid-span vertical deflection is presented in Figure 17. From the figure a maximum vertical displacement of 0,34 m can be observed when the temperature had reached its maximum value. In the cooling phase the displacement decreased to 0,27 m, corresponding to the plastic deformation that was produced in the beam during the fire.

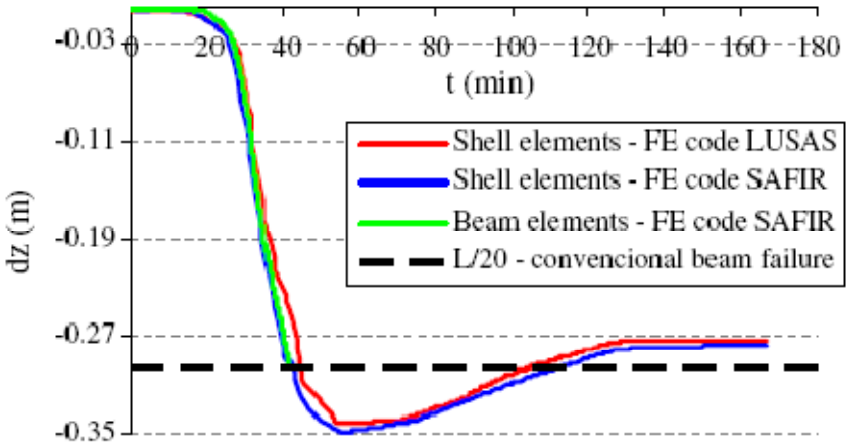

Figure 17 Development of mid-span deflection (13)

The development of the axial force is presented in Figure 18, where "line 1" corresponds to a point close to the column.

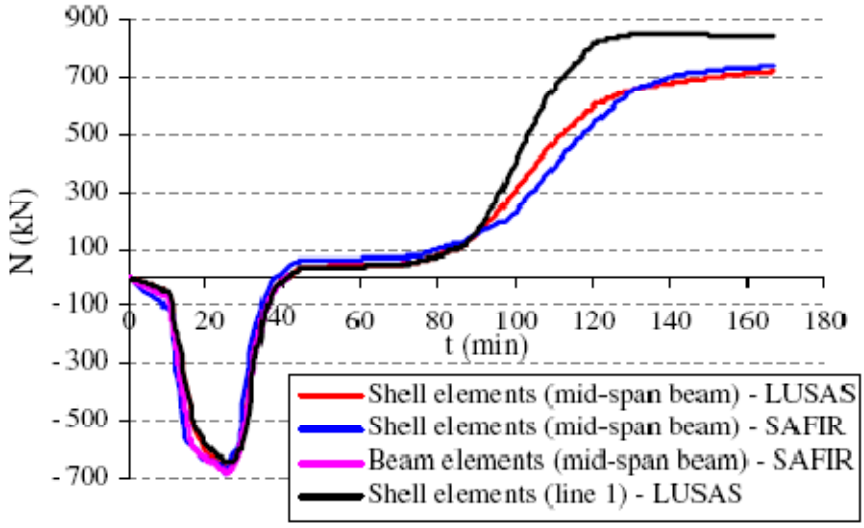

Figure 18 Development of the axial force (13)

Santiago et al. divides the behaviour of the beam into different stages. In the first stage (t < 9 min) the thermal expansion increases the axial compression and sagging moment without large displacements. In the second stage (9 min < t < 26 min) the internal forces increase rapidly. Stage three (26 min < t < 45 min) involves a decrease of the internal forces due to loss of material strength and large deflections. In the fourth stage (45 min < t < 55 min) the beam behaviour changes from bending to catenary and tensile forces are produced while the bending moments are reduced. In the last and fifth stage (t > 55 min) the cooling starts, increasing the tensile forces and hogging moments as the material recovers its strength and stiffness and the material starts to contract. It's also worth noticing that the axial force is not constant along the beam during cooling.

Santiago et al. also studied the local behaviour at the connections as well as performed a parametric study of the same reference case, but these are not presented here.

2.5.4 Moss & Bong

P.J. Moss et al. (14) and M.W. Bong (15) performed a numerical study on the fire behaviour of steel portal frame industrial buildings, as the one presented in Figure 19, with the help of SAFIR. The main purpose of the study was to explore design measures to avoid the outward collapse of the wall panels, but it also involved analysis on the cooling phase, using the Eurocode external fire curve with a decay phase, as seen in Figure 20.

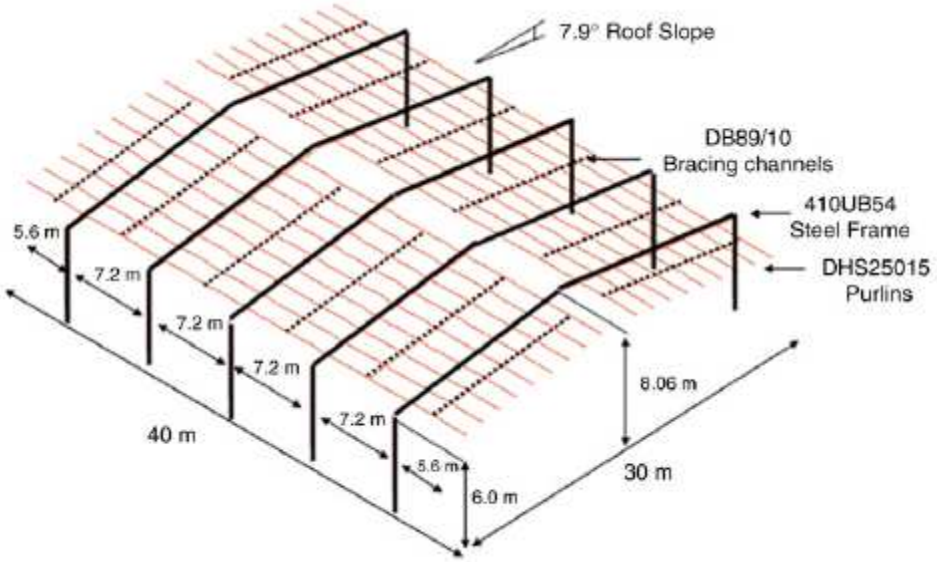

Figure 19 Portal frame industrial building (14)

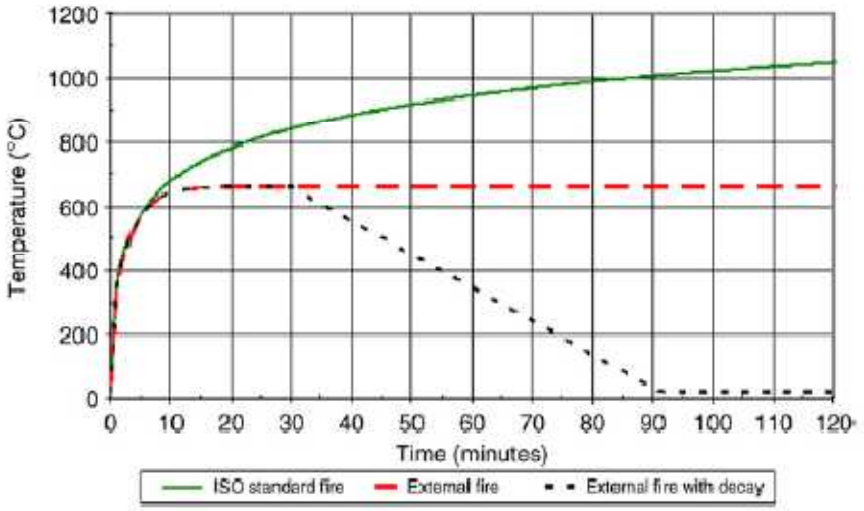

Figure 20 Time-temperature curves used in the analysis (14)

The analysis of the external fire curve with decay phase was performed assuming that the ends of the purlins where axially restrained and that the whole building was exposed to the fire. During the analysis, no collapse was observed during the 120 minutes that was simulated. In the case of the external fire without decay phase, the analysis was performed both with and without axial restraint at the ends of the purlins. The analysis showed that the building collapsed without the axial restraints, but was able to last one hour of fire exposure without collapsing when axial restraints were used.

During the first minutes of the fire, the apexes of the portal frames deflected upwards due to thermal expansion of the columns and rafters. When axial restraints at the ends of the purlins were provided, the purlins initially buckled out-of-plane due to thermal expansion, but stabilised themselves after a few minutes as the buckling was concentrated in one of the central bays. Later on the axially restrained purlins provided stability to the building through catenary action making it last longer compared to the case where no axial restraint was provided.

The purlin axial restraint forces developed during the external fire with decay phase are shown in Figure 21. From the figure the magnitude of the compressive forces developed during the first 15 minutes due to thermal expansion can be observed. After this the forces started to decrease as the temperature increased, reducing the strength of the steel and increasing the vertical displacements. When the decay phase started at 30 min, the compressive forces were reduced and became tensile as the building underwent thermal contraction and the material regained its strength. This shows that the largest forces in many connections may be developed during the decay phase of the fire. No catenary action of the purlins can however be observed from the restraint force diagram as no tensile forces are developed before the decay phase, which seems a bit unexpected as the building suffered from vertical displacements, as seen in Figure 22. The maximum temperature being quite low during the analysis (660 °C) and the fact that the vertical displacements downwards were quite small during the heating phase might have been the reasons for the absence of catenary action. Figure 22 also shows that the structure suffered from small permanent deformations after the fire.

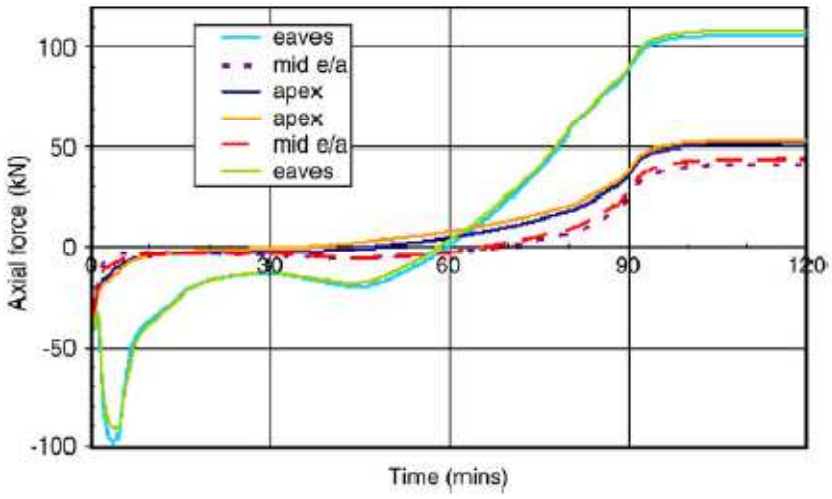

Figure 21 Purlin axial restraint forces during the external fire with decay phase (14)

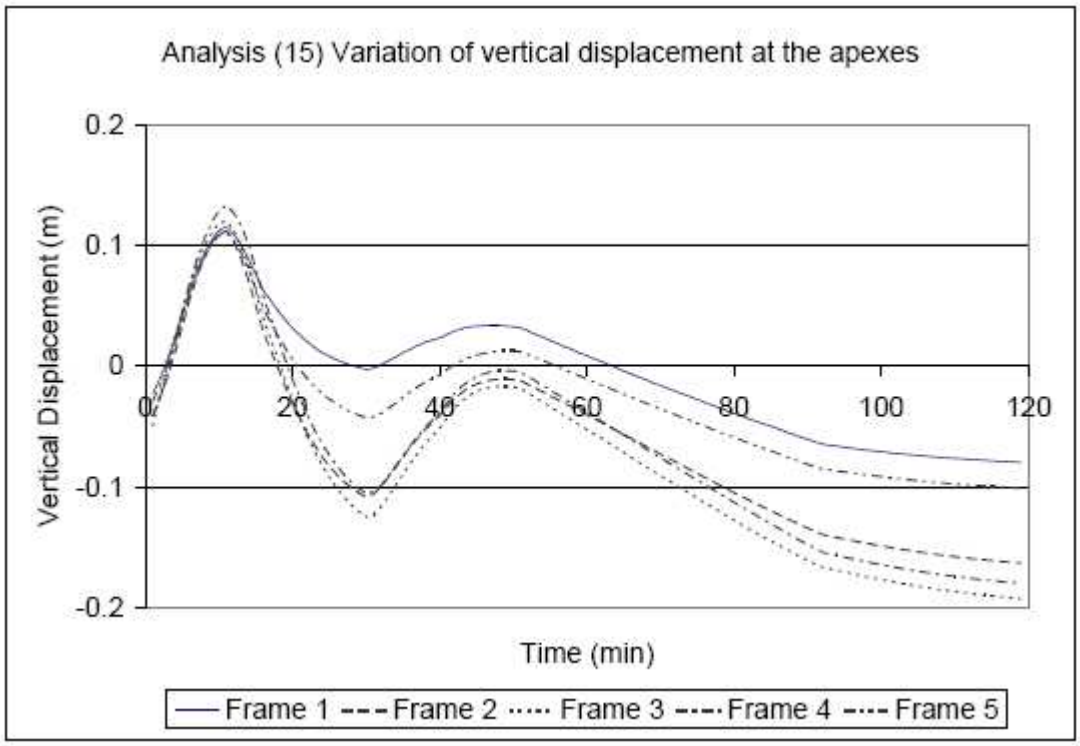

Figure 22 Variation of vertical displacement at the apexes for the external fire with decay phase (15)

2.5.5 Lu, Mäkeläinen and Outinen

Lu et al. (16) performed a numerical study on the behaviour of cold-formed Z-shaped steel purlins in fire, using a 3D finite element model with both geometric and material non-linearity made in ABAQUS/Explicit. The main purpose of the study was to achieve understanding on the failure mechanism of the purlin and how the number of spans affects the behaviour of the purlin.

The studied structure was a roof construction consisting of lightweight Z-shaped purlins supporting sandwich panels, as shown in Figure 23. The sandwich panels were screwed to the purlins, which in turn were bolted to U-shaped steel consoles welded to the supporting members. Only the internal face of the sandwich panels was considered in the analysis and was modelled as a 0,5 mm thick steel sheeting. The thickness of the purlins was 2 mm. The steel grade of both purlins and sheeting was S350GD+Z.

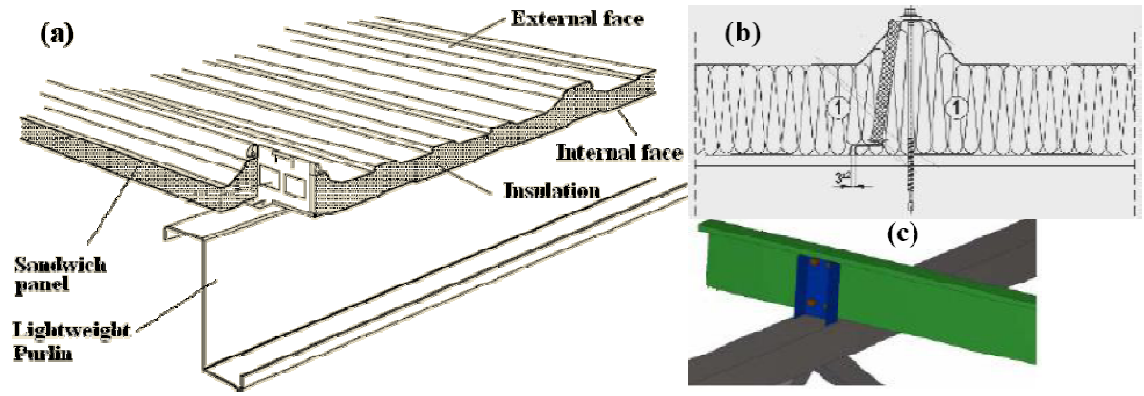

Figure 23 Studied roof structure (16)

Four different FE models were analysed; one single-span without sheeting, one single-span with sheeting, one two-span with sheeting where only one span was heated and one two-span with sheeting where both spans were heated. The length of the spans was 6020 mm. The structure was loaded by a mechanical load of 0,73 kN/m^2 and heated according to the standard fire curve in EN 1993-1-2, so that the full mechanical load was applied before the heating began.

The first model without any steel sheeting was made in order to study whether the sheeting needs to be included in the model or not, as it greatly influences the calculation efficiency. Compared to the other models where the sheeting was included, the first model suffered from large out of plane deformation very early at about 150 °C. Hence it could be concluded that the steel sheeting provided needed restraint against lateral-torsional and flexural buckling in the models and had to be included.

The development of the axial forces at the left support of the three models including the steel sheeting is presented in Figure 24. In all the models the purlins were initially in compression due to thermal expansion but then developed into tension due to the catenary action. The maximum compressive force occurred at about 120 °C, after which it started to drop due to inelastic buckling at the left support. In the two two-span models a second drop occurred at about 500 °C due to inelastic local buckling at the right support. Tensile forces were developed at 500 °C for the one-span model and at 560 °C for the two-span models as the purlins went into catenary action due to degradation of material strength and stiffness.

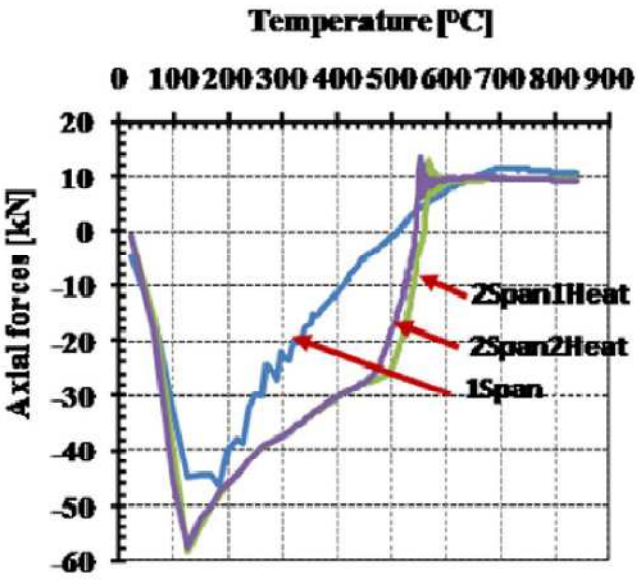

Figure 24 Axial forces developed at left support (16)

The study also incorporated a great deal of analysis on the out of plane displacements and different buckling phenomena, but this will not be discussed in any more detail here.

2.6 Tie forces

2.6.1 Tie forces according to Eurocode

In Annex A of Eurocode 1991-1-7 (17) rules and methods for designing buildings to sustain localised failure from an unspecified cause, i.e. an accident, without disproportionate collapse are given. According to section A.5 of Annex A, "each continuous tie, including its end connections, should be capable of sustaining a design tensile load of T_i for the accidental limit state in the case of internal ties, and T_p, in the case of perimeter ties, equal to the following values:"

$$for\ internal\ ties\ T_i = 0{,}8(g_k + \psi q_k)sL\ or\ 75\ kN, whichever\ is\ the\ greater$$

$$for\ perimeter\ ties\ T_p = 0{,}4(g_k + \psi q_k)sL\ or\ 75\ kN, whichever\ is\ the\ greater$$

where

g_k	characteristic self-weight [kN/m^2]
q_k	characteristic variable load [kN/m^2]
s	spacing of ties [m]
L	span of the tie [m]
ψ	relevant factor in the expression for combination of action effects for the accidental design situation (i.e. ψ_1 or ψ_2 in accordance with expression (6.11b) of EN 1990) [-]

As fire according to Eurocode is regarded as an accidental action, the effects of a localised fire can be compared to the horizontal tie forces, presented above.

2.6.2 Wald

F. Wald et al. (18) presented results from full-scale fire tests on the axial forces that are developed in the connections of the members subjected to fire, including the cooling phase, with the purpose to compare these forces with the tying forces used in design (Annex A of EN 1991-1-7: 2006) to prevent progressive collapse. The tests were carried out at Cardington, UK, in 2003 and in Ostrava, the Czech Republic, in 2006. The tests compromised complete buildings, but the results presented and used here consider mainly single beams of the buildings.

In the Cardington test flexible end plates were used for the beam to column connections and fin plates for the beam to beam connections. The steel grades ranged from S275 to S355 for beams, columns and connections and the used bolts were of grade 8.8. The columns were fire protected and the slab worked as a composite structure with the beams. Sandbags were used as the applied load and wooden cribs as fire load. Strain gauges were used to determine the axial forces in the connections during the fire. During the fire test local buckling of the lower flange of beams were observed due to axial restraint of the beams and rotational stiffness of joints, which most often is neglected in design. Compressive forces as high as 462 kN (for the beams above the fire) and tensile forces of up to 344 kN (for the beams beneath the fire) were measured during the test.

In the article F. Wald et al. did not calculate the tie forces according to Eurocode 1991-1-7 for the Cardington test. It was only concluded that the tie forces predicted by Eurocode are too small.

In the Ostrava test the beam to beam and beam to column connections were designed as simple end plate connections. The steel grade is not mentioned in the article. The steel columns were partially encased in the walls and the exposed parts were fire protected. The slab was not connected to the beams and did hence not work as a composite structure. Also here wooden cribs were used as fire load. Thermocouples, strain gauges and displacement transducers were used to monitor the structure during the fire. Deformations and lateral-torsional instability of the beams were observed during the test but no collapse occurred. Compressive forces as high as 300 kN (for the beams above the fire) and tensile forces of up to 215 kN (for the beams beneath the fire) were measured during the test.

For the Ostrava test Wald et al. compared the tie forces according to Eurocode to the measured values. The tie forces according to Eurocode were calculated to be 57 kN, meaning that the minimum value of 75 kN should be used. This was however still quite a lot smaller than the values measured in the test, hence it was concluded that the tie forces predicted by Annex A of Eurocode 1991-1-7 were too small.

In both tests the maximum forces were measured prior to the fire reaching its maximum temperature. The direction of the forces remained the same long into the cooling phase, when it ultimately changed direction (compression to tension and tension to compression) but remained small compared to the forces reached in the heating phase.

2.6.3 Horizontal forces according to "Fire Safety of Industrial Hall"

A research project was carried out by the steel industry in Europe in order to develop a design guide for single storey industrial halls exposed to ISO standard fire. The study was made for several different configurations of lengths, heights and number of bays, both for portal and lattice frames, aiming to prove that steel single story industrial buildings are safe in the case of fire without passive fire protection. (19)

The design guide deals with several aspects of fire safety for industrial buildings, but the main point of interest for the present study is the calculation of the tensile forces appearing at the top of a cold portal frame resulting from fire in the adjacent compartment, as seen in Figure 25, where the left compartment is under fire. These forces can be compared to the tie forces presented above according to Eurocode.

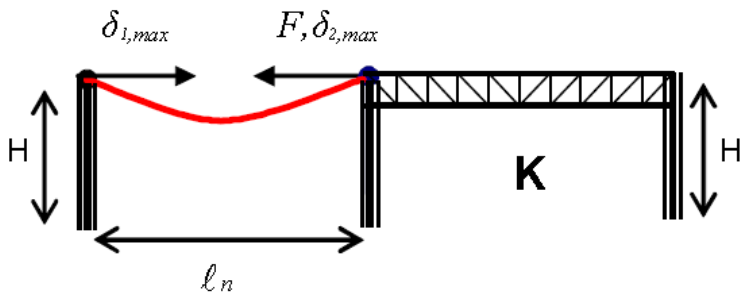

Figure 25 Tensile force acting on frame adjacent to fire compartment (19)

According to the guide the tensile force is calculated in four steps. In the first step the coefficient, c_p, related to the slope of the roof is chosen according to:

$$for\ portal\ frames: c_p = \begin{cases} 1.19\ for\ 0\ \%\ slope \\ 1.16\ for\ 5\ \%\ slope \\ 1.10\ for\ 10\ \%\ slope \end{cases}$$

$$for\ lattice\ frames: c_p = 1.45$$

In the second step a coefficient, n_{eff}, related to the number of heated bays, n, in the fire compartment:

$$for\ portal\ frames: n_{eff} = \begin{cases} 0.5\ at\ the\ end\ of\ the\ frame\ , n = 1 \\ 1.0\ in\ the\ middle\ of\ the\ frame, n = 1 \\ 1.0\ at\ the\ end\ of\ the\ frame, n \geq 2 \\ 2.0\ in\ the\ middle\ of\ the\ frame, n \geq 2 \end{cases}$$

$$for\ lattice\ frames: n_{eff} = \begin{cases} 0.6\ at\ the\ end\ of\ the\ frame\ , n = 1 \\ 1.0\ in\ the\ middle\ of\ the\ frame, n = 1 \\ 1.0\ at\ the\ end\ of\ the\ frame, n \geq 2 \\ 1.0\ in\ the\ middle\ of\ the\ frame, n \geq 2 \end{cases}$$

In step three the total vertical load, q_{tot} [N/m], which the frame is subjected to, is determined for the case of fire using the load combination coefficients defined in the corresponding national annexes.

In the fourth and last step the tensile lateral force is calculated according to:

$$F = c_p \cdot n_{eff} \cdot q_{tot} \cdot l$$

where

F	tensile lateral force [kN]
c_p	coefficient related to the slope of the roof [-]
n_{eff}	coefficient related to the number of heated bays [-]
q_{tot}	total vertical load [kN/m]
l	span of the heated bay [m]

This lateral tensile force is intended to be used as an additional horizontal load for stability check of the remaining structure. In the scope of this study the force can however as already mentioned be compared to the tie forces predicted by the Eurocode, even though the force calculated according to the design guide is only intended for multi-bay structures. By taking the n_{eff} coefficient as 1,0, and by replacing the uniform line load and span of the bay by the total load, we get the same type of formula as for the tie force in the Eurocode, i.e.:

$$F = c_p \cdot 1.0 \cdot Q_{tot}$$

where

Q_{tot}	total vertical load acting on the frame [kN]

In this formula, the only difference to the Eurocode tie force is the first coefficient, which is slightly larger according to the design guide and depends on the slope of the roof, whereas the coefficient in the Eurocode formula is 0,4 or 0,8, depending on where the tie is situated.

2.7 Conclusions on literature review

There is very little information available on the mechanical properties of steel after fire exposure, as opposed to the mechanical properties of steel during heating. J. Outinen (6) and B.R. Kirby et al. (7) however performed tests on different structural steels that had been exposed to elevated temperatures. Both studies showed largely the same results; in most cases the strength of the steel is almost unaffected, but a safe approach would be to limit the utilization after fire exposure to 90 % of the nominal yield strength. As the actual strength of structural steel nowadays usually is quite a lot larger than the nominal yield strength, for the purpose of this study, the mechanical properties of the steel can be assumed to be fully regained during the decay phase of the fire. Further research on the subject, incorporating different steel grades and temperature ranges, would of course be of great use as there is so little material available.

When studying the behaviour of a structure during the decay phase of the fire, the model for the strain reversal, taking the effects of permanent strains into account, is essential. Both linear and curvilinear models with different degree of complexity have been developed and studied (2) (3) (8) (9). There is however very little information available on the differences in implementing the different models and how well the models works. Iu et al. (8) presented a comparison of the different models, based on a numerical analysis of a simply supported beam, showing small differences in the results, but no connection to a real fire test was made. Hence, more information on this area would be valuable, even though the user seldom gets to choose the model herself/himself when it comes to doing structural analyses with the help of FEM-software, as some strain reversal model is readily included in the software.

A few different fire tests including the decay phase have been performed on different restrained beams and sub-frames consisting of columns and beams connected by different types of joints (10) (11) (12). The general behaviour in all tests was the same; as the temperature of the beam increases a large compressive force is developed in the beam due to the axial restraint. As the temperature increases further the steel loses its strength and the compressive force decreases. Next the deflection start to grow rapidly as the bending resistance is reached and the beam goes into catenary and tensile forces are developed in it. In the decay phase the temperature starts to decrease causing the beam to contract and the tensile force to increase, leaving a residual tensile force. The fire tests showed the importance of the decay phase of the fire, the studies were however only made on the behaviour of restrained single-span beams. Even though the behaviour of beams indeed is important, the behaviour of trusses remains untested.

Axially restrained beams and purlins have also been studied numerically with the help of different FEM-software, showing basically the same behaviour as the real fire tests (13) (16). This in fact means that there is not always a need to perform real fire tests, but the structure can be studied with the help of advanced FEM-software.

There is very little information available on the behaviour of steel skeleton buildings during the decay phase of the fire. Only one numerical study (14) (15) where the behaviour of a whole building was studied and where the decay phase was included could be found. The study was performed on a steel portal frame industrial building, showing that the building was able to

sustain the fire using axial restraint at the ends of the purlins. Additional studies on the topic is absolutely necessary and of great importance to gain better understanding on the global behaviour of steel skeleton buildings taking the decay phase of the fire into account, both buildings with portal frames and buildings with roof-trusses need to be studied.

The forces developed in members and connections when exposed to fire, including the decay phase, can be compared to the tie forces presented in Eurocode 1991-1-7 (17). F. Wald (18) performed such a comparison based on the results from the full-scale fire tests on restrained beams in Cardington, UK, and Ostrava, the Czech Republic, and concluded that the forces predicted by the Eurocode were much too small. The question on how to evaluate the axial forces, which in fact can be very large, developed in structural members during the event of a fire remains unanswered and would be an important topic for future research.

3 SOFTWARE

In structural fire safety design several different kinds of software are used, fire simulation software and FEM-software being the two main categories.

Fire simulation software or programs are for the purpose of structural fire safety mainly used to evaluate the temperature development of the gas or directly the structural members. The different programs range from simple one- or two zone software, such as O-Zone and CFast, to advanced field models, such as FDS. FDS is based on computational fluid dynamics and is one of the most advanced fire simulation software. It has also been thoroughly verified and validated and is continuously being developed.

FEM-software is widely used to study structures at ambient temperature, some of the most common in Finland being Autodesk Robot Structural Analysis Professional and Bentley Staad.Pro. These ambient temperature FEM-software also often offer the possibility to do a simple fire resistance analysis, generally a linear analysis based on the ISO 834 standard temperature curve and the equations presented in Eurocode. This is however not enough when the desire is to do a more comprehensive non-linear analysis with arbitrary temperature curves.

In order to truly study the behaviour of structures exposed to fire, FEM-software being able to handle both geometrical- and material non-linearity is needed. There are several general purpose FEM-software, such as Abaqus FEA and Ansys, but these suffer from being quite difficult to use and they generally do not contain the needed tools out of the package, but need a great deal of development work before the actual analysis can be performed. With the help of some kind of pre-processor purpose built for structural fire safety design, the general purpose FEM-software could prove to be very practical, but at the current state they remain out of range for everyday engineering concerning both price and usability. There are only a few FEM-software, such as SAFIR and Vulcan, developed with the purpose to analyse structures exposed to fire, but these will be dealt with below in this study.

One of the main problems, or risks, with many FEM-software is that they often work as a black box; a certain input gives a certain output, but there is very little information on how the output actually is calculated. In order to overcome this problem the theory behind the software need to be documented in great detail to enable verification and testing, otherwise the user can only choose to trust the results or not. In other words the software need to be both verified and validated properly before being put into everyday use.

Another serious risk with both FEM- and fire simulation software is that a user without the proper competence can get a certain output without knowing if the input was correct. Put in other words, there is a possibility that the user can get output he or she desires by modifying the input. This means that the complex and advanced software require competence from the user in order to ensure the correctness of the results.

Future research work could be put on integrating the different parts of the design, i.e. the ambient temperature design, the fire simulation as well as the elevated temperature design, in

order to avoid making several models of the same structure. The different FEM-softwares also need development in order to make them more efficient and to improve their usability.

3.1 SAFIR

3.1.1 Background

SAFIR is a nonlinear program, based on the Finite Element Method (FEM), developed at the University of Liege, Belgium, for the simulation and analysis of the behaviour of structures subjected to fire. It can be used to study structures in one, two or three dimensions both at ambient and elevated temperatures. Available are truss, beam, solid and shell elements as well as several material models containing the stress-strain behaviour at elevated temperatures. (20)

In the first step of the analysis, the thermal analysis, the temperature distribution of the different members is calculated. The fire exposure can be given either as the gas temperature as a function of time or as the heat flux on the surface as a function of time, based on which the software calculates the temperature of the members. (20)(21)

In the second step it may be necessary to perform a torsional analysis if using 3D beam elements for the different types of members. The result from this analysis is added to the output from the thermal analysis. (20)

The third and last part of the analysis is the structural analysis, where the behaviour of the structure under static and thermal loading is determined. In this part the results from the first two parts are used as input, along with the main input-file. This part of the analysis is performed as an iterative step-by-step procedure, where the information about the behaviour of the structure is saved for each time step until failure of the model occurs or the desired end time has been reached. (20)

In each part the input is given as text files, which has to be created either manually or with the help of some pre-processor. For simple thermal analyses the pre-processor SafirWizard is available from the University of Liege. For more general purposes the third-party pre-processor GID, developed by CIMNE (International Center for Numerical Methods in Engineering), can be used to create the input files. (20) (21)

3.1.2 Experience of usage

SAFIR was used to study the CEE industrial hall and its behaviour under fire. The model was built up by 3D beam elements as the desire was to stick to a pure bar model, without any shell elements. No pre-processor was used to create the input files, as the future purpose was to develop an interface between SAFIR and other softwares, such as FDS, in order to create the model and run the analysis automatically.

Despite intensive effort, the model kept ending prematurely and failed to simulate the whole fire scenario. Failure seemed to be caused by buckling of some member or by large strains, preventing convergence to be reached. Seeking help from J.M. Franssen at the University of Liege and altering the model made the simulation run a bit further, but it still kept failing for the same reasons. According to Franssen nobody had to his knowledge tried to analyse such a complete building with SAFIR.

3.1.3 SAFIR in literature

A. Santiago et al. (13) used both SAFIR and LUSAS, a general purpose commercial nonlinear finite element software, to study steel beams in a sub-frame for a whole fire scenario, including the decay phase. In the study SAFIR was used for two alternative analyses, using both beam and shell elements. It was noted that the decay phase could not be studied with the analysis using only beam elements, as the model became numerically unstable even before the maximum temperature was reached. However, the analyses using shell elements performed with SAFIR and LUSAS showed good agreement in results.

On the other hand, P.J. Moss et al. (14) used SAFIR to study a part of a steel portal frame building. By discretizing the portal frames into beam elements, they succeeded in studying the complete fire scenario, including the decay phase, despite of large deflections. Hence, in that case there was no need to use shell elements in order to be able to study the decay phase, leaving the question of why SAFIR did not perform well in this study open.

O. Vassart et al. (22) performed a benchmark comparison of three different FEM programs; ANSYS, ABAQUS and SAFIR. The benchmark consisted of a single story steel portal industrial hall subjected to ISO fire, for which the analysis was carried out both in two and three dimensions. For the three dimensional case both a static and dynamic analysis was made, as only the dynamic analysis was able to handle post local failure. The comparison showed that the three programs give close results. It's not directly stated, but the structure seems to have been studied using beam elements, again indicating that SAFIR at least for simpler cases should be able to handle post local failure and large deflections using beam elements.

3.2 Vulcan

3.2.1 Background

Vulcan is a commercial Finite Element Analysis (FEA) software developed at the University of Sheffield in the United Kingdom, to be used for studying buildings in the case of fire, taking into account the whole structure as well as both geometrical and material non-linearity. It can deal with steel beam-column elements and concrete slabs, as well as the composite effect between steel members and concrete slabs in three dimensions. Standard stress-strain curves and full thermal expansion characteristics, defined as functions of temperature for both uniform and non-uniform temperature distributions, are included in the material models for both steel and concrete. The results have thoroughly been validated against test data, including the results of the large scale fire tests performed at Cardington, UK. (23)

The structural model is made up of finite beam-column, spring, shear connector and slab elements. 3-noded line elements are used to represent the beam-columns and the cross-section of the elements is divided into segments, allowing the temperature, stress and strain to vary in the cross-section. Steel-steel connections are represented by a 2-noded spring element of zero length with the same number of nodal degrees of freedom as the beam-column elements. If a composite floor is modelled, the interaction between the steel beams and the concrete slabs is represented by a 2-noded shear connector element of zero length with three translational and two rotational degrees of freedom at each node. (23)

Vulcan can also deal with the geometric non-linearity of the concrete slabs, by modelling the slab as layers of concrete and steel. Cracking and crushing are also taken into account in the analysis. (23)

Vulcan is developed aiming at simplicity and high speed of use, taking advantage of a graphical user interface. The geometry of the structure and other inputs are created with the help of the graphical user interface, making manual creation of input files unnecessary in most cases. It is also possible to import models from CAD. The results are also presented graphically. (23)

Detailed information on the creation of the Vulcan input file and on how structural information can be exported from Tekla Structures and temperature data from FDS to Vulcan will not be presented here, but is given in Appendix A as it doesn't form a crucial part of this study.

3.2.2 Learning process

3.2.2.1 Visit at the University of Sheffield

In order to complete the research work a powerful tool for analysing steel structures exposed to fire, including the decay phase of the fire, was needed. After trying to use Safir without success, it was decided to turn to the finite element analysis software Vulcan, developed at the University of Sheffield in the United Kingdom. To be able to efficiently learn and study the software it was necessary to visit the University of Sheffield, where Professor Ian Burgess and Dr. Florian Block from Buro Happold assisted in the learning process. During the visit mainly one type of building was studied, a one storey industrial hall with an all steel skeleton made up of columns, beams, roof trusses, purlins and diagonals. This type of building was chosen as it is widely used for industrial halls, but no design rules for the decay phase of the fire are available.

3.2.2.2 Completion of visit

The learning process was started by studying the basics of Vulcan in Finland before leaving for Sheffield. After arriving in Sheffield the target was discussed with Professor Ian Burgess, who suggested a way of working towards the goal. First of all one frame including columns and a roof truss was modelled in Vulcan and studied both at ambient and elevated temperatures. The results at ambient temperature were compared to a Robot Structural Analysis Professional 2011 model, showing good agreement between the models. Also the analyses at elevated temperatures showed promising results, up to the point of buckling, and high usability of Vulcan. Whenever a problem occurred Professor Ian Burgess helped solving it. At no time the calculation times for Vulcan were unreasonably long.

Dr. Florian Block aided mainly in the practical usage of Vulcan and gave some valuable tips about how to configure the models and how to overcome some usual problems.

The next step in the process was to go in the third dimension adding purlins and several frames to the model. This of course added to the complexity of the model and also the calculation times grew substantially. Also this model was analysed at ambient temperature and compared to a Robot model, and again the models showed very good agreement, the difference being within ten percent. For the three dimensional models at elevated temperatures the calculation times grew substantially and problems with convergence occurred.

The main problem to overcome seemed to be getting the analyses run beyond buckling. When buckling happens the structure becomes unstable and it gets numerically difficult for the software to solve the equations, hence the analysis fails to converge. The normal version of Vulcan does not contain a dynamic solver, but there is a research version begin developed that does contain a dynamic solver, which should make it possible to continue the analysis beyond buckling. However, the research version does not at this point seem as a realistic approach for engineering work as it does not have any graphical pre- or post-processor and is yet to be validated, but may well prove useful in research work.

Another way of overcoming the problem with buckling suggested by Block and Burgess would be to run a first analysis of the complete model until one member buckles, then remove that member from the model and run the analysis again from the beginning. The buckled member can be removed as it does not carry any substantial load anymore and does not contribute to the stiffness. In the second analysis the model would behave differently until the point where the removed member had buckled in the first run, but would quite well simulate the situation after the removed member would have buckled. This second analysis would then be run until the next member buckles, which would then be removed from the model and a third analysis would be performed. This would then be continued until the maximum temperature and final state of the structure during the heating phase is reached. By combining the deflection- and force curves from the subsequent analyses so that each analysis contributes to only a part of the whole behaviour, the real situation including buckling can be studied. The problem with this approach is how to deal with cooling. The deformed members regain their strength and start carrying load, so at some point it would be necessary to include them in the model again. This is however quite difficult as it is not possible to know what their deformed shape would be and at what point they should be included in the model again.

A small discussion was also held with Professor Roger Plank from the University of Sheffield about the targets of the research. During this and several other discussions with Professor Ian Burgess the importance of the stiffness of the building became quite clear. Especially the horizontal stiffness of the building will greatly affect what kind of forces will develop during the decay phase of the fire. If the horizontal stiffness of the building is small, it is not likely that any substantial forces, which would have to be taken into account in the design of the building, will develop in the decay phase. However if the horizontal stiffness is large, e.g. in the case when there is a concrete slab on top of the steel members in a composite structure, substantial forces that would have to be taken into account in the design of the building will most probably develop in the decay phase of the fire.

3.2.2.3 Accomplishments during the visit

During the visit a quite good understanding of the usage of Vulcan and its' possibilities in fire engineering was achieved. Furthermore the discussions about the problems of the decay phase of the fire were very educational and valuable, giving a good idea on what to focus on and where efforts should be put in order to gain usable information from the research. Especially the stiffness of the structure proved to be very important and ways of studying it was discussed.

3.2.2.4 Future advantages and co-operation

During the visit it was agreed that the co-operation would be continued through e-mail discussions, by sharing information and taking advantage of possible synergy effects from the different research projects going on in Sheffield and Tampere. Professor Ian Burgess and Professor Roger Plank showed great interest in the ongoing research work on the effect of the decay phase of the fire on steel and composite structures and stated their interest in maintaining contact throughout the project. Dr. Florian Block also promised to help out with the usage of Vulcan by e-mail contact.

3.2.3 Analysis test

Test analyses were performed on a CFRHS100x100x5 beam with a length of 2000 mm and steel grade S355 in order to check how Vulcan performed under various loading cases and boundary conditions. The analyses were mainly performed at ambient temperature but some tests were also made at elevated temperature, using both the Eurocode and Ramberg-Osgood material models.

Generally there was no significant difference between the results from the analyses at ambient temperature using the two different material models. However, at elevated temperature the analyses using the Eurocode model seemed to give larger internal forces and deformations, which is natural due to the difference in material models.

Under pure compression Vulcan limits the load to the Euler critical buckling load according to (24):

$$N_{cr} = \frac{\pi^2 \cdot EI}{(KL_c)^2}$$

where

N_{cr}	Euler critical buckling load [N]
E	modulus of elasticity [N/mm^2]
I	second moment of area [mm^4]
K	column effective length factor [-]
L_c	unsupported length of column [mm]

In pure tension Vulcan limits the load according to the yield strength of the beam and in pure bending according to the plastic bending resistance. It however seems as shear and torsion are not checked for properly, the beam did not fail in such load cases, but as shear and torsion seldom are critical, especially for roof trusses, this should not pose any larger problem or affect the analysis. The combined effect of normal forces and bending moments seem to be dealt with properly.

4 CASE STUDY – CEE HALL

The main object of study is the all steel CEE-Hungary hall by Ruukki, as seen in Figure 26, operating as a warehouse. (25)

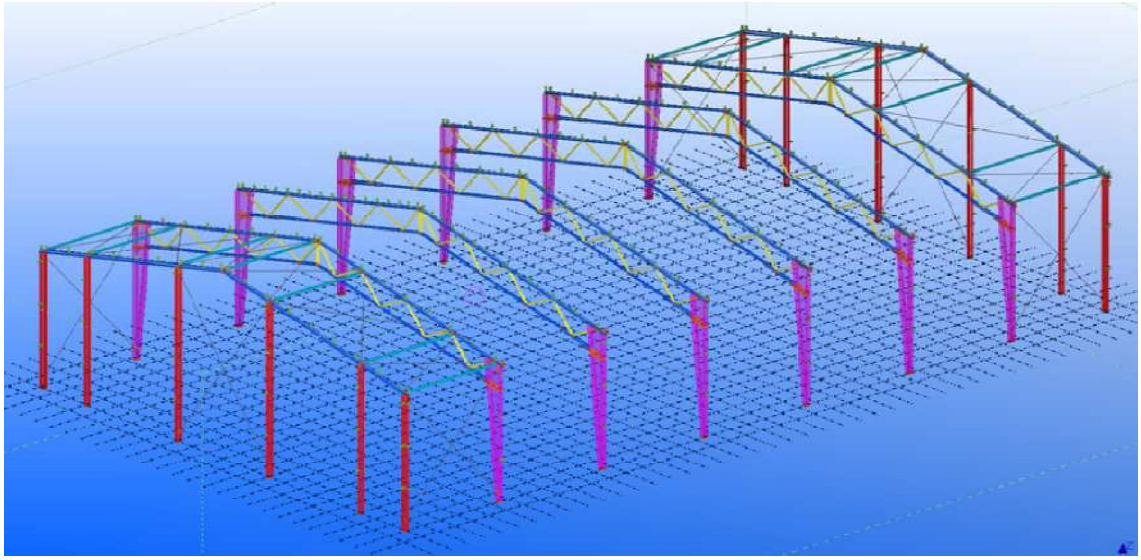

Figure 26 CEE hall (25)

The hall consists of 6 frames with a span of about 24 m as well as end columns and edge beams. The spacing between the six frames is 6 m and the distance from the last frames to the ends of the building is 5,5 m, making the total length 41 m. The height of the building varies from about 6,5 m to 8,8 m. The main frames consist of columns, made of welded trapezoidal unsymmetrical I-profiles, and roof trusses made of cold-formed rectangular hollow section (CFRHS) tubes. The end columns are IPE profiles and the edge beams cold-formed rectangular hollow section (CFRHS) tubes. The bracing at the walls and roof are steel wires. The walls and roof are light weight steel structure and the roof purlins are Z profiles. The steel grade of all structural members is S355. (25)

The main frame of the CEE hall can be seen in Figure 27 along with dimensions and truss profiles. (25)

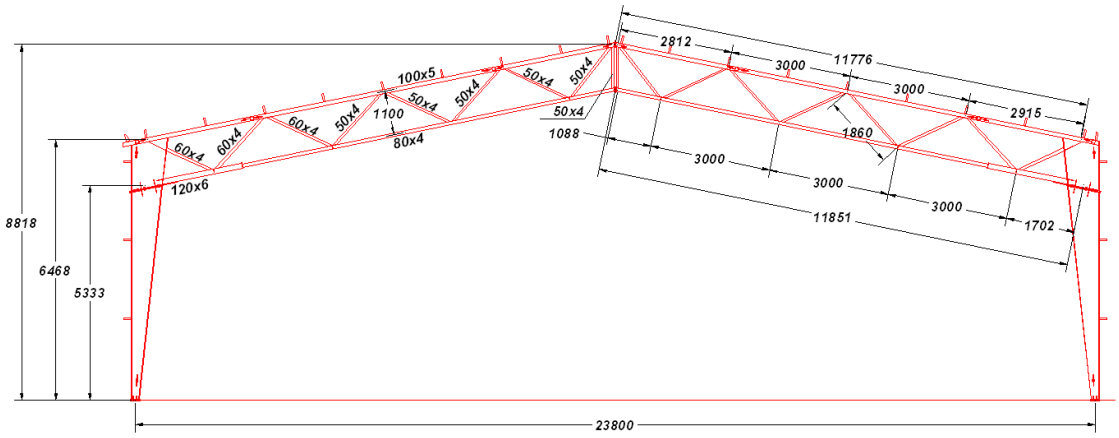

Figure 27 Main frame (25)

In the structural analysis the model is simplified by removing all eccentricities, replacing the main columns with IPE profiles, the bracing with CFRHS tubes and the purlins with CFRHS tubes. The profiles of the structure can be found from Figure 28. (25)

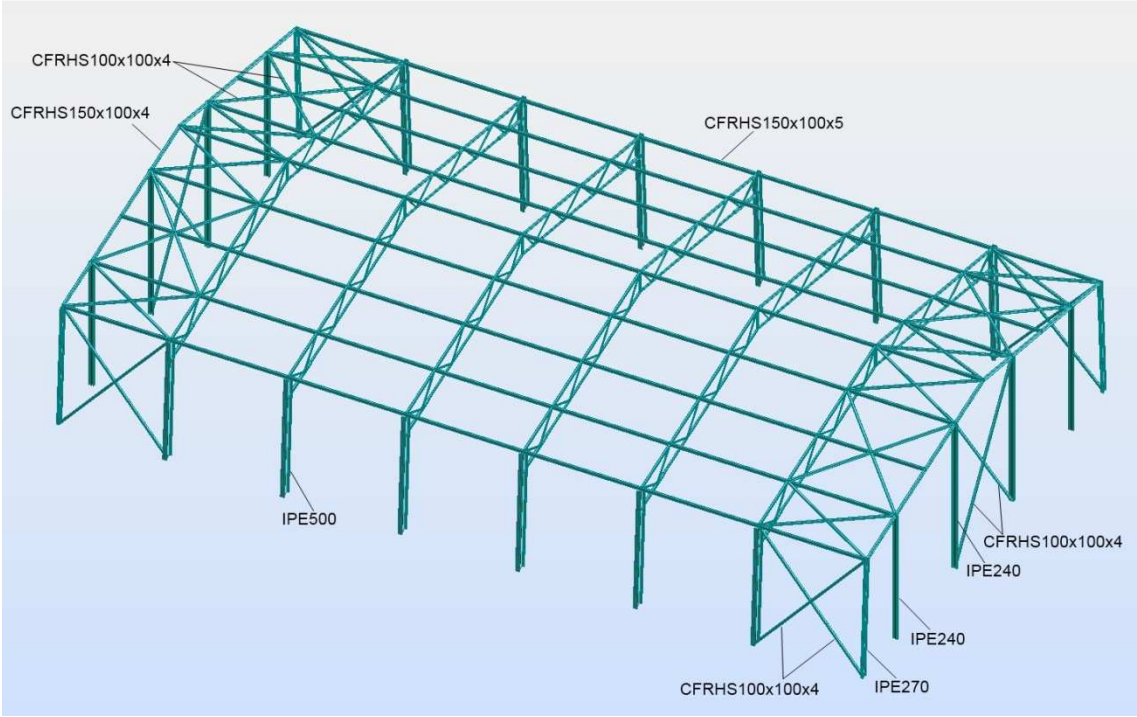

Figure 28 Profiles of structural analysis model

The structure is subjected to a dead load of 0,4 kN/m on the purlins, a snow load of 1 kN/m^2, corresponding to a uniform vertical load of 1,5 kN/m on the purlins, as well as a wind load of 0,50 kN/m^2 acting on the walls. In the case of fire the most critical load combination involves the characteristic dead load with a combination factor of 1,0 as well as the snow load with a combination factor of 0,4, giving a total uniform vertical line load of 1 kN/m on the purlins. (25)

4.1 Tie forces according to Eurocode

The internal tie force for the main frame of the CEE-hall is calculated according to Eurocode as follows:

$$T_i = 0{,}8(g_k + \psi q_k)sL = 0{,}8\left(\frac{0{,}27kN}{m^2} + 0{,}4 \cdot \frac{1kN}{m^2}\right) 6m \cdot 24m = 77{,}2kN$$

$$or\ 75kN, whichever\ is\ greater$$

Hence, the horizontal force that the frame has to withstand is 77 kN.

4.2 Development of analysis model

The following initial analyses were performed in order to develop the analysis model and to determine where the effort to study the structure in more detail should be put. All the analyses were performed using the smoothed Ramberg-Osgood material model for steel.

4.2.1 2D main frame analysis at ambient temperature

A two dimensional model of one main frame, where the out of plane deformations were restricted, was made and analysed linearly with both Vulcan and Autodesk Robot Structural Analysis Professional 2010 to enable a comparison between the results of the two different software. The frame was subjected to 17 point loads of 6 kN each, corresponding to the loads transferred from the purlins, as seen in the screenshot from Vulcan in Figure 29. Fixed connections were used at all joints except the base connections of the columns, which were hinged but restrained against torsion. This solution was chosen as it is quite similar to the real situation with a welded truss and rather stiff connections, furthermore the analysis becomes much easier for Vulcan to solve.

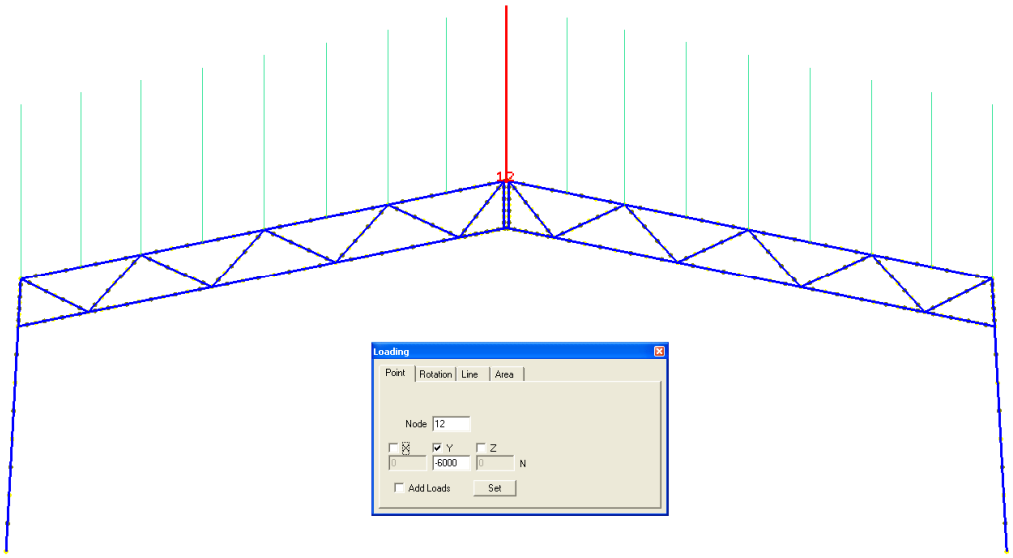

Figure 29 2D frame, 6 kN point loads

In the Vulcan model each member was divided into four finite elements and each cross-section was divided into 10x10 elements.

The maximum displacement at mid span was 26 mm in both models, showing great agreement between the results. The support reaction according to Vulcan was 51 kN in the vertical direction and -25,2 kN inwards in the horizontal direction. Robot gave the same value for the vertical reaction and a slightly bigger value of -25,8 kN for the horizontal reaction. Also the member forces were very similar in the models, verifying the accuracy of the Vulcan model.

4.2.2 3D main frame analysis at ambient temperature

The 3D frame analysis was performed in the same way as the 2D analysis, the only difference being that the out of plane deformations weren't restricted. The frame was laterally supported only at the top chord at the points where the purlins would be connected, at the columns where the bottom chords were connected, at mid-span where the bottom chords are connected as well as in the middle of the bottom chords where there would be lateral supports in the real structure.

The results from the 3D frame analysis did not differ from the corresponding 2D analysis. This was of course due to the fact that the load level at ambient temperature was so low that essentially no out of plane deformations, which would influence the behaviour of the frame, took place.

4.2.3 2D main frame analysis at elevated temperature

The same model, restricted against lateral deformation, as in the 2D main frame ambient temperature analysis was exposed to the temperature curve in Figure 30 with a maximum temperature of 600 °C and analysed non-linearly in Vulcan. The temperature of the steel was set to directly follow the temperature curve using the uniform temperature pattern in Vulcan, i.e. no lag in the temperature increase was taken into account.

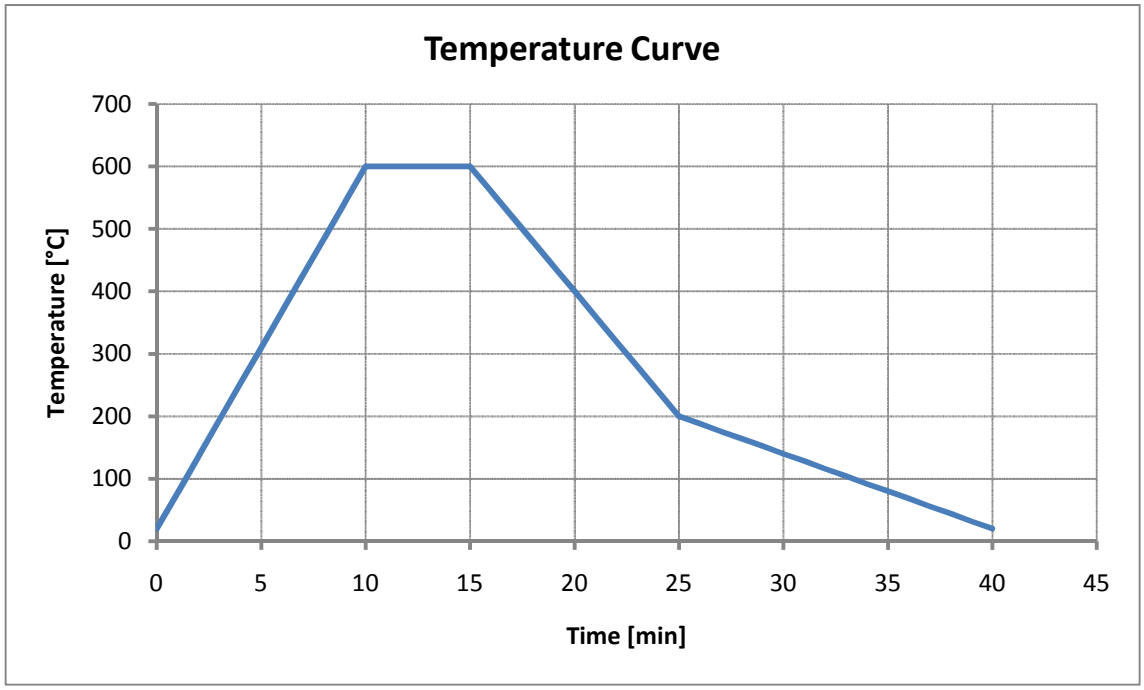

Figure 30 Steel temperature curve, maximum of 600 °C

The vertical deflection of the top node of the main frame can be seen in Figure 31. From the figure it can be seen that at first the node deflected downwards due to loading but then

started to deflect upwards due to thermal expansion. The final deflection after 40 minutes, when the temperature had gone back to 20 °C, was only slightly larger, 0,13 mm, than at the beginning of the analysis. This very small difference may be considered to be within the accuracy of the analysis model.

The horizontal force at the right base connection can be seen in Figure 32. From the figure it can be seen that the force increased in the heating phase but decreased back to the original value in the decay phase of the fire.

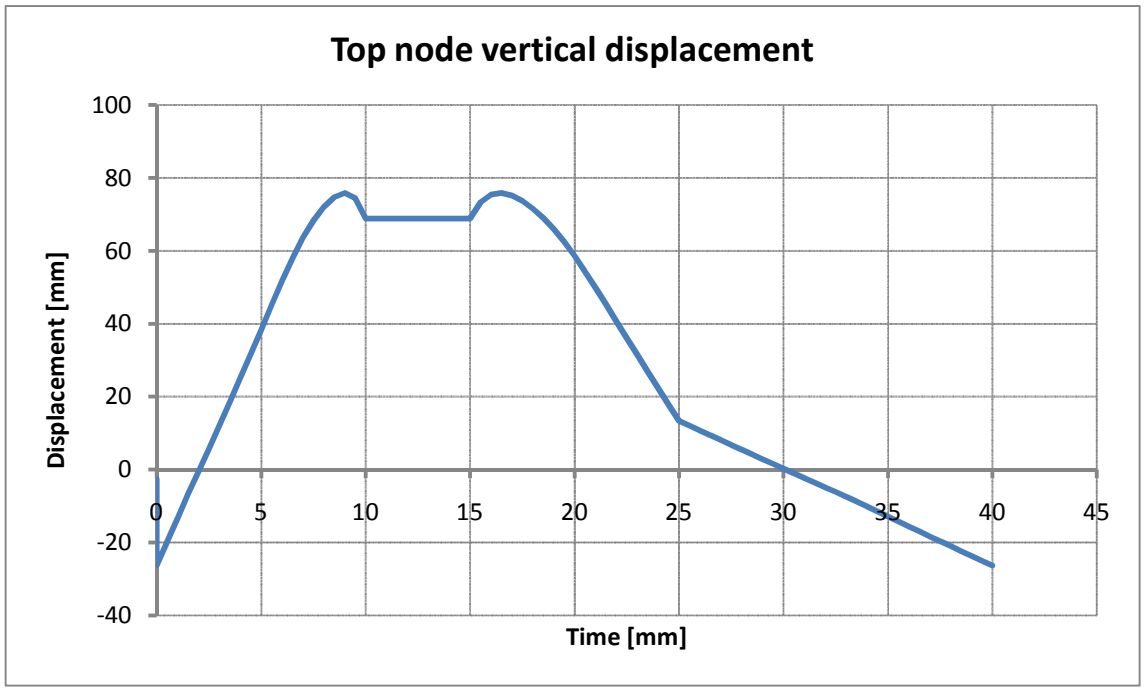

Figure 31 Vertical displacement at top node

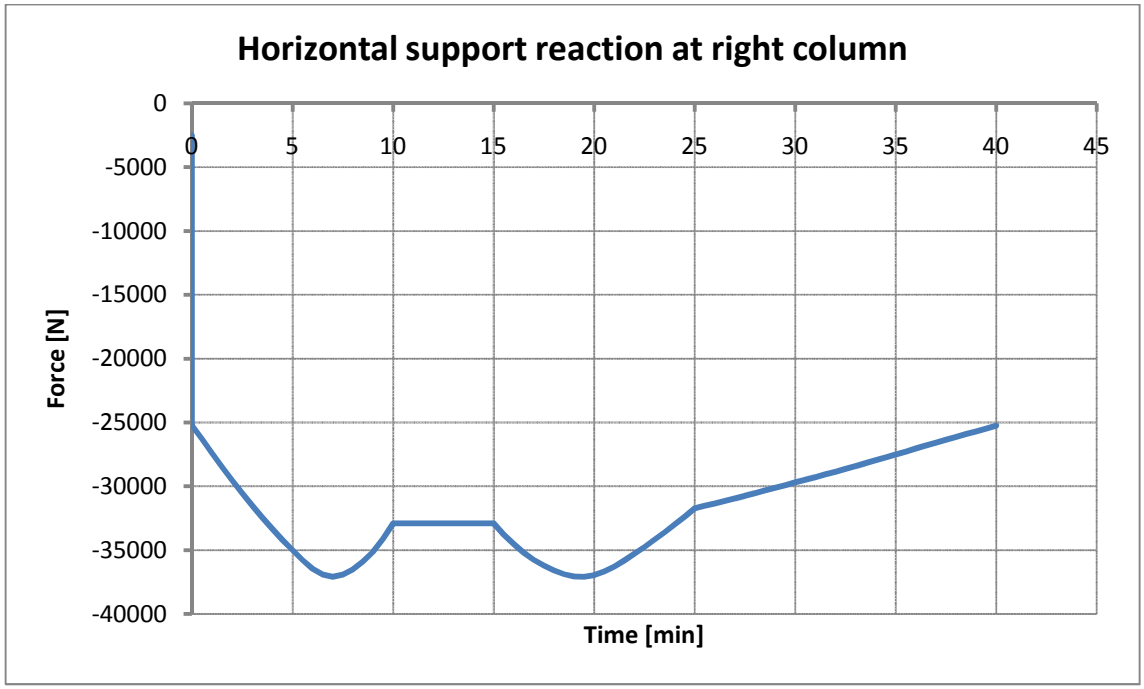

Figure 32 Horizontal support reaction of the base connection

The reason for the "valleys" in the displacement and force diagrams was that the structure had begun to deflect downwards at about 7 minutes as the steel started losing its strength due to the increasing temperature. Basically the beginning of a runaway phenomenon, where the structure deflects rapidly, could be seen. At the same time and for the same reason the horizontal support reaction was decreasing between 7 and 10 minutes. The reverse could be noticed when the temperature began to decrease back to ambient value.

As neither the deflections nor the forces at the end of the analysis differed from the values at the beginning, it could be concluded that no permanent deformations had taken place due to the temperature exposure.

4.2.4 2D main frame analysis at elevated temperature, fixed supports

The same model as in the previous section was also analysed with fixed base connections and exposed to the same temperature curve with a maximum of 600 °C.

The vertical deflection at the top node can be seen in Figure 33. From this figure it can be observed that the frame basically behaved in the same way as the frame with pinned base connections, except that there is no "valley" in the graph, i.e. no runaway of the deflection had begun. The initial displacement was smaller and the maximum deflection was much bigger than in the case of the pinned base connections. The reason for this was of course that the frame had a much higher degree of restraint when the base connections were fixed. This restraint also led to a permanent increase of the deformation at the top node of 10,3 mm downwards, compared to the initial loaded state.

The horizontal support reaction of the right column is presented in Figure 34. As for the vertical displacement it can be seen that the general behaviour was the same as in the case with pinned base connections, but the forces were substantially larger. Also here the permanent deformation can be observed, as the final horizontal support reaction was 25,1 kN smaller than before the temperature exposure. Here it can also be noticed that the force had begun to decrease at about 7 minutes as the strength of the steel started to degrade, as was the case in the frame with pinned base connections.

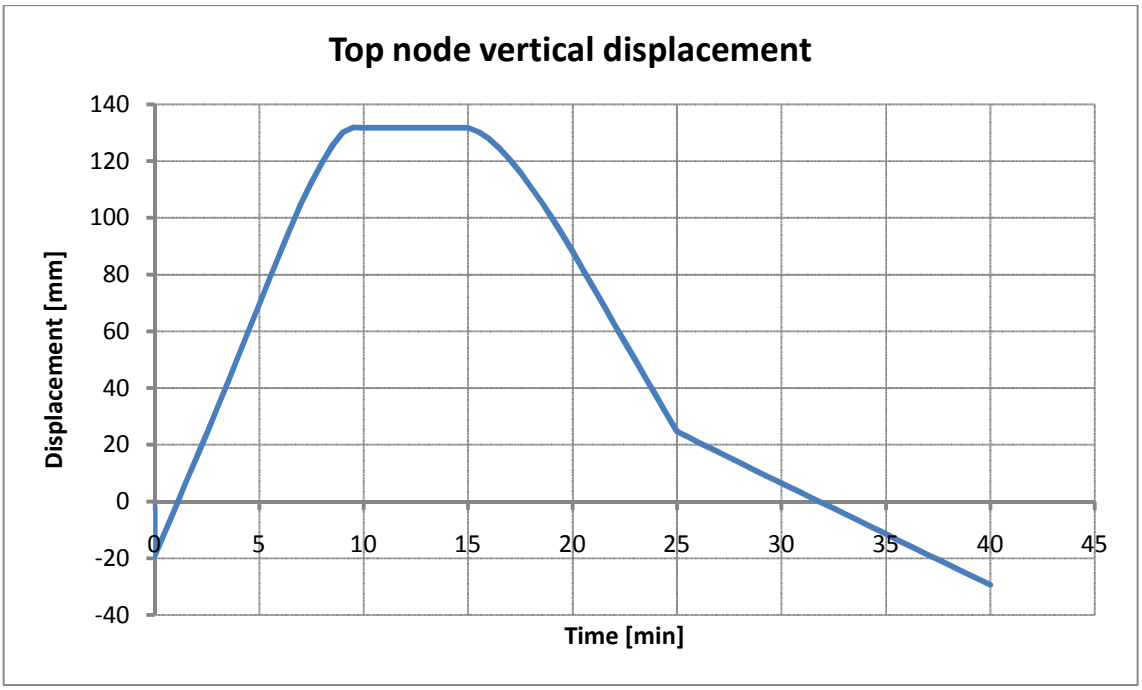

Figure 33 Vertical displacement at top node

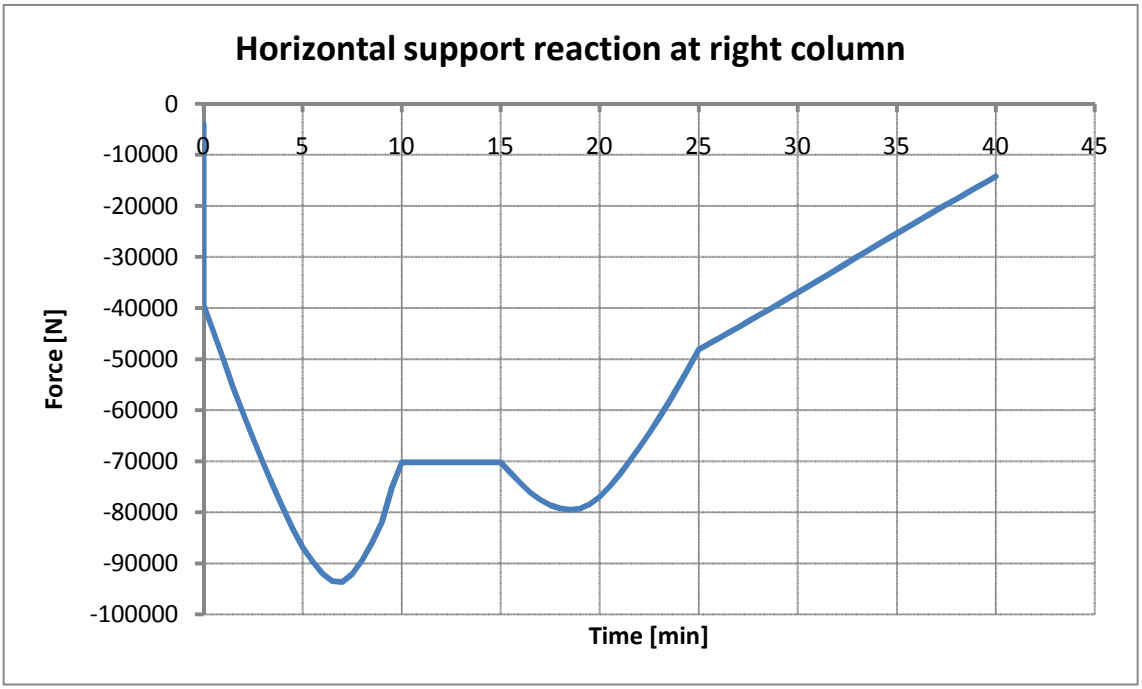

Figure 34 Horizontal support reaction of the base connection

The shape of the loaded main frame with fixed supports before the temperature exposure can be seen in Figure 35, where the deformations are scaled with a factor of 20. The shape of the frame after temperature exposure is shown in Figure 36, from where the permanent deformation can be observed.

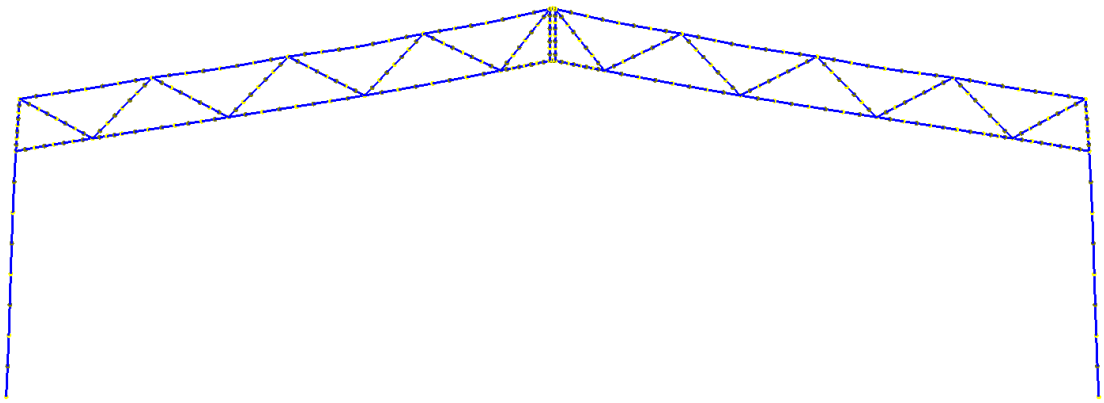

Figure 35 2D main frame with fixed supports before fire

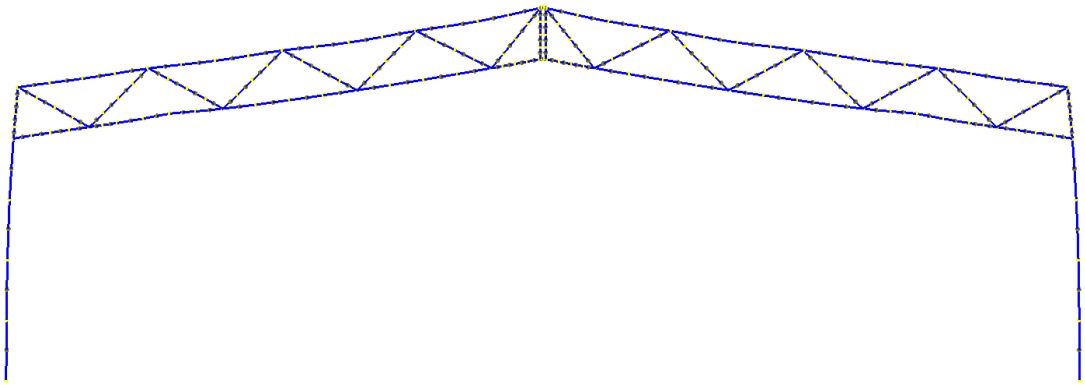

Figure 36 2D main frame with fixed supports after fire

The results from the analysis clearly showed the importance of the degree of restraint on the structure; a higher degree of restraint leads to larger forces and can hence also cause permanent deformations at an earlier stage than for the case with a lower degree of restraint.

4.2.5 3D main frame analysis at elevated temperature

The 3D model of the main frame was also analysed non-linearly in Vulcan exposed to the same temperature curve as in the 2D model, with a maximum temperature of 600 °C.

The vertical deflection at the top node is presented in Figure 37 and the horizontal support reaction in Figure 38. From the figures it can clearly be seen that the frame behaved exactly in the same way as in the 2D case.

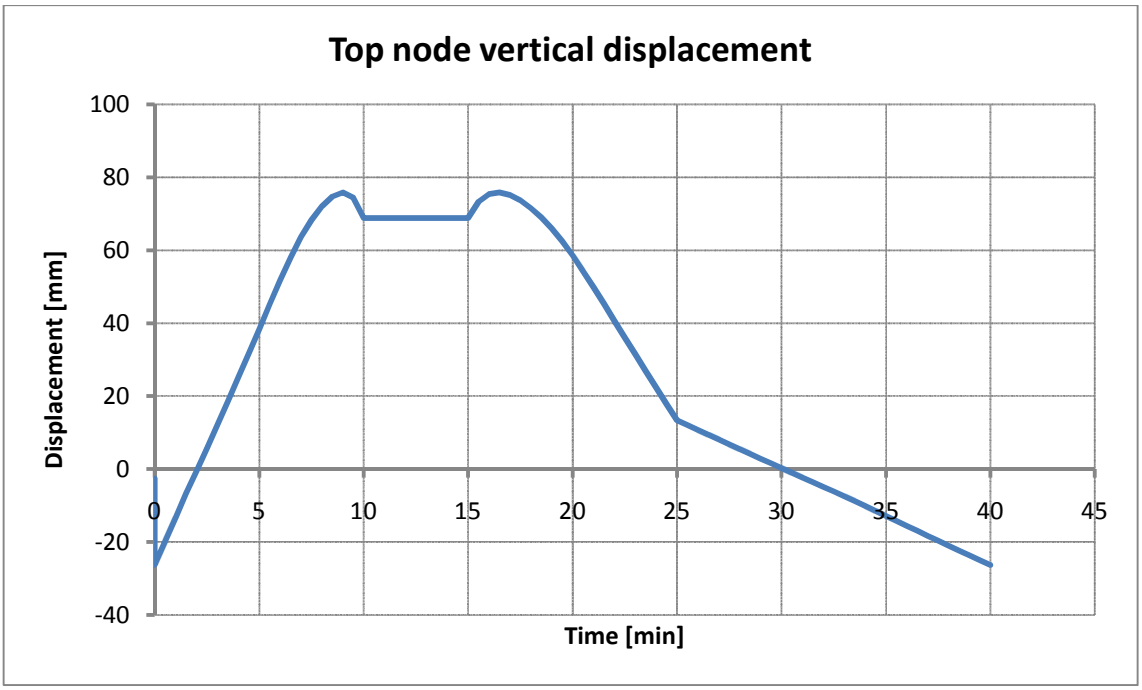

Figure 37 Vertical displacement at top node

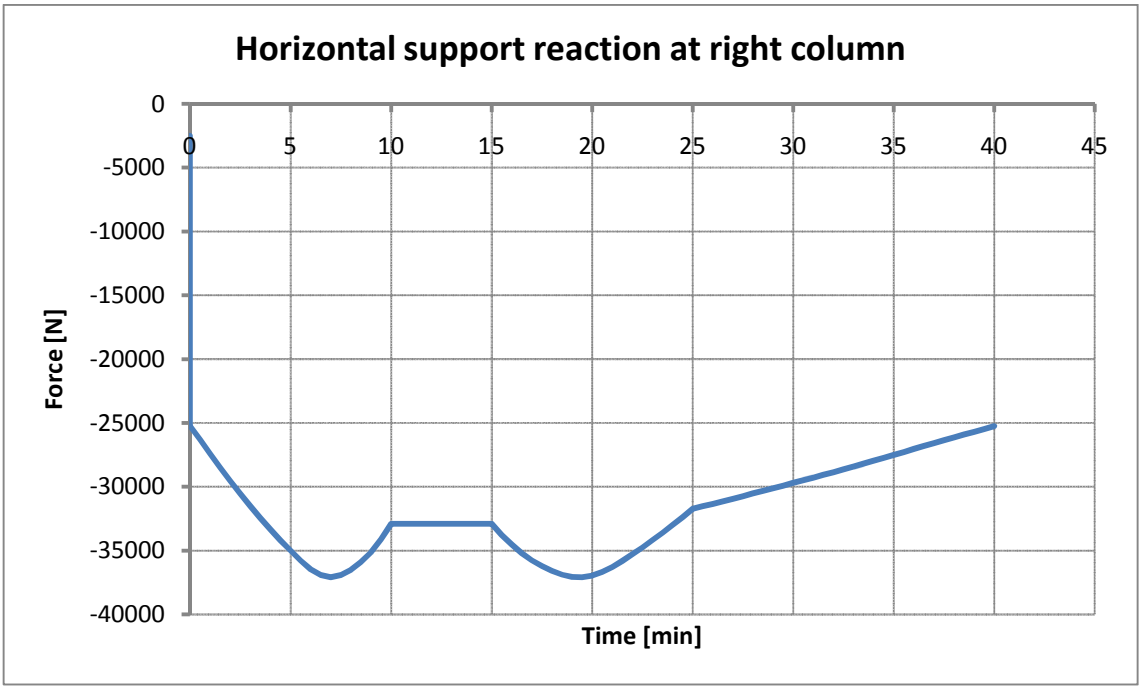

Figure 38 Horizontal support reaction of the base connection

The results from this analysis showed that the load level was so low that the temperature exposure up to 600 °C did not affect the integrity of the structure nor did any lateral deformations take place.

4.2.6 3D main frame analysis at elevated temperature, fixed supports

The 3D model was also analysed with fixed base connections and exposed to the same temperature curve as above, with a maximum temperature of 600 °C.

The vertical deflection of the top node can be seen in Figure 39. As for the 2D frame with fixed base connections, there is no clear valley in the displacement graph, i.e. no runaway had taken place in the heating phase. The permanent increase of the deformation of the top node was 10,2 mm downwards.

The horizontal support reaction of the right column is presented in Figure 40, showing great agreement with the corresponding 2D frame. Also in this case the final horizontal support reaction was smaller than before the temperature exposure, the difference being 25,1 kN.

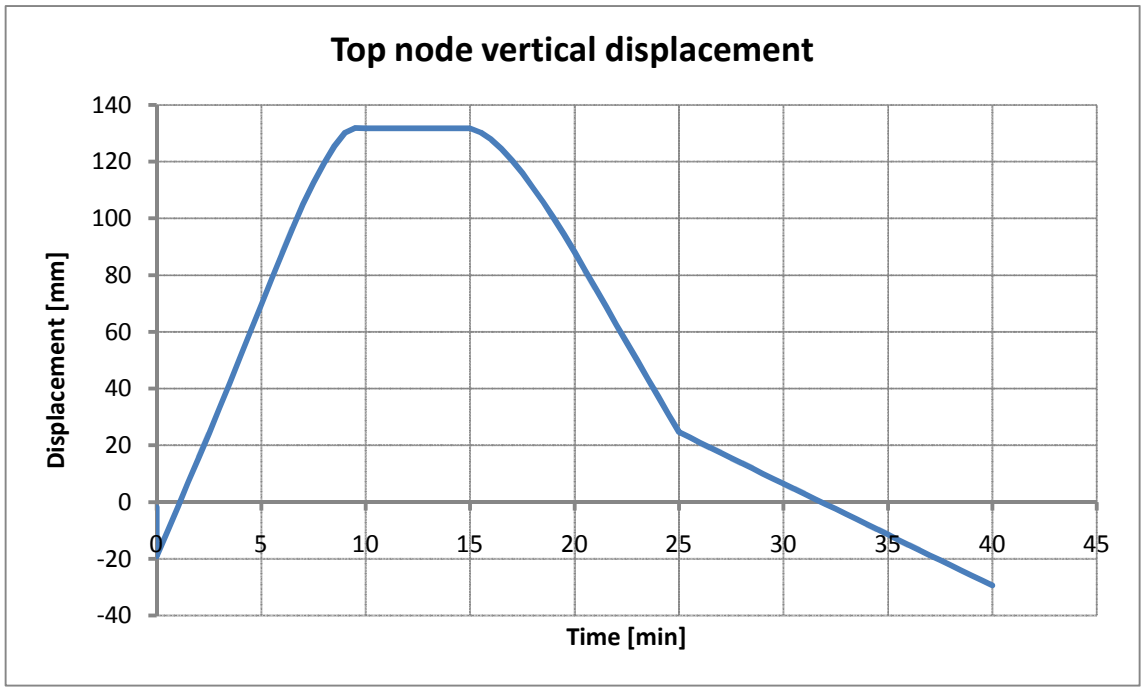

Figure 39 Vertical displacement at top node

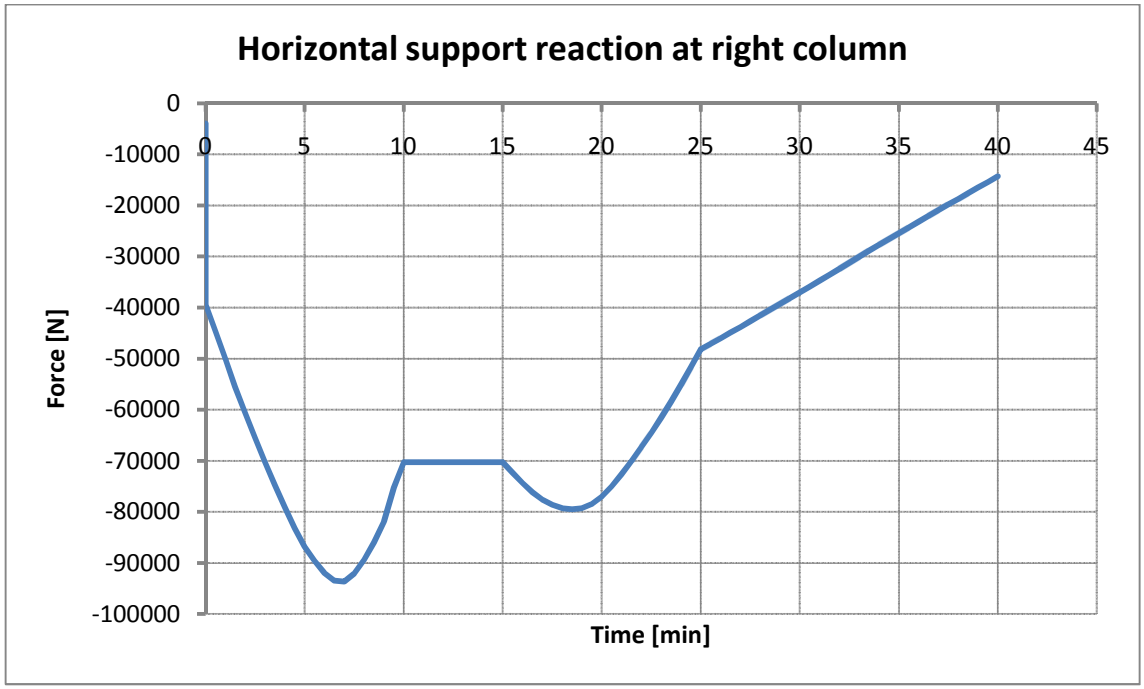

Figure 40 Horizontal support reaction of the base connection

The results from this 3D analysis showed that the structure behaved very much in the same way as in the case of the 2D frame with fixed base connections. This means that even with fixed base connections a temperature exposure of 600 °C does not pose any problems for the structure, but as for the corresponding 2D case it shows the importance of the degree of restraint.

4.2.7 3D main frame analysis at elevated temperature, Eurocode temperature pattern

The 3D main frame with pinned base connections was also analysed using the inbuilt Eurocode temperature pattern in Vulcan, i.e. the temperature development of the steel was calculated according to Eurocode with the help of the section factors, based on the same temperature curve as above. In this case the temperature of the different members, with different cross-sections, varied depending on the section factors. In the analysis the coefficient of heat transfer by convection, α_c, was 25 W/m^{2}K, whereas the correction factor for the shadow effect, k_{sh}, the emissivity of the fire, ε_f, and the configuration factor, Φ, were all taken as 1. The surface emissivity of the member, ε_m, was 0,7. The temperature of the top chord can be seen in Figure 41, from where it can be noticed that the maximum temperature of 550 °C naturally was lower than the 600 °C in the previous cases, where the steel temperature was assigned to follow the temperature curve.

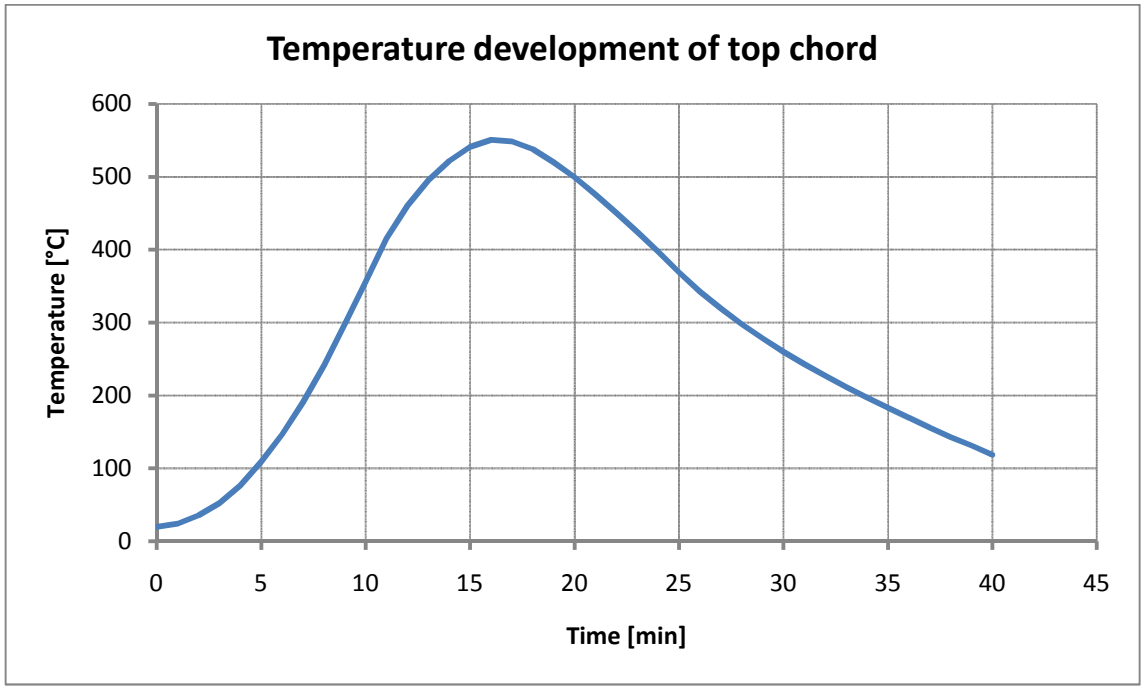

Figure 41 Steel temperature development of top chord

The vertical displacement at the top node up to 40 minutes can be seen in Figure 42. From the figure it can clearly be seen that the maximum displacement of 75 mm was only marginally smaller than in the case using the uniform temperature pattern in Vulcan, giving a displacement of 76 mm. Hence, even though the temperature of the top chord was lower using the Eurocode temperature pattern, the vertical displacement was essentially the same in both models. The reason for this was that the temperature of the large sections (IPE500) of the columns increased slower than the rest of the structure, due to the smaller section factor of the

columns, causing the material of the columns to retain more of its stiffness than the trusses, leading to a higher degree of restraint on the truss.

The horizontal force at the right base connection of the frame can be seen in Figure 43, from where it can be noticed that the maximum force actually was larger than in the case using a uniform temperature pattern. The reason for this is the same as for the displacements, i.e. the larger restraint provided by the columns, also causing the horizontal shear forces to grow larger in the columns. This is confirmed by Figure 44, from where it can be seen that the horizontal displacement at the top right corner of the frame was smaller using the Eurocode temperature pattern, and by Figure 45, from where it can be observed that the horizontal force at the right end of the top chord was substantially larger using the Eurocode temperature pattern.

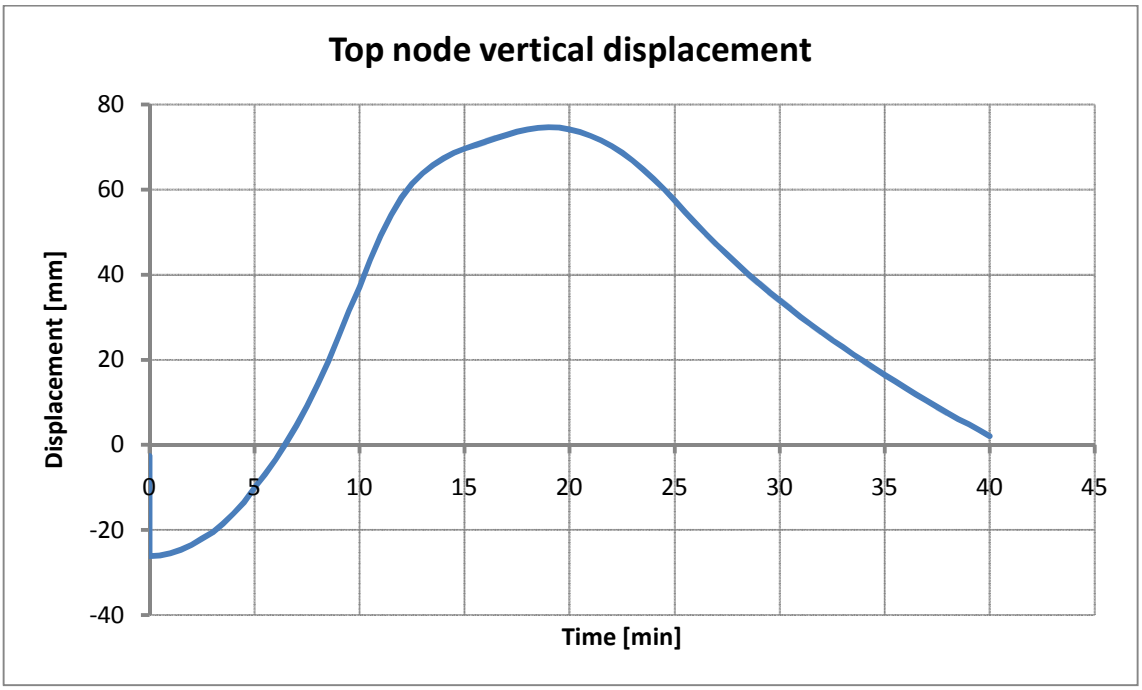

Figure 42 Vertical displacement at top node

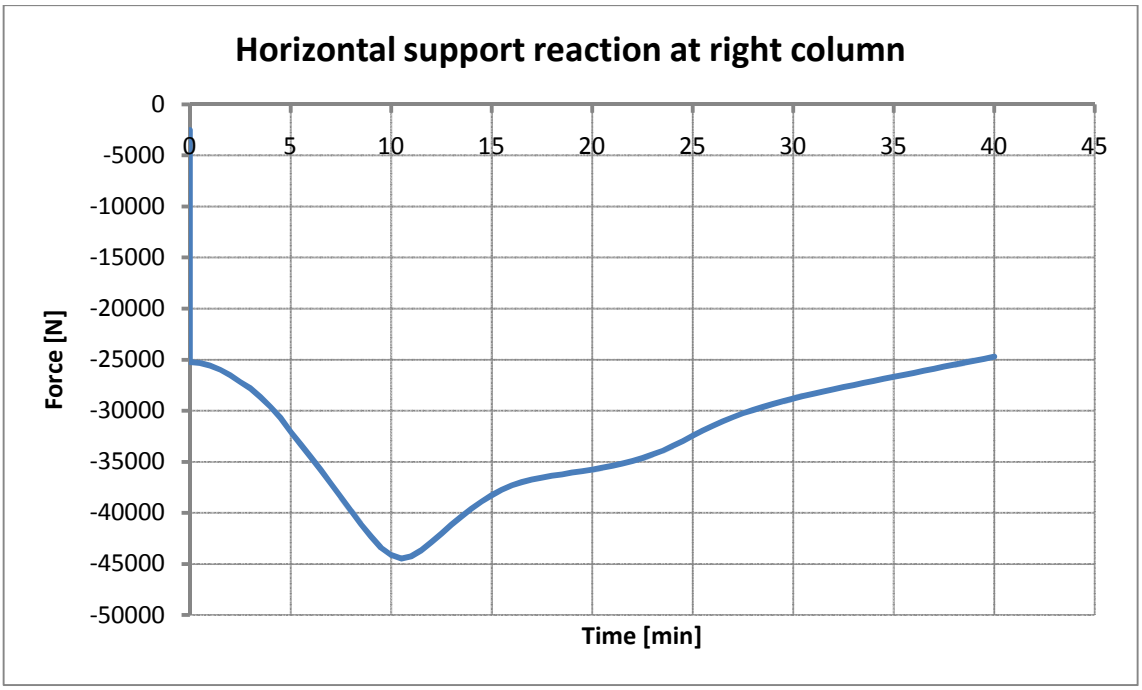

Figure 43 Horizontal support reaction of the base connection

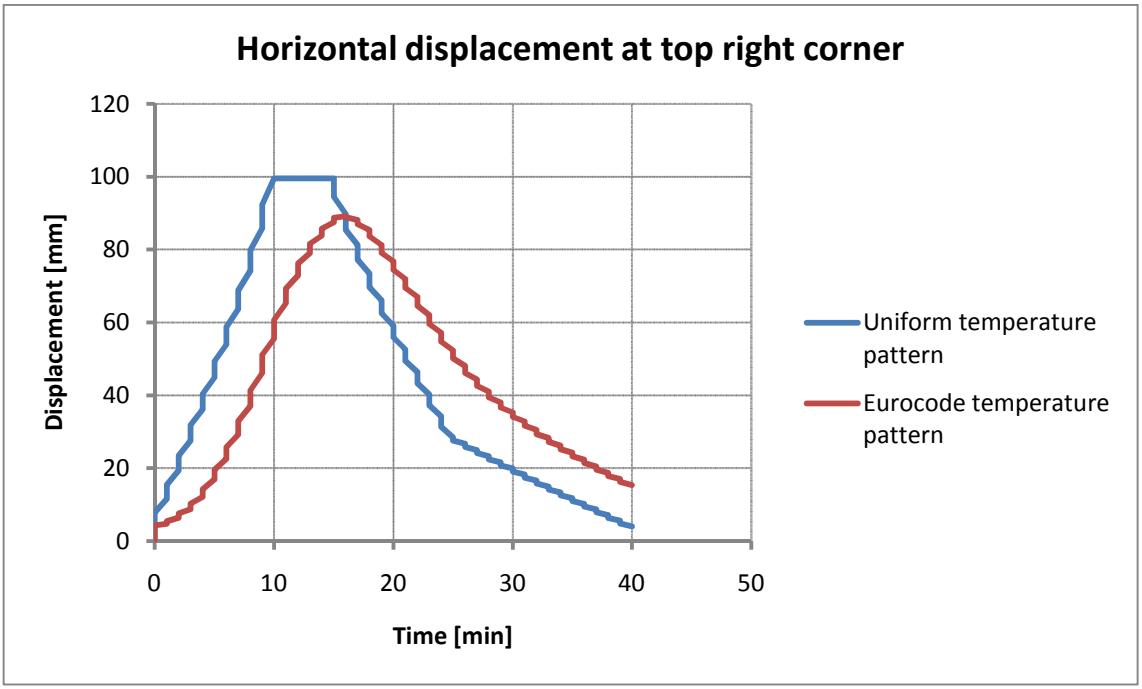

Figure 44 Comparison of horizontal displacement at top right corner

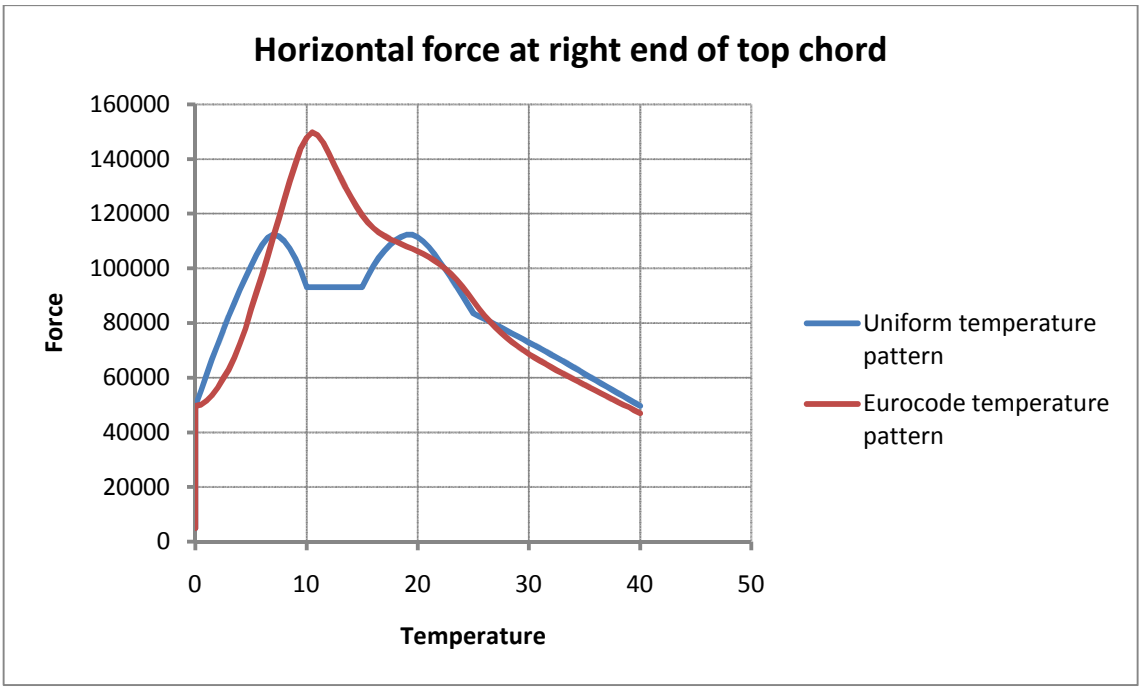

Figure 45 Comparison of the horizontal force at the right end of the top chord

The problem with using the Eurocode temperature pattern in Vulcan is that the calculation time grows very large, even for this simple frame analysis the calculation time was in the range of 12 h. It is of course natural that the calculation time increases as the complexity of the model grows, but it is not reasonable that the calculation time grows with a factor in the range of 50 compared to the case using the uniform temperature pattern. Hence, in order to save time without losing too much accuracy, the best option seems to be to calculate the temperature of the steel in e.g. Excel and then assign only a few temperature curves to different groups of members with approximately the same temperature development. Especially the columns may need to be assigned different temperature curves than the truss if there is a large difference in the section factor, as the stiffness of the columns is very important in evaluating the forces developed in the structure during the temperature exposure.

4.2.8 Local fire 1: mid-span fire

In the previous cases the gas temperature was set to rise similarly throughout the whole structure. In the following cases the behaviour of the structure when subjected to local fires will be studied in more detail.

The mid-span part, marked with red in Figure 46, of the 3D main frame with hinged base connections was exposed to the temperature curve presented in Figure 47 reaching 800 °C, whereas the remaining part of the structure was exposed to the fire curve presented in Figure 48 reaching 300 °C. The uniform temperature pattern was used in Vulcan, i.e. the steel was set to follow the gas temperature. The analysis was run until 40 minutes when the temperature had reached ambient level again.

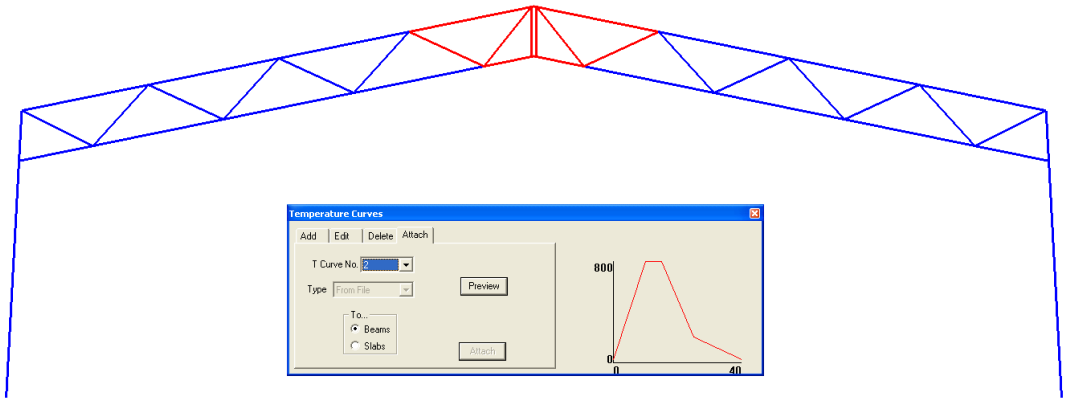

Figure 46 Local fire 1; parts exposed to 800 °C

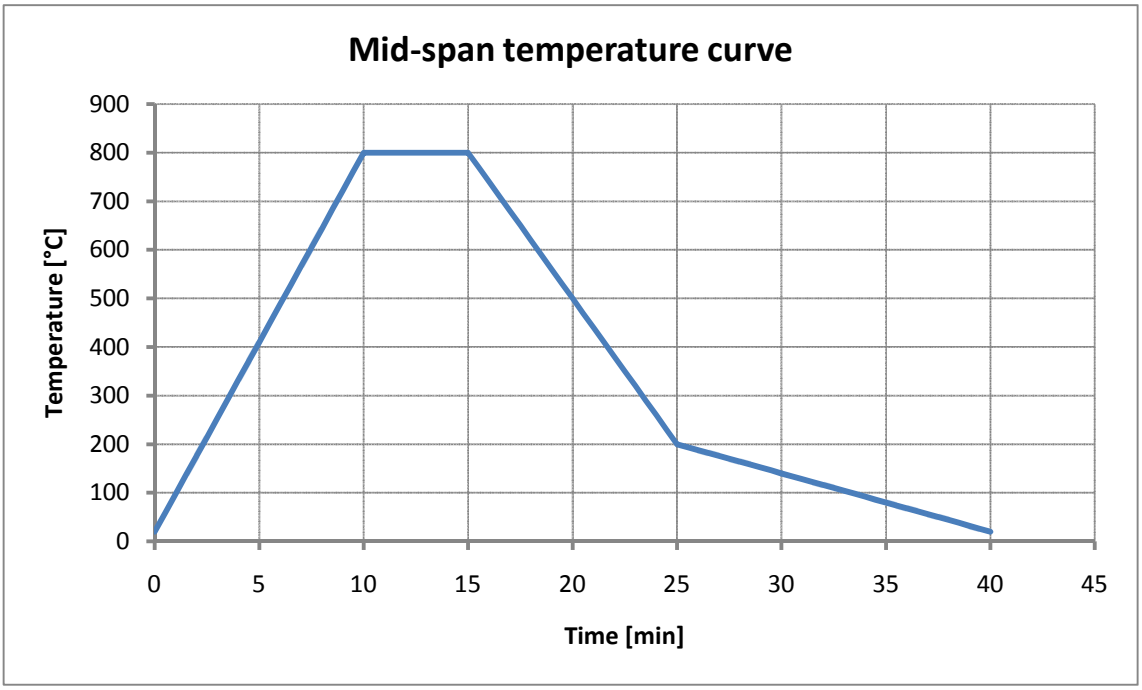

Figure 47 Local fire 1; steel temperature curve reaching 800 °C

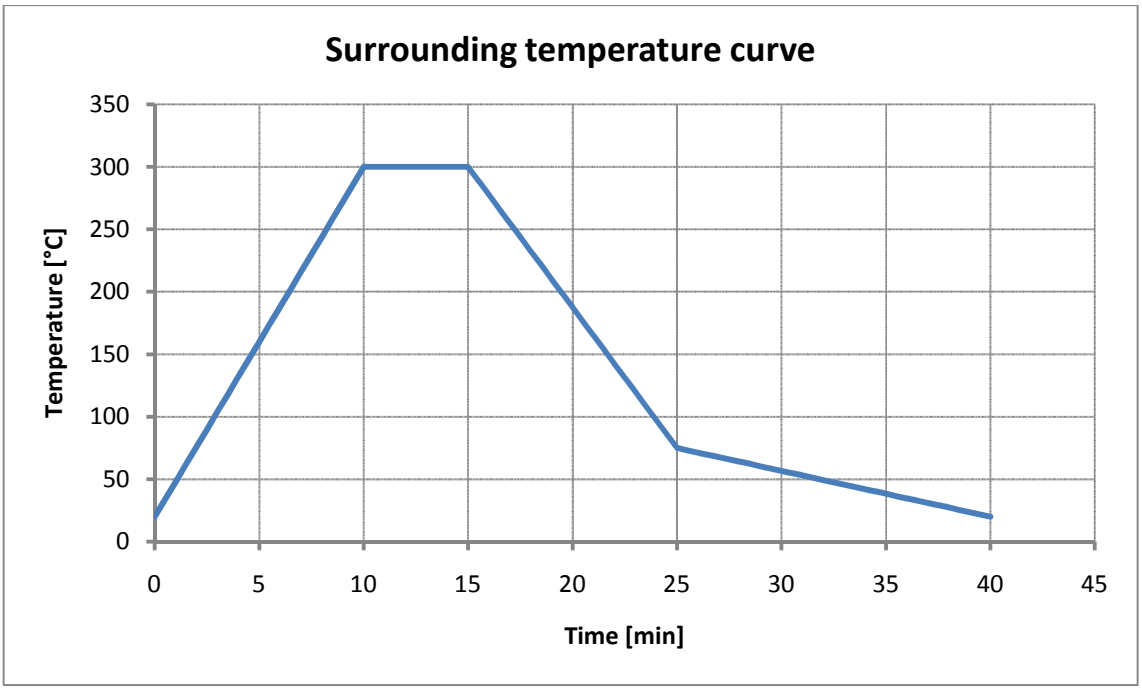

Figure 48 Local fire 1; steel temperature curve of remaining structure, reaching 300 °C

During the heating phase of the analysis the parts of the upper chords closest to the apex of the truss started to undergo substantial deformation at approximately 8 minutes, but the structure as a whole remained stable. The deformation of the roof truss every 5 minutes, as well as at 9 minutes, until 40 minutes, when the temperature had decreased back to 20 °C, can be seen in Figure 49, scaled by a factor of 5.

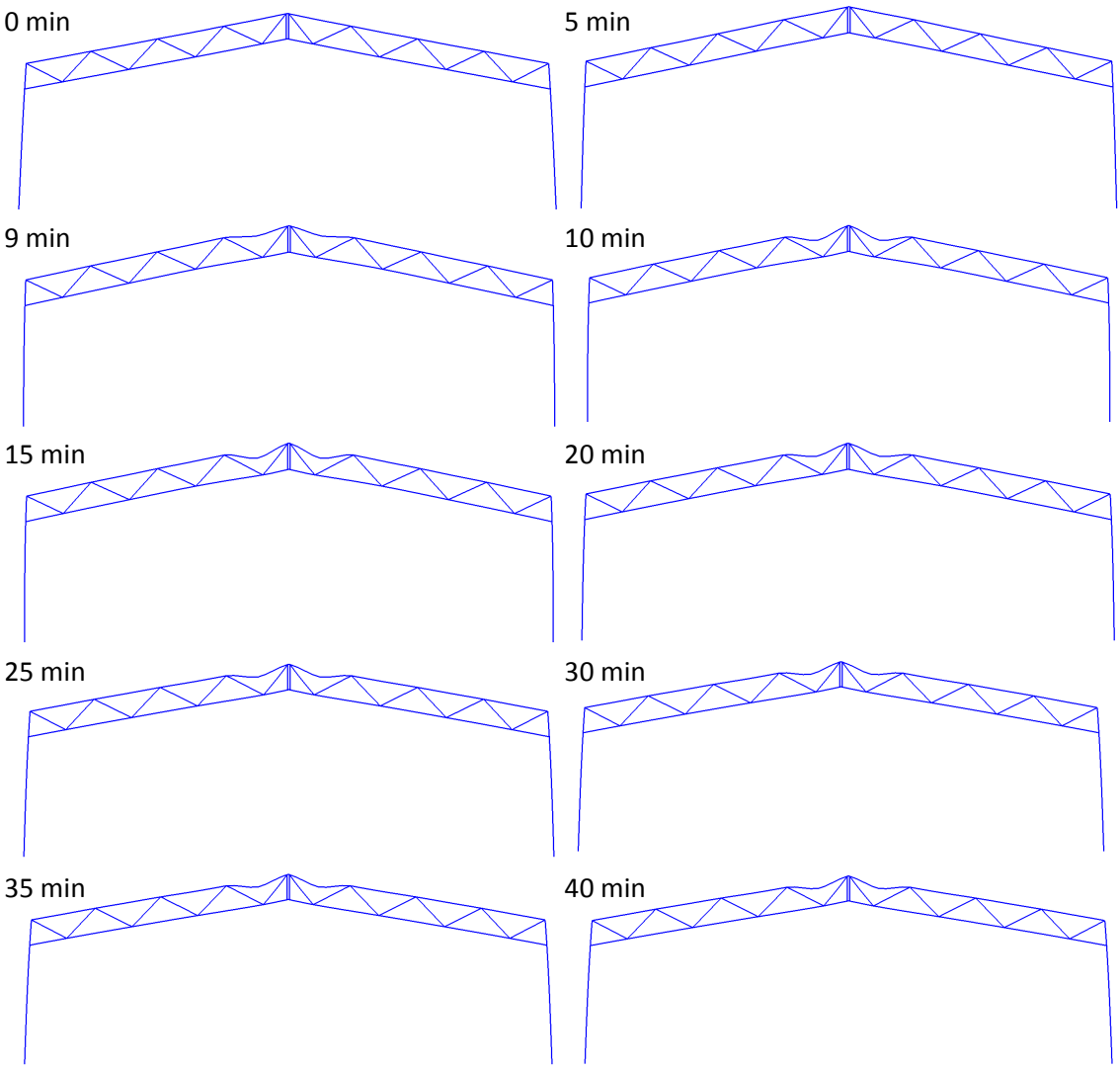

Figure 49 Local fire 1; 0-40 min

The vertical displacement of the top node can be seen in Figure 50, from where the deformation of the upper chord can be noticed as a drop in the displacement. The final deflection at mid-span was 40,6 mm larger than the initial value.

The horizontal support reaction of the right base connection is presented in Figure 51, from where the deformation of the top chords can be noticed as a sudden increase in the horizontal force. From the figure it can also be noticed that the horizontal support reaction was largest in the cooling phase of the fire, more precisely at the end of the analysis, reaching -40,9 kN. It should however be pointed out that this value can vary significantly depending on the cooling rate of both the local temperature curve and the curve of the remaining structure.

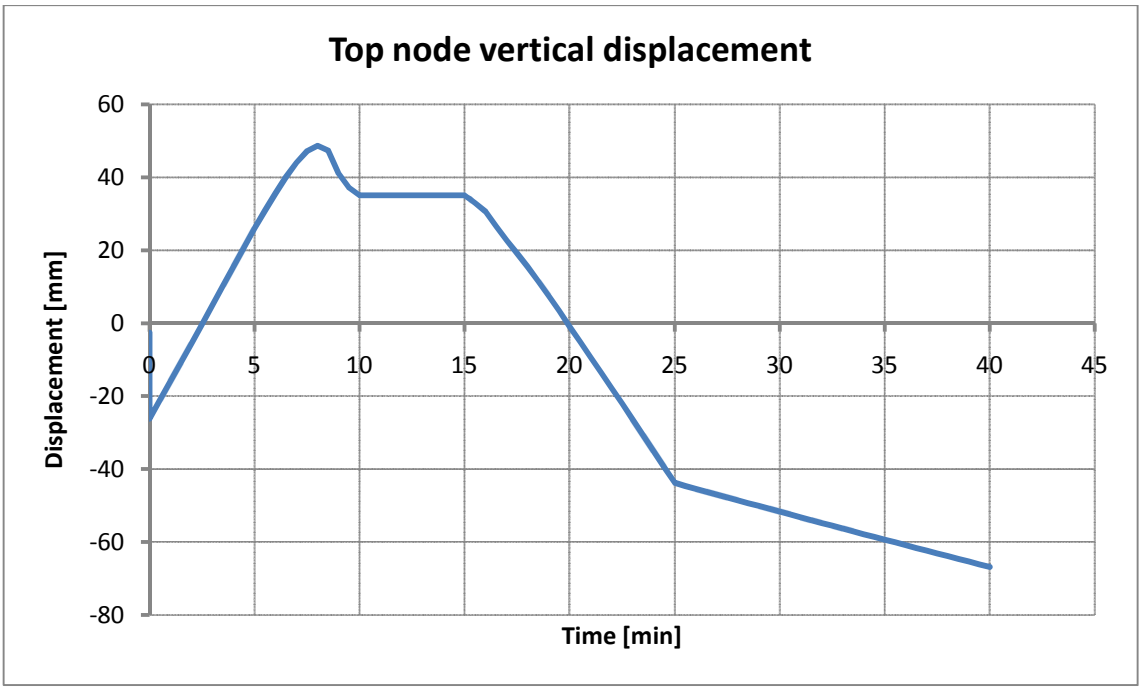

Figure 50 Local fire 1, vertical displacement at top node

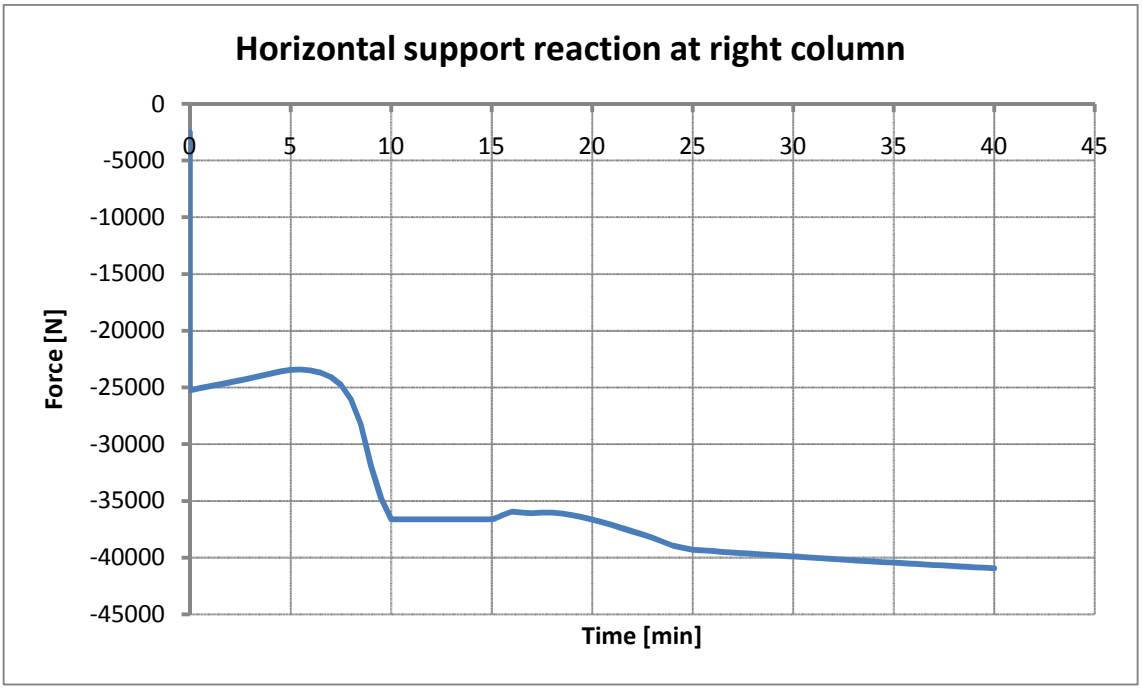

Figure 51 Local fire 1, horizontal support reaction of the base connection

In this first analysis replicating the effects of a local fire to the structure it was shown that even though the truss underwent significant permanent deformations a stable solution could be found in Vulcan and the analysis could be performed all the way back to ambient temperature. The results furthermore showed the importance of the decay phase as the horizontal support reaction at the base of the columns indeed was largest in the end of the analysis.

4.2.9 Local fire 2: mid-span fire, fixed base connections

A similar analysis was also performed using fixed base connections. In order of the analysis to be able to run to the end, it was however necessary to decrease the maximum temperature to 700 °C as the analysis otherwise failed in the heating phase. Again the uniform temperature pattern was used in Vulcan.

The vertical displacement of the top node is presented in Figure 52, from where it can be observed that the frame with fixed base connections was not heated enough for any substantial permanent deformations to take place. The permanent increase in vertical deflection remained at a modest 0,7 mm.

The horizontal support reaction at the right column base connections is presented in Figure 53, also confirming that basically no permanent deformation took place.

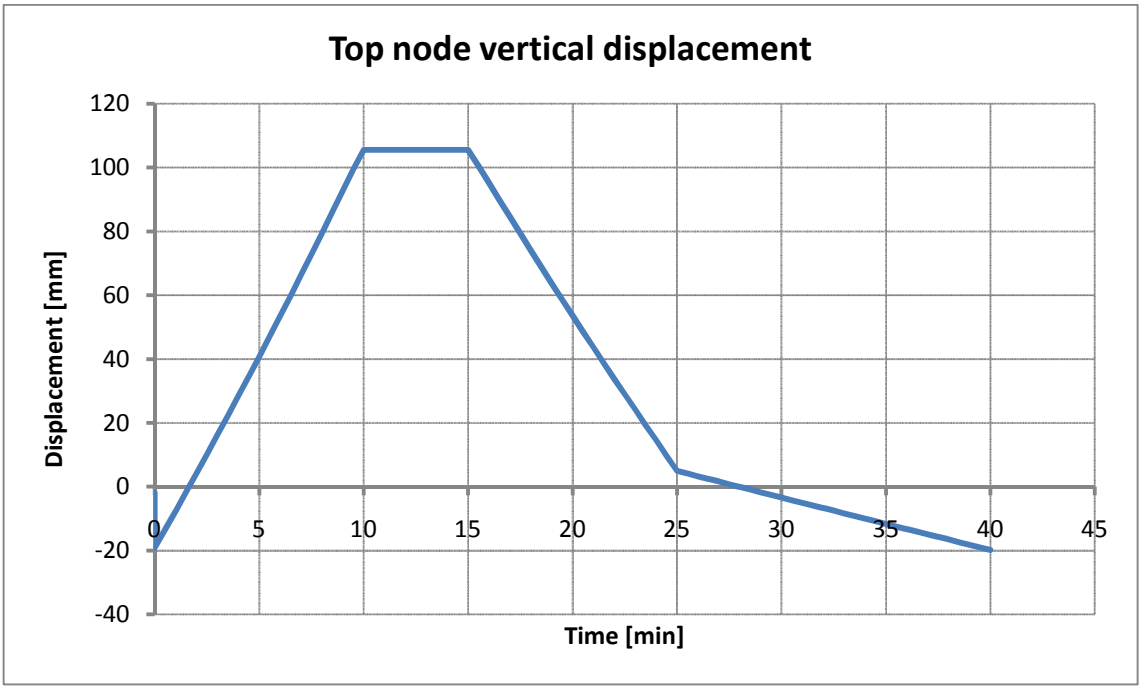

Figure 52 Local fire 2, vertical displacement at top node

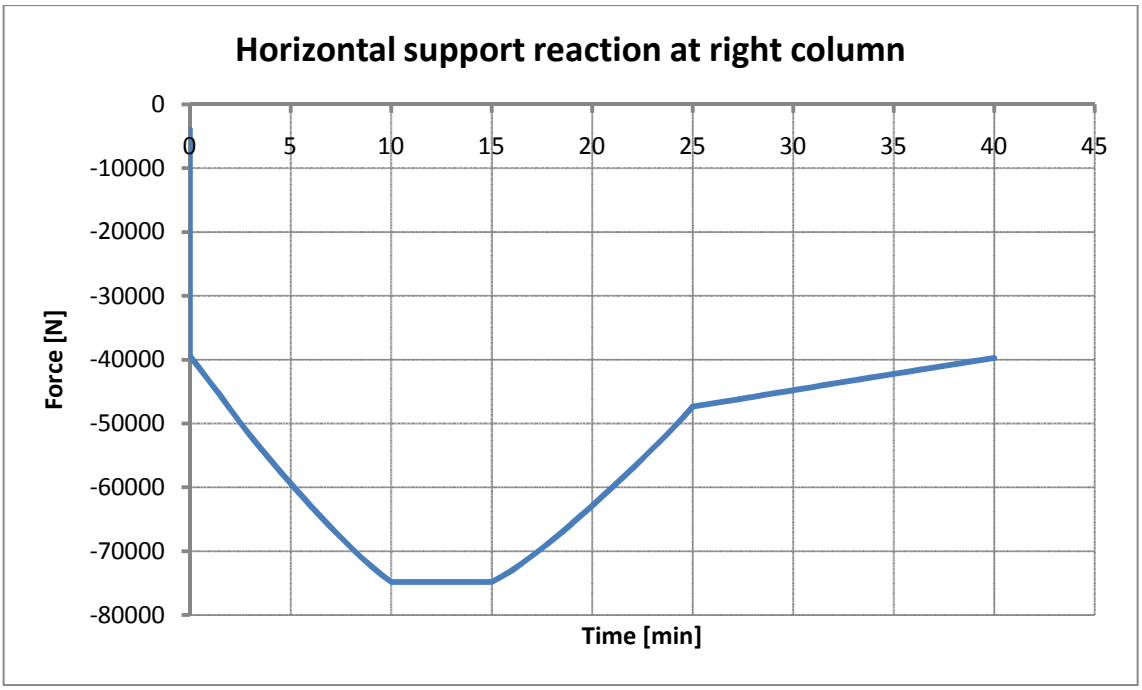

Figure 53 Local fire 2, horizontal support reaction of the base connection

As it was necessary to lower the maximum temperature to 700 °C in order to get the model to run without failure no direct comparison to the previous model can be done. Again it can however be concluded that the degree of restraint plays a significant role in the behaviour of the structure.

4.2.10 Local fire 3: mid-span fire, temperature groups

In the third mid-span local fire the members of the top chord were divided into a few groups and assigned different temperature curves with the maximum temperature ranging from 800 to 300 °C, according to Figure 54, Figure 55, Figure 56 and Figure 57, using the uniform temperature pattern in Vulcan.

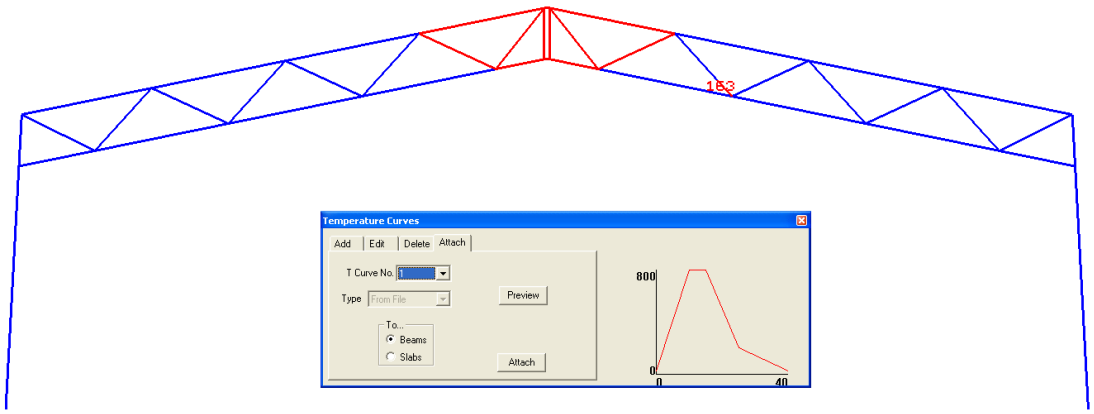

Figure 54 Local fire 3; mid part exposed to 800 °C

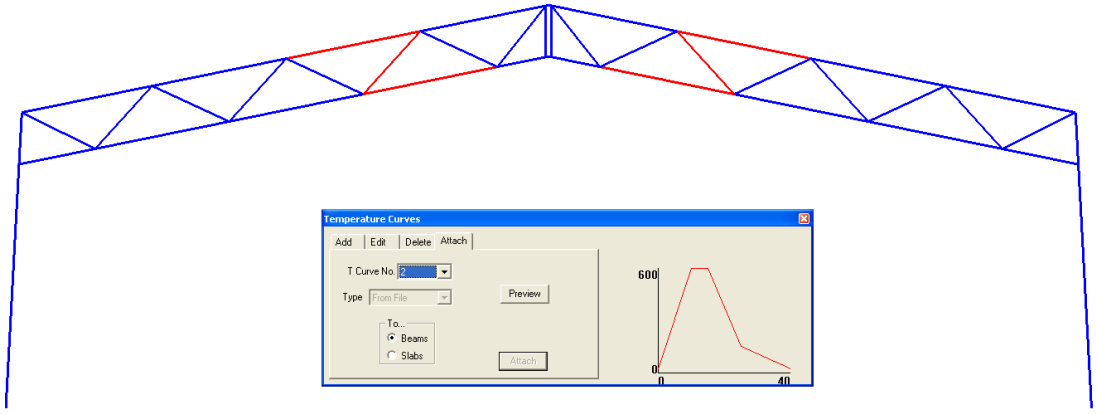

Figure 55 Local fire 3; parts exposed to 600 °C

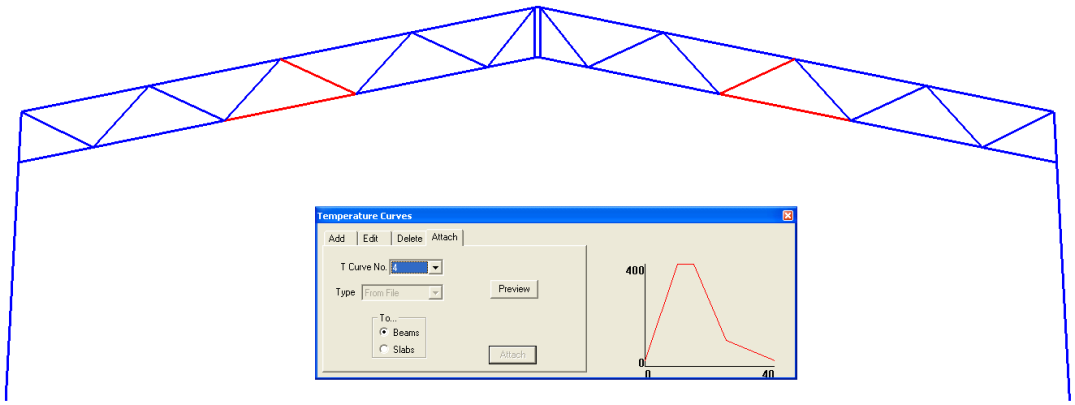

Figure 56 Local fire 3; parts exposed to 400 °C

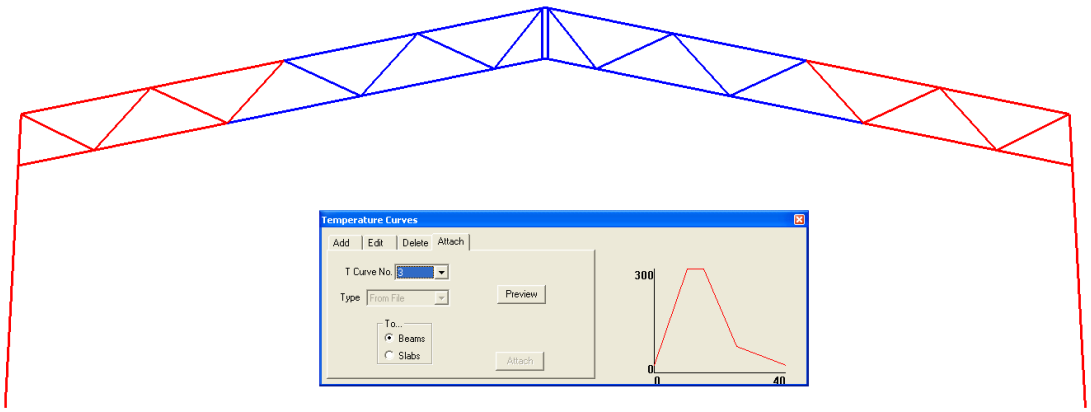

Figure 57 Local fire 3; parts exposed to 300 °C

The frame behaved essentially in the same way as in the mid-span local fire 1 scenario, where only two temperature curves were used; the two upmost parts of the top chords deformed at about 9 minutes but the frame remained stable. Figure 58 show the deformation of the roof truss every 5 minutes, as well as at 9 minutes, scaled by a factor of 5. Figure 59 gives a detailed view of the deformed shape of the mid part of the truss at 10 minutes into the analysis, scaled by a factor of 5.

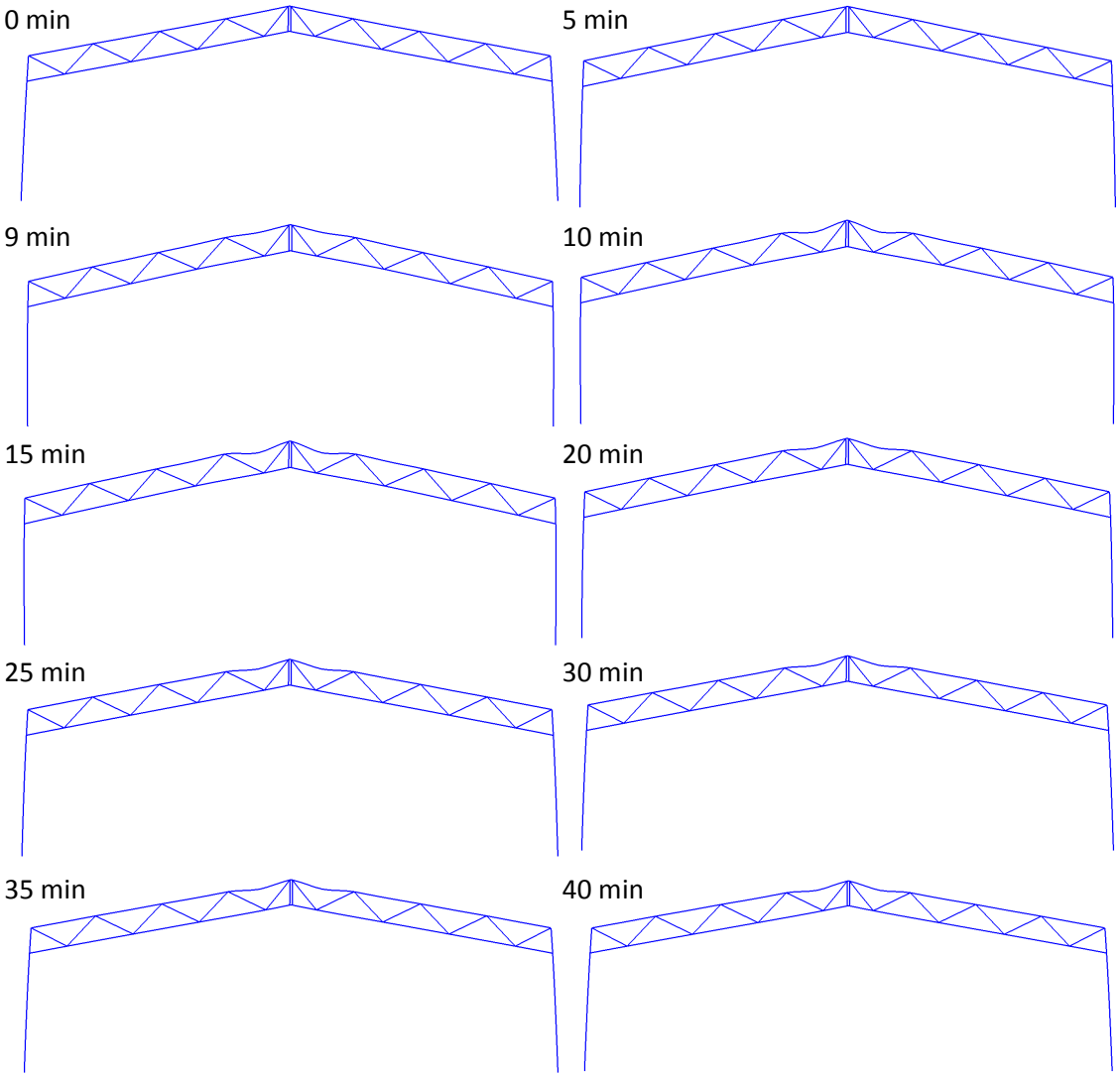

Figure 58 Local fire 3; 0-40 min

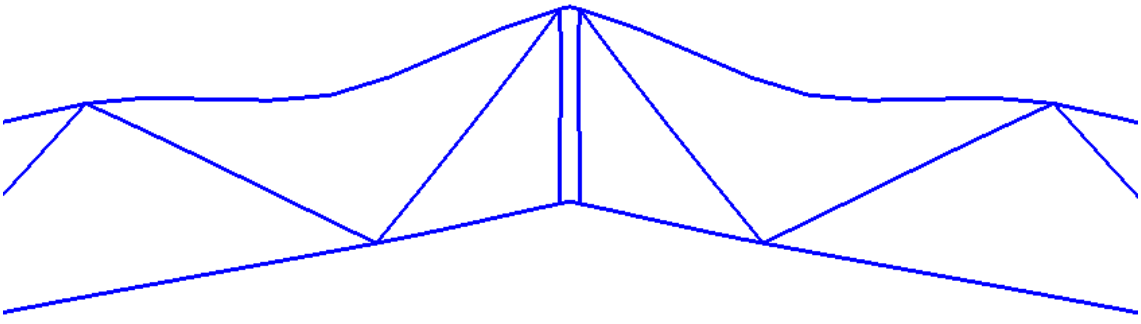

Figure 59 Local fire 3; deformed shape of mid part of truss at 10 min

The vertical displacement of the top node is presented in Figure 60. In the figure there is however no clear indication of large deformations taking place at the top chord in the heating phase. The vertical deflection was permanently increased by 17,1 mm, i.e. a much smaller increase than in local fire 1.

The horizontal support reaction of the base connection at the right column is presented in Figure 61. From the figure it can be noticed that the largest force took place during the period of constant temperature between 10 and 15 minutes, reaching 36,4 kN, or almost the same as in local fire 1 where the force was 36,6 kN in the constant temperature plateau. In the cooling phase the horizontal support reaction however decreased opposed to local fire 1 where it increased. The final horizontal support reaction was 6,6 kN larger than the initial value.

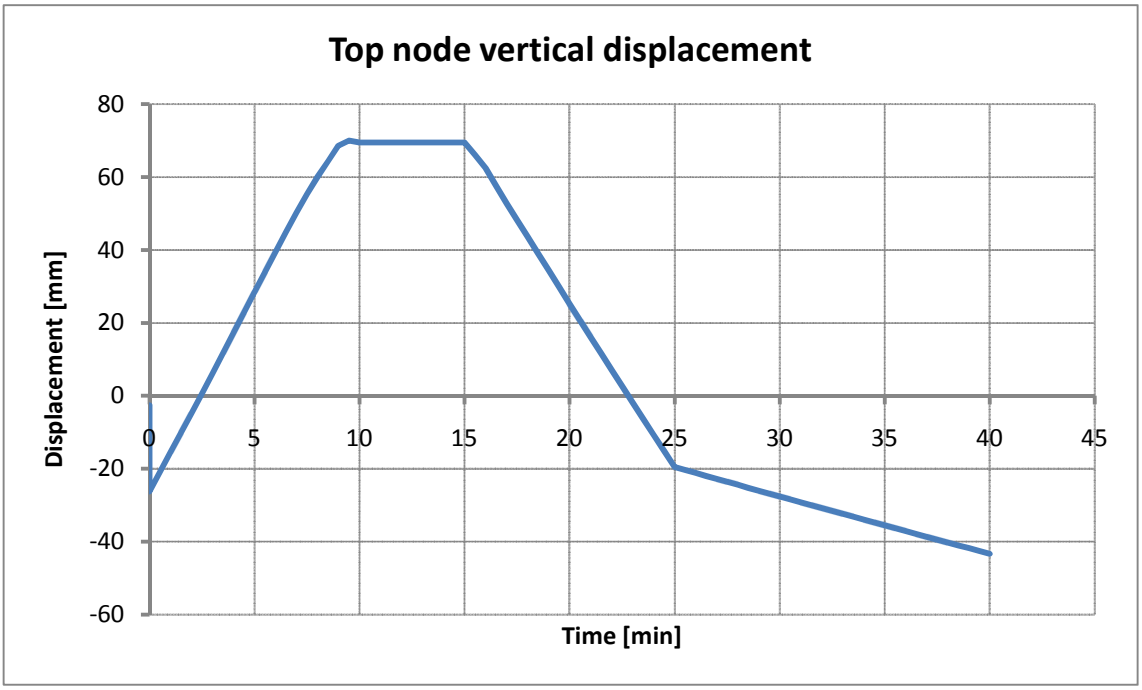

Figure 60 Local fire 3; vertical displacement at top node

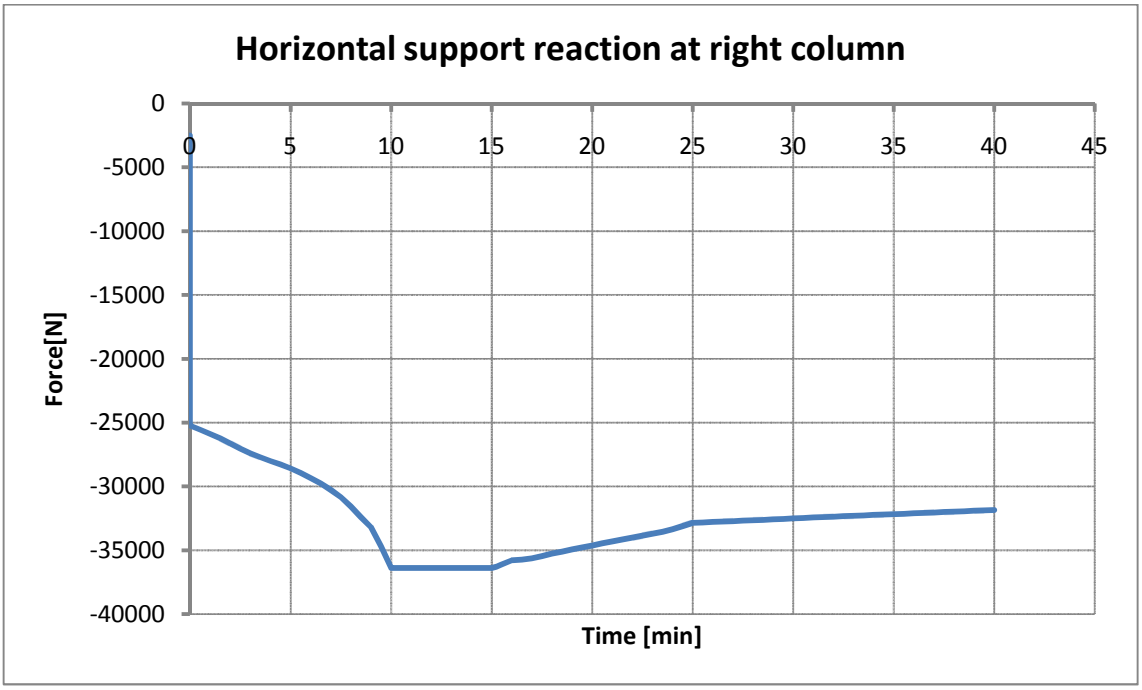

Figure 61 Local fire 3; horizontal support reaction of the base connection

As in local fire 1, the structure underwent permanent deformations at both sides of the apex of the roof. This could however not be observed clearly from the figures of the vertical displacement and the horizontal support reaction in the same way as for local fire 1. The largest horizontal support reaction took place in the stationary phase, opposed to local fire 1 where the support reaction reached its maximum at the end of the decay phase.

4.2.11 Local fire 4: fire at column

In the fourth local fire analysis the local temperature exposure was put at the right end of the frame, so that the end of the truss was exposed to the highest temperature of 600 °C and the column 400 °C, as seen in Figure 62 and Figure 63. A few members of the truss were also exposed to a temperature curve reaching 300 °C, as seen in Figure 64, whereas the remaining part of the structure was kept at ambient temperature, as seen in Figure 65. The uniform temperature pattern was used in Vulcan.

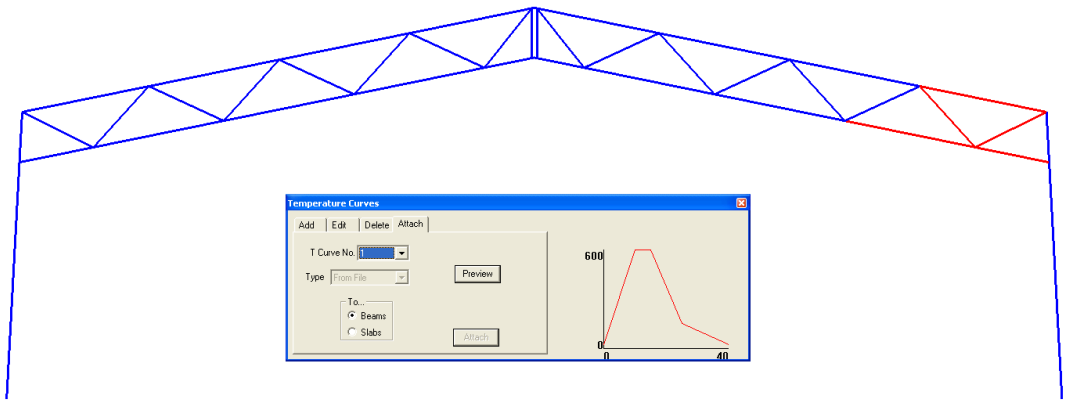

Figure 62 Local fire 4; parts exposed to 600 °C

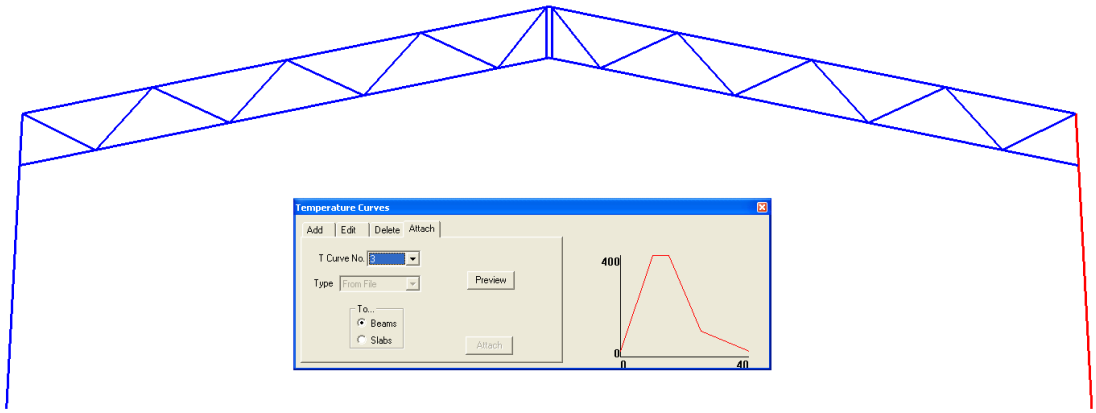

Figure 63 Local fire 4; parts exposed to 400 °C

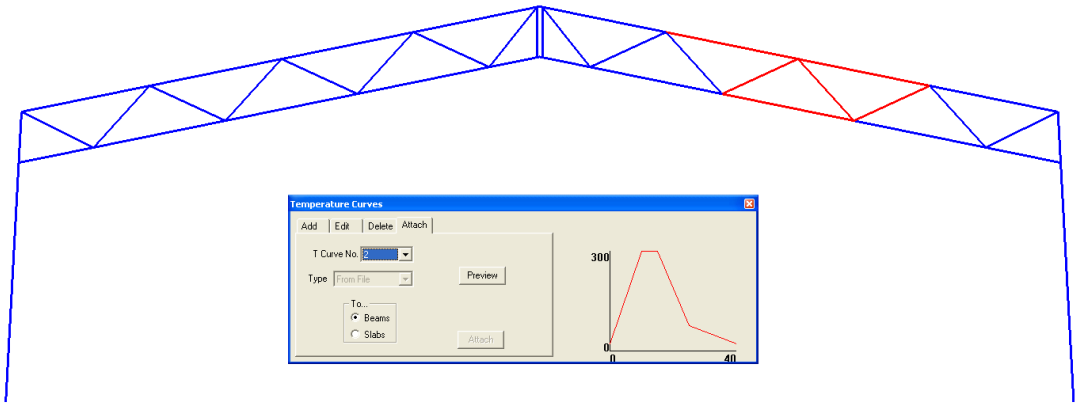

Figure 64 Local fire 4; parts exposed to 300 °C

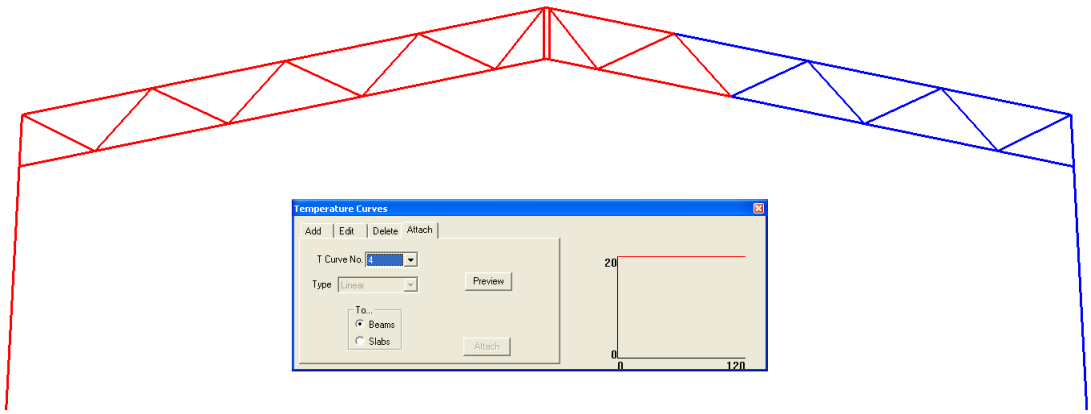

Figure 65 Local fire 4; parts at ambient temperature (20 °C)

The deformed shape of the frame at 15 minutes into the analysis is presented in Figure 66, from where the effects of the thermal expansion clearly can be observed as the deformations are scaled to a factor of 20. No plastic deformations however took place.

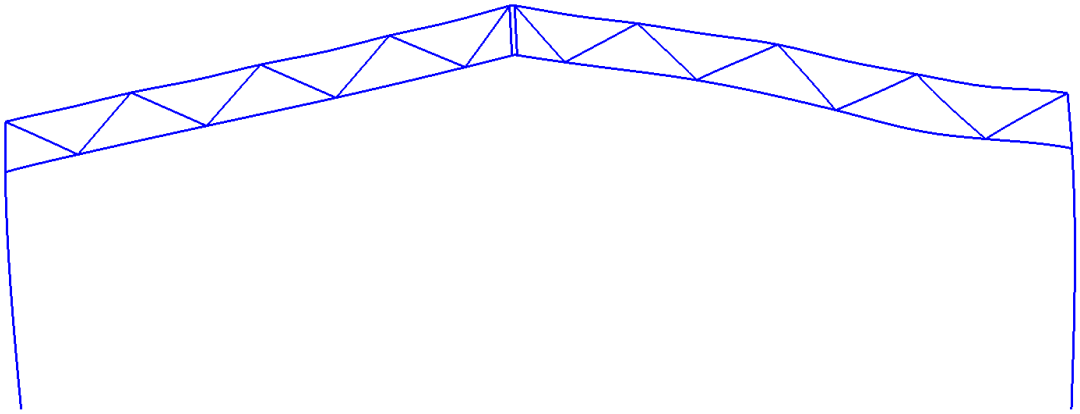

Figure 66 Local fire 4; deformed shape at 15 min

The vertical displacement of the top node is presented in Figure 67 and the horizontal support reaction in Figure 68, both figures showing that no additional permanent deformation took place due to the fire exposure.

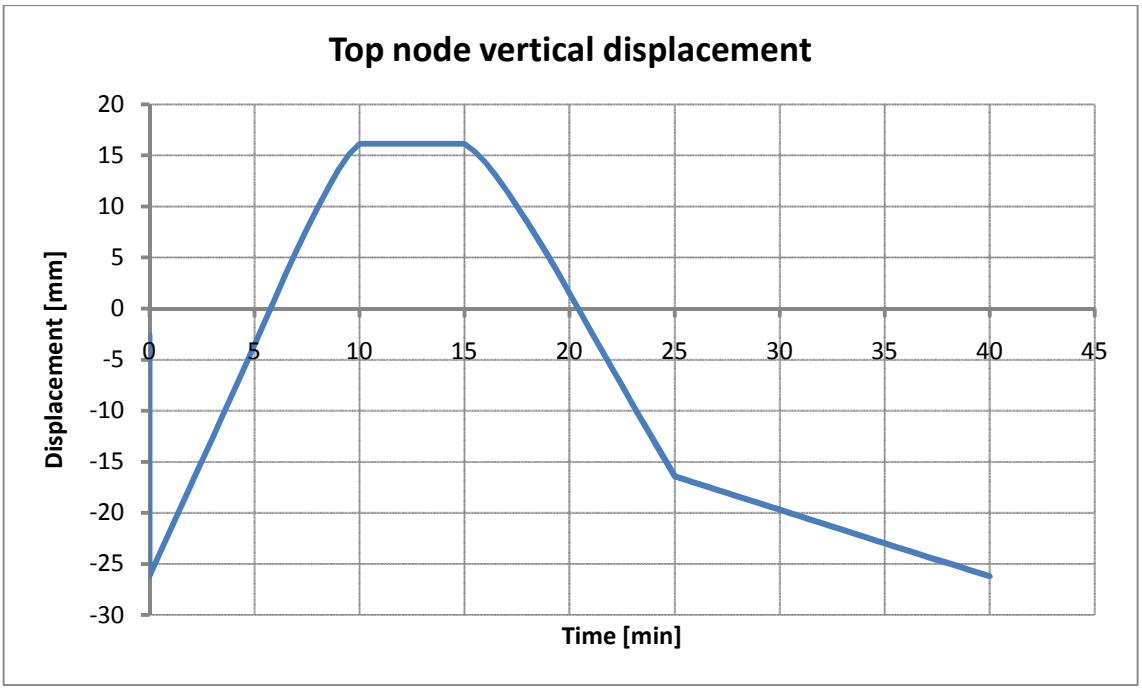

Figure 67 Local fire 4; vertical displacement at top node

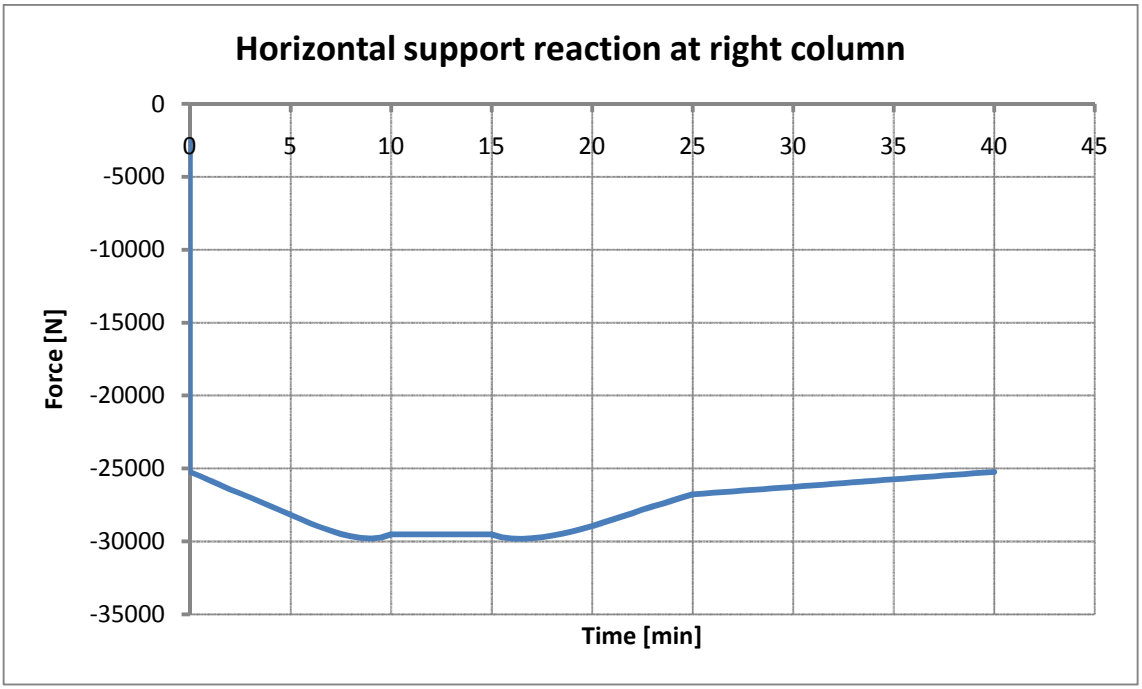

Figure 68 Local fire 4; horizontal support reaction of the base connection

The temperatures reached in this analysis were not high enough for the structure to suffer from any permanent deformations nor could anything significant be observed in the behaviour of the structure.

4.2.12 Local fire 5: three frames, mid-span fire

An analysis was performed on a model made up of three main frames connected by hinged roof purlins and supported in the direction of the purlins at one of the end frames. The base connections of the columns where hinged. All other connections were fixed. No eccentricities

were considered. The mid part of the mid frame, marked with red in Figure 69, was exposed to the fire curve seen in Figure 47, reaching a maximum temperature of 800 °C, whereas the remaining part of the structure was exposed to the fire curve seen in Figure 48 reaching 300 °C, again using the uniform temperature pattern in Vulcan.

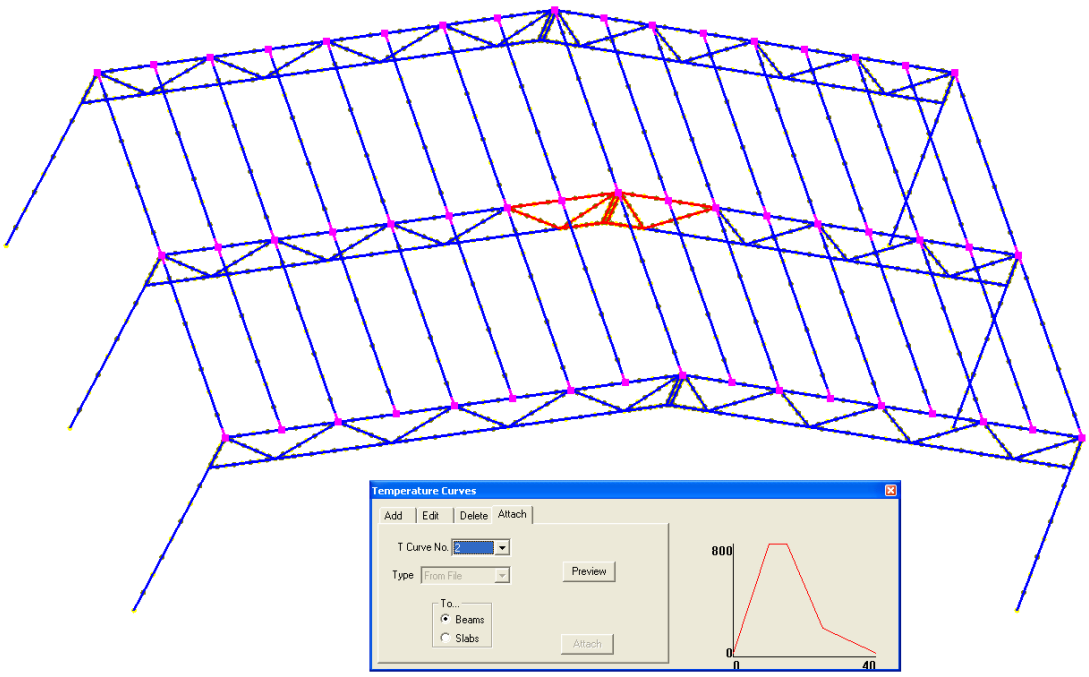

Figure 69 Local fire 5; parts exposed to 800 °C

The deformed shape of the structure at every 5 minutes, as well as at 9 minutes, can be seen in Figure 70, scaled by a factor of 5. The mid-frame behaved in a very similar manner to the frame in local fire 1, where only the mid-frame was included. It was however noticed that the left part of the top chord deformed more than the right part, even though the structure was symmetrical. The reason for this remains unclear.

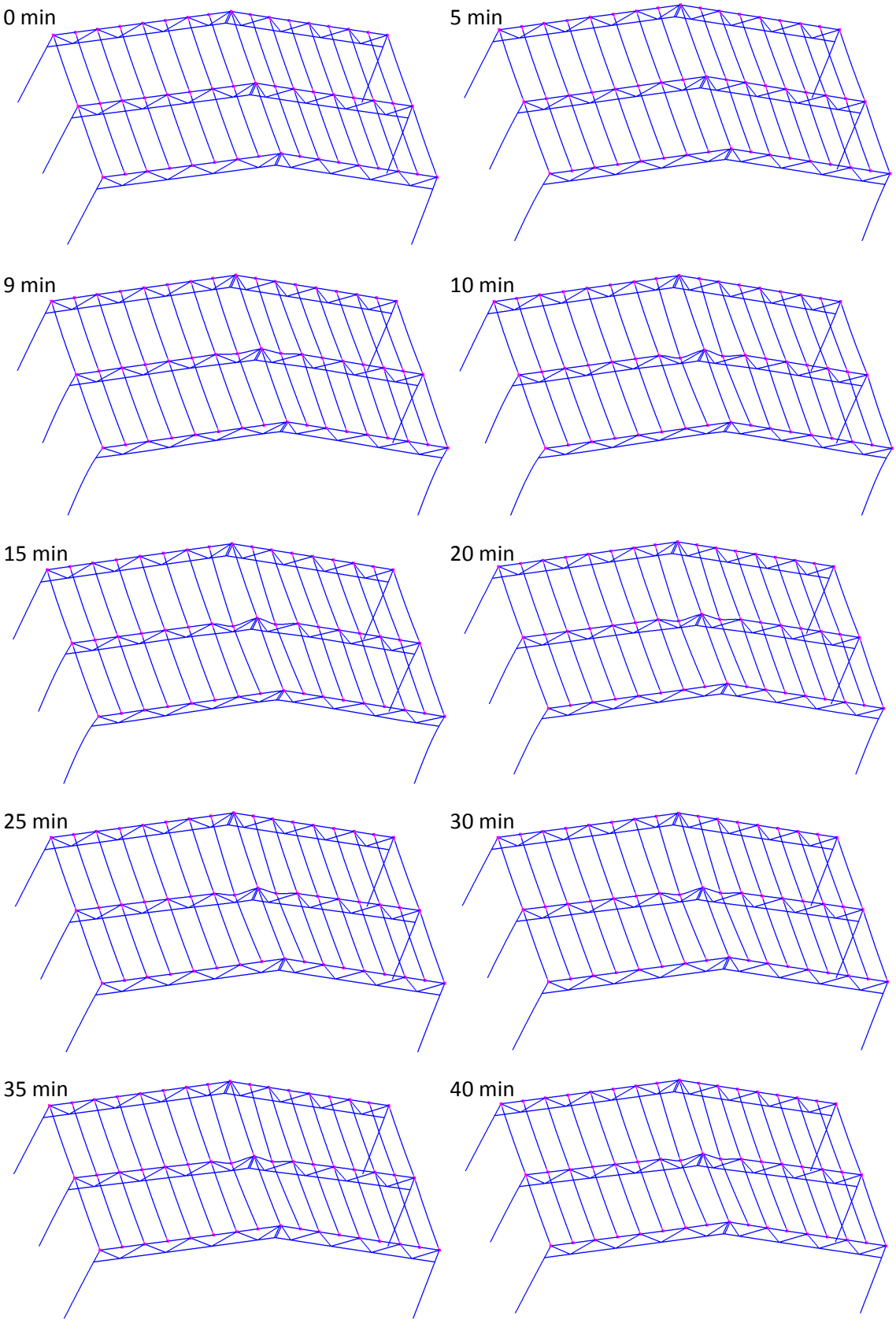

Figure 70 Local fire 5; 0-40 min

The vertical displacement of the top node of the mid frame is presented in Figure 71. The final deflection was 41,1 mm larger than the initial value before the temperature exposure, i.e. almost exactly the same increase in deflection as in local fire 1 with only one frame.

The horizontal support reaction of the base connection at the right column of the mid frame is presented in Figure 72, which verifies that the mid frame behaved very similarly to the single frame in local fire 1. The largest horizontal support reaction took place in the end of the decay phase, reaching a value of 40,7 kN.

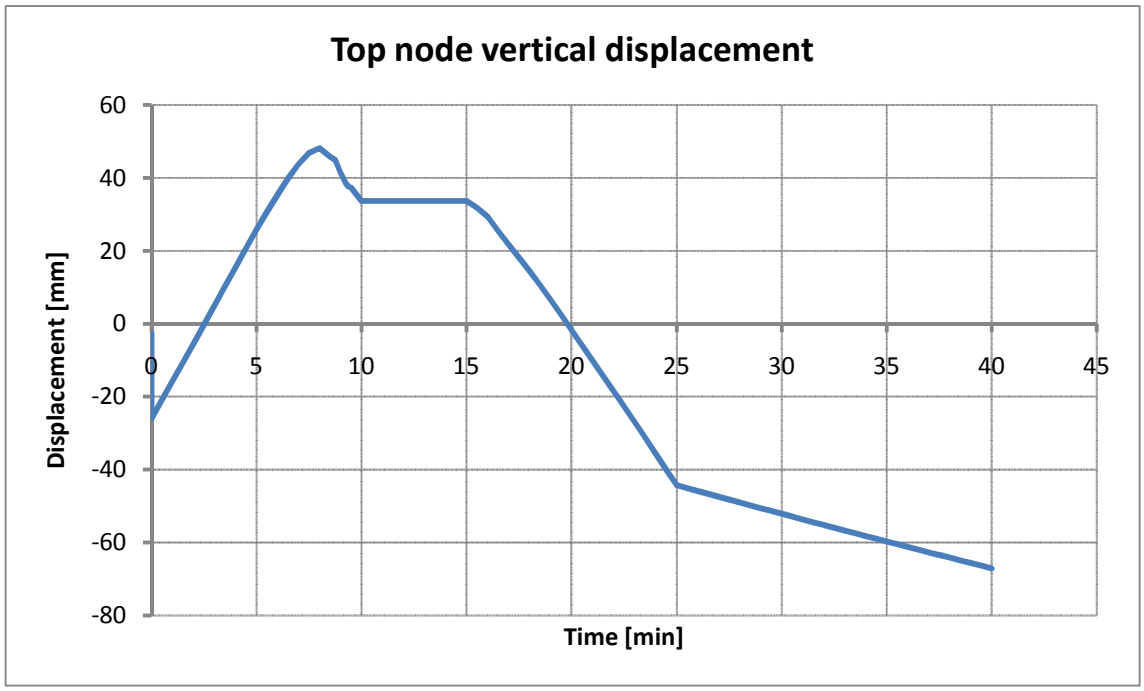

Figure 71 Local fire 5; vertical displacement at top node

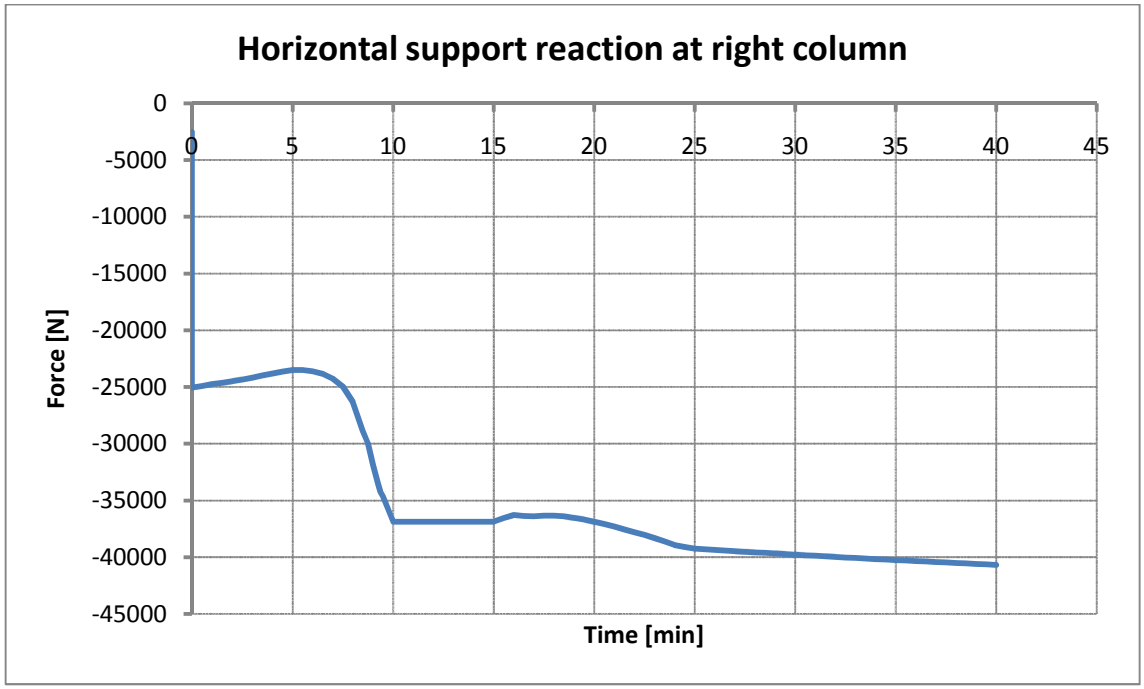

Figure 72 Local fire 5; horizontal support reaction of the base connection

The results for the mid-frame of this analysis showed great agreement with the results from local fire 1 where only one frame was included. This indicates that the behaviour of one frame does not depend on the adjacent frames or the purlins in any larger extent. The results for the purlins from this analysis are not presented as the boundary conditions of the structure were not completely symmetrical with respect to the mid-frame in order to avoid a too high degree of lateral restraint.

4.2.13 Local fire 5, comparison of material models

As the test analyses showed that the two different material models for steel gave slightly different results at elevated temperatures, the same analysis was also performed using the Eurocode model instead of the Ramberg-Osgood model to compare if there was any significant difference.

The results for both material models are compared in Figure 73 and 74. From the figures it can be noticed that the difference between the results was quite small. The analysis using the Ramberg-Osgood model showed a slightly smaller deflection at the top node from the end of the heating phase onwards and the horizontal support reaction at the base of the column of the mid-frame was slightly smaller in the cooling phase. The largest difference in the deflection between the two models was about 6 mm and the largest difference in the support reaction about 2 kN. The differences in the results were small and can be considered as negligible. It seems to be more reasonable to use the material model which is numerically more stable in order to improve convergence. Hence, it's advisable to use the smoothed Ramberg-Osgood model, rather than the Eurocode model which contains sharp edges which could pose numerical problems.

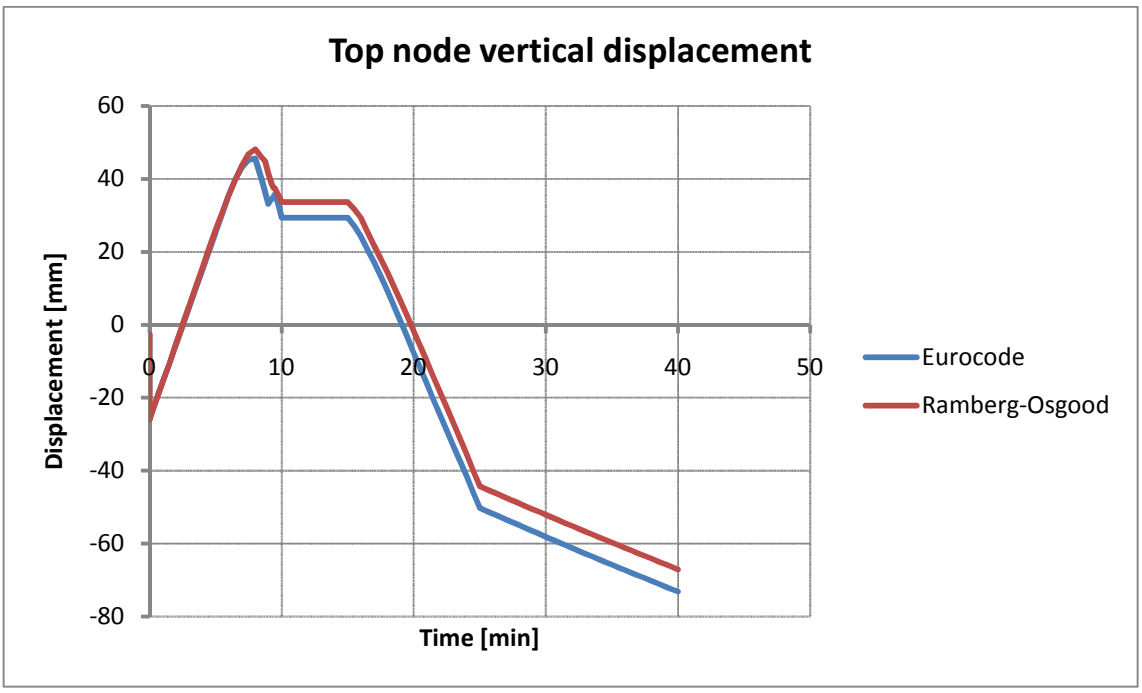

Figure 73 Local fire 5; comparison between material models for vertical displacement at top node

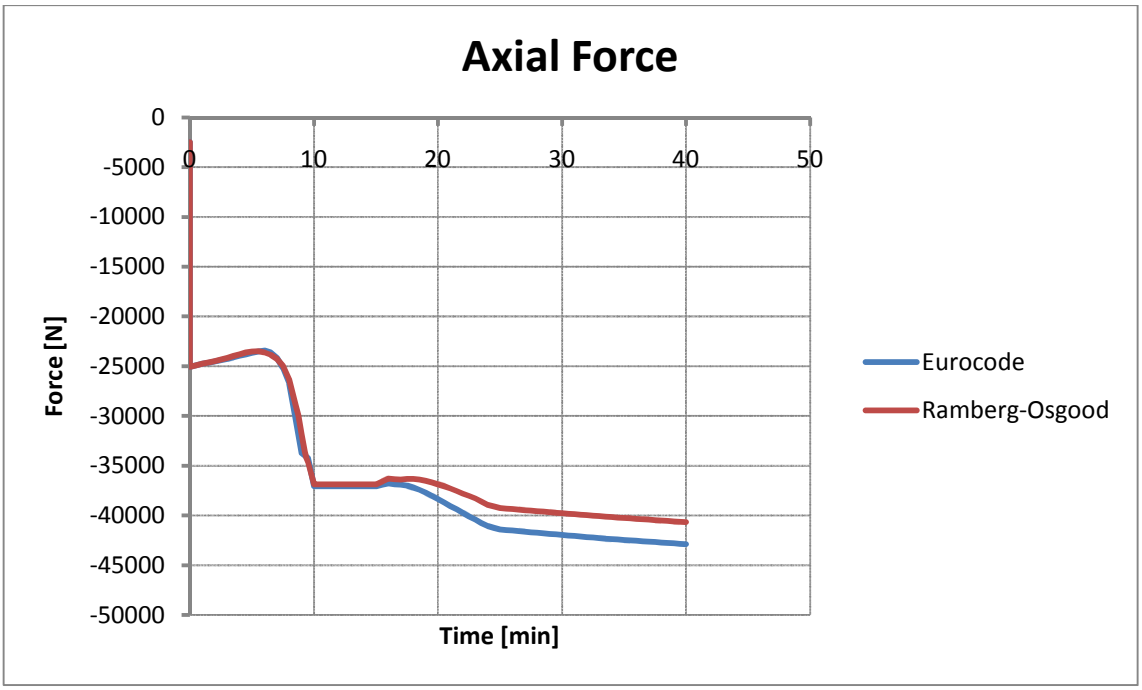

Figure 74 Local fire 5; comparison between material models for horizontal support reaction at base connection

4.3 Final analyses

In order to simplify the analysis and to save valuable calculation time only the three mid frames of the hall was studied in the final analyses, using the smoothed Ramberg-Osgood material model and the uniform temperature pattern in Vulcan. The stiffness of the remaining structure was taken into account by modifying the boundary conditions of the three mid frames.

The stiffness of the hall is mainly provided by the bracings in the walls and roof between the last two frames at both ends of the hall. The hall was modelled and analysed non-linearly at ambient temperature using Autodesk Robot Structural Analysis Professional 2010. By applying a thermal load of 300 °C to the roof purlins indicated by red circles in Figure 75, the stiffness of the structure could be evaluated. It was concluded that the stiffness was provided mainly by the bracings in the walls and the outermost bracings in the roof. The longitudinal stiffness was evaluated at each point where the purlins would be connected to the end structures and translated into springs with corresponding stiffness, as seen in Figure 76, simply by dividing the axial forces in the purlins by the horizontal displacements at the ends of the purlins in the direction of the axis of their length. E.g. for the outermost purlins the axial force was 250,97 kN and the displacement 14 mm, leading to a spring stiffness of about 17900 N/mm.

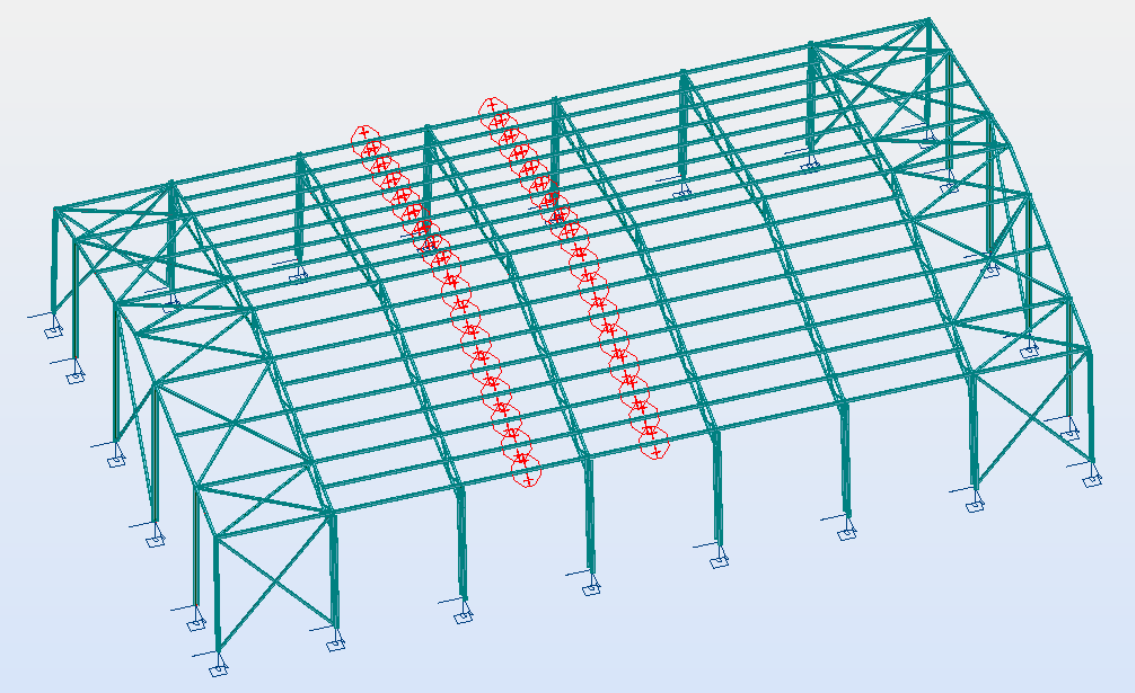

Figure 75 Stiffness analysis model in Robot

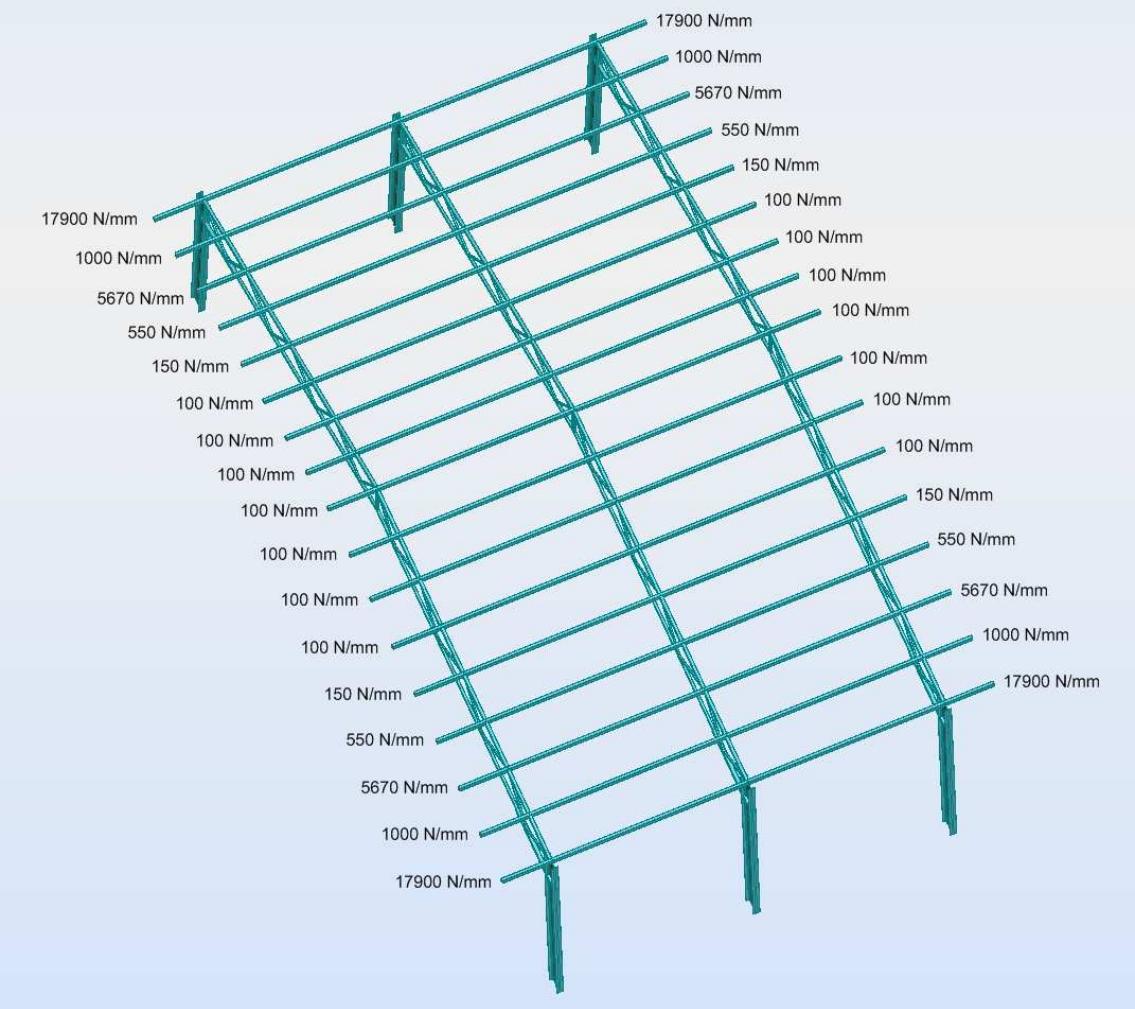

Figure 76 Spring stiffness

In Vulcan the stiffness of the surrounding structure was applied at the supports. 1/4th of the length of the purlins connecting the mid frames to the end structures were incorporated in the model as the springs need to be assigned to beam elements in Vulcan. Furthermore it was not desirable to assign the springs directly to the truss neither to include the whole purlins as they would have increased the complexity of the model and hence also the needed calculation time. Supports, as well as springs with axial stiffness according to Figure 76, were applied at the ends of the end purlins. Apart from the axial stiffness presented in Figure 76 all the other properties of the different springs were the same; fixed in the vertical direction, fixed in the direction of the truss, fixed for torsional moment of the purlins and free for bending moments in both directions. Hence the supports carried vertical forces, but this should not affect the behaviour of the structure as the connections to the trusses were pinned, and by testing it was also concluded that the vertical forces carried by the supports were very small. Furthermore it seemed to be more realistic that the connecting purlins gave some degree of vertical support, which indeed was the case for the real structure.

4.3.1 Mid-span local fire

The mid-span local fire analysis was performed on a model essentially the same as the local fire 5 initial analysis, see Figure 69, but incorporating the stiffness of the surrounding structure as described above. The base connections of the columns as well as the purlin connections were hinged, all other connections were considered as fixed. No eccentricities were incorporated in the model. The purlins between the ends of the frames were removed from the model as they would otherwise buckle and cause the analysis to stop. The mid part of the mid frame, marked with red in Figure 77, was exposed to the fire curve seen in Figure 47, reaching a maximum of 800 °C, whereas the remaining part of the structure was exposed to the fire curve seen in Figure 48, reaching a maximum of 300 °C, which also was the case for local fire 5 initial analysis. These temperature curves were chosen in order to keep the analysis simple. The uniform temperature pattern was used in Vulcan, i.e. the steel temperature was assigned to directly follow the gas temperature.

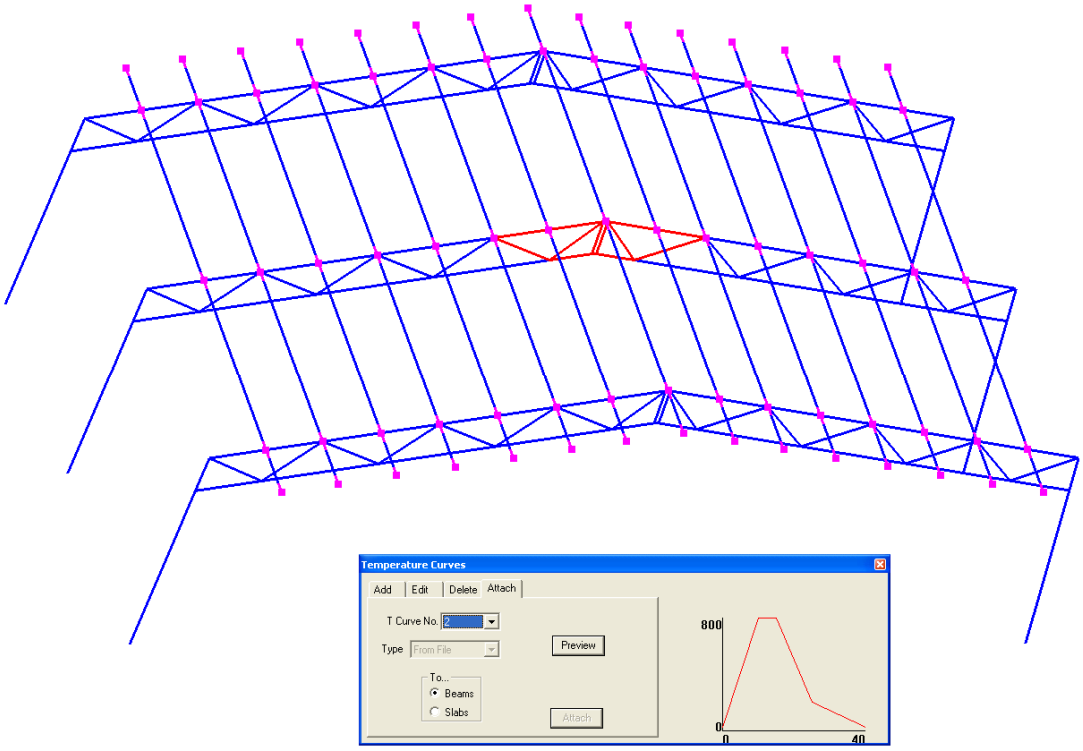

Figure 77 Final analysis, mid-span local fire; members exposed to 800 °C marked with red

Vertical uniform line loads of 1 kN/m, representing the self-weight of the structure as well as the snow load, were applied to the roof purlins according to Figure 78.

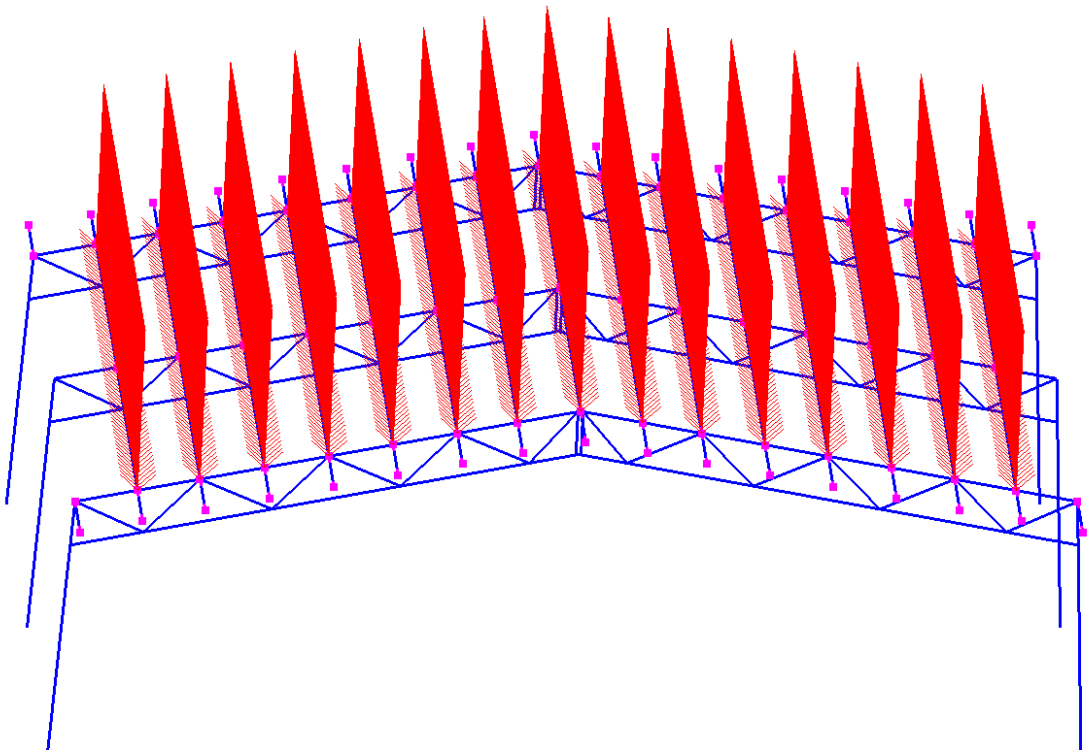

Figure 78 Final analysis, mid-span local fire; line loads

The structure was also loaded by 3 kN point loads representing the loads from the structures omitted from the model, as seen in Figure 79. Furthermore horizontal point loads of 1,7 kN were also applied in the middle of the bottom chords to represent the initial imperfection of L/1000, i.e. 12 mm, of the truss halves. The horizontal point loads were assigned to act in opposite directions in order of the total horizontal force acting on the structure to remain at zero and as the bottom chords would otherwise bend unnaturally to one side.

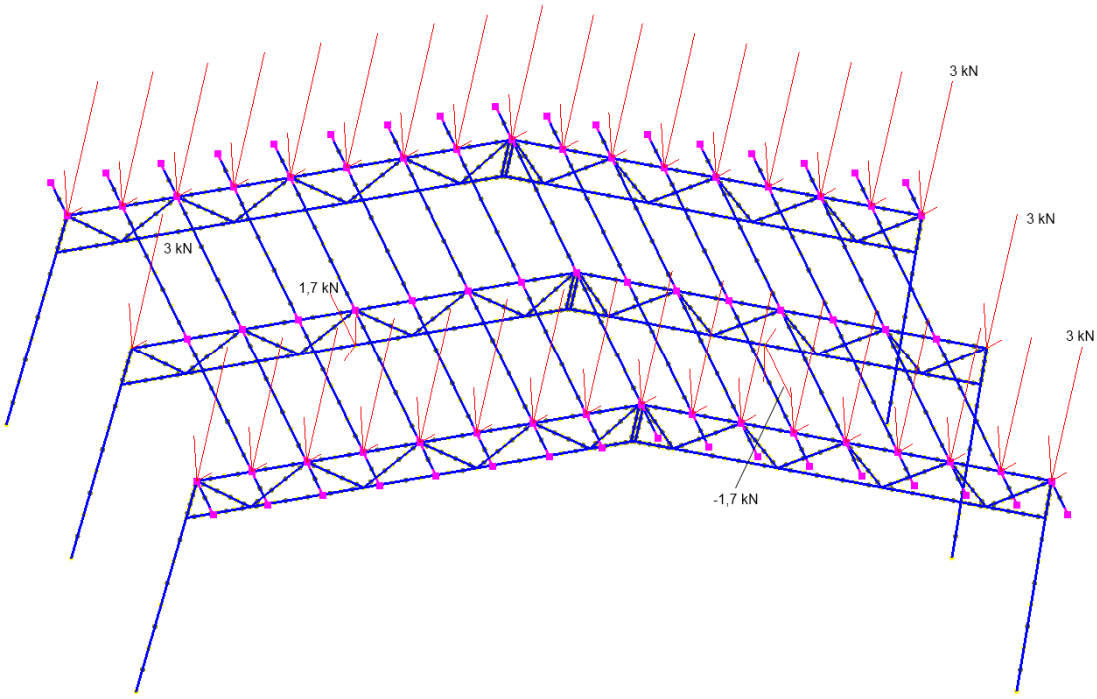

Figure 79 Final analysis, mid-span local fire; point loads

The deformed shape of the structure at every 5 minutes, as well as at 9 minutes when the top chord started to deform rapidly, can be seen in Figure 80, scaled by a factor of 5. The mid-frame behaved in a similar manner to the frame in both local fire 1 and local fire 5, except that no asymmetrical behaviour was found for the upper chords in this analysis.

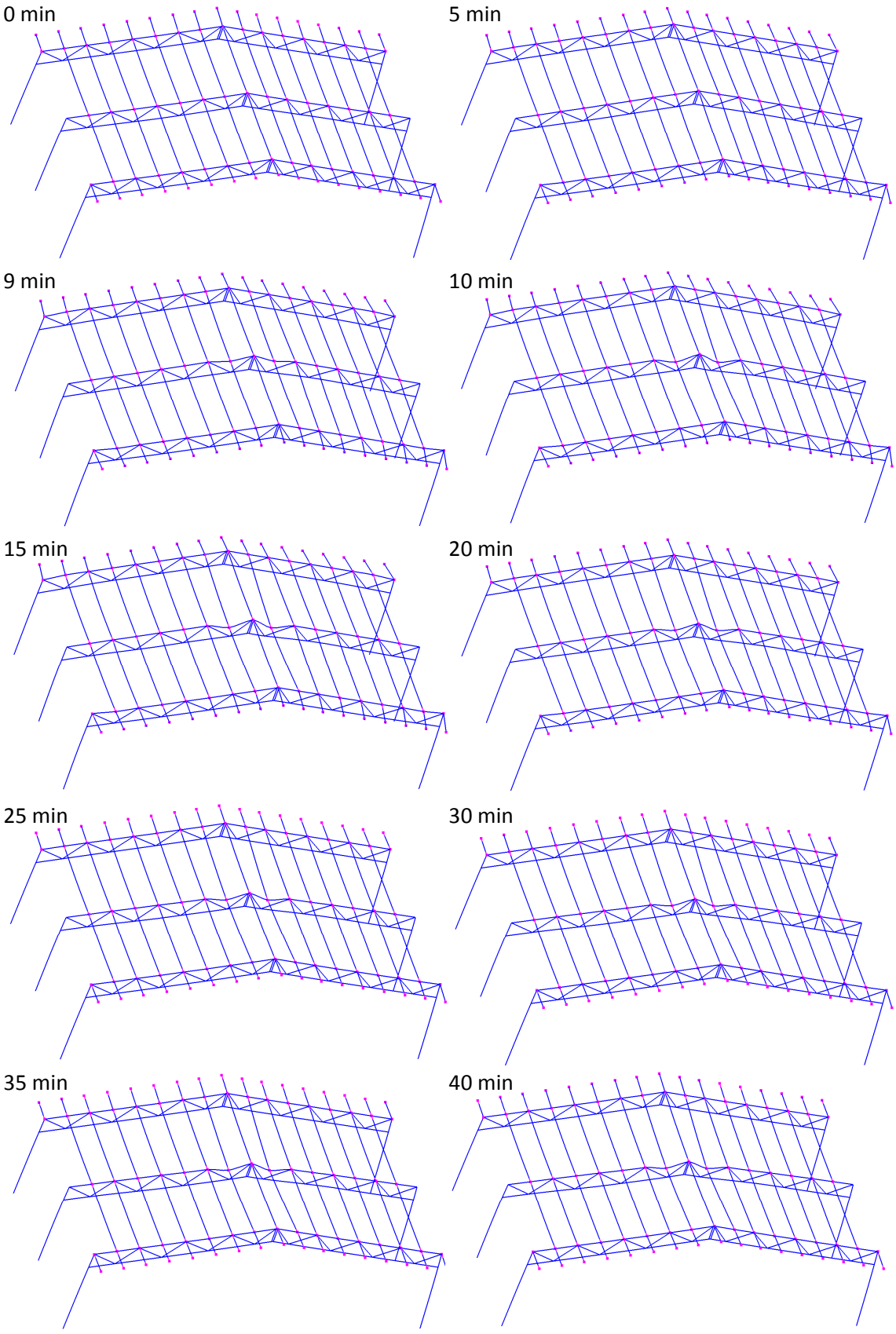

Figure 80 Final analysis, mid-span local fire; 0-40 min

The vertical displacement of the top node of the mid frame is presented in Figure 81. The final deflection was 40,5 mm larger than the initial value before the temperature exposure, i.e. somewhat smaller than in the local fire 5 initial analysis.

The horizontal support reaction of the base connection at the right column of the mid frame is presented in Figure 82, which verifies that the mid frame behaved very similarly to the mid frame in local fire 5. The largest horizontal support reaction took place in the end of the decay phase, reaching a value of 40,5 kN, i.e. almost the same as in the local fire 5 initial analysis.

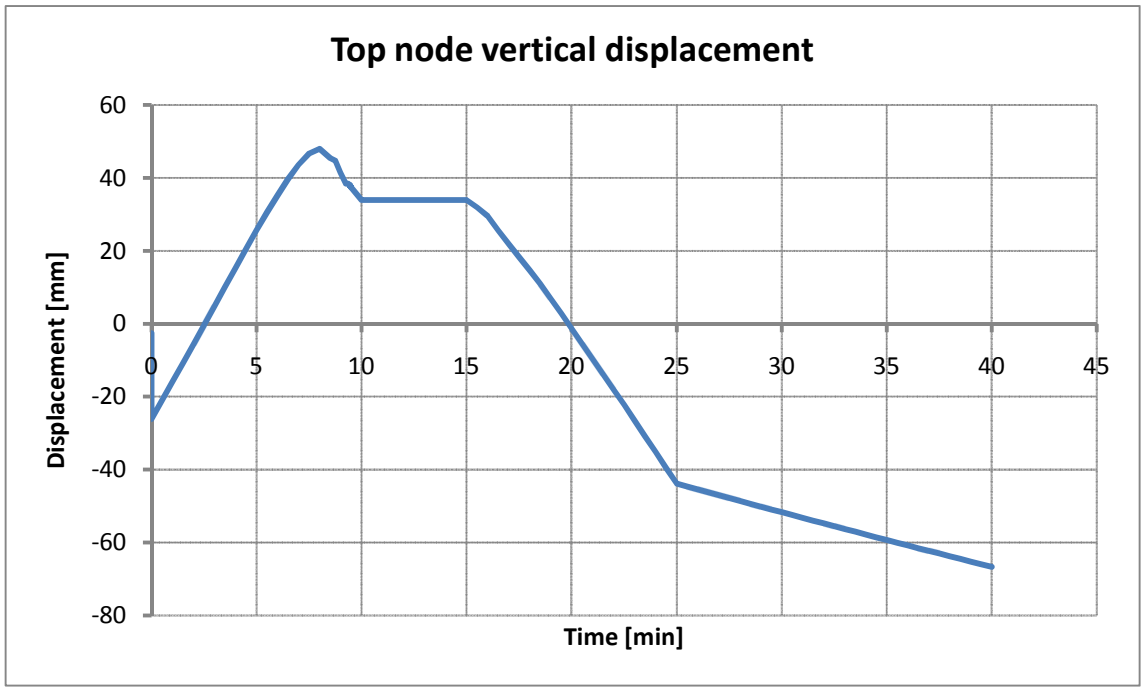

Figure 81 Final analysis, mid-span local fire; vertical displacement at top node

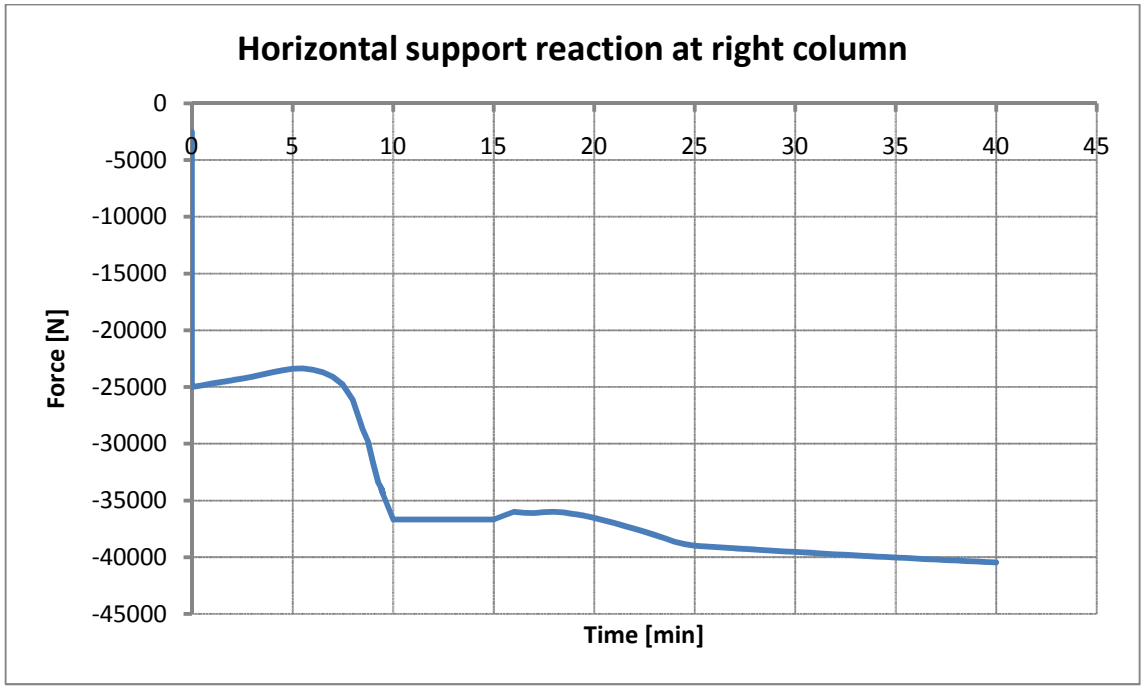

Figure 82 Final analysis, mid-span local fire; horizontal support reaction at base connection

From Figure 80 it can quite clearly be observed that the parts of the upper chords closest to the top of the truss have undergone permanent deformation and would not carry load in the same way as before the fire exposure. This is confirmed by Figure 83, which describes the axial force in the left deformed member as a function of time. Before the fire, the member was in compression, but as the member was heated and the deformation started to grow, the force decreased and was eventually developed into a tensile force in the decay phase. This would in other words mean that the truss behaved differently in the decay phase and after the fire than before the fire exposure.

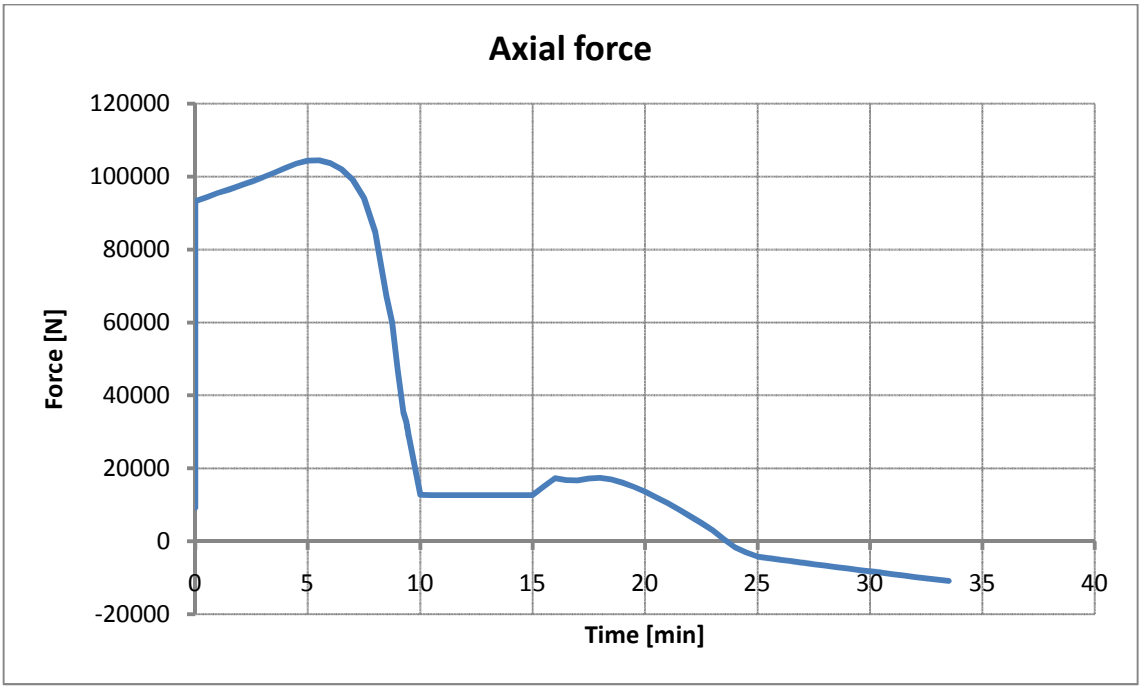

Figure 83 Final analysis, mid-span local fire; top chord axial force

Generally if a steel member has a certain capacity in compression, taking buckling into account, it will be able withstand at least the same force in tension. However, a member designed for tension will not necessarily withstand the same force in compression. Hence it is especially important to check for members designed for tension at ambient temperature but that develop compressive force during or after the fire, as well as members suffering from increasing compressive force.

As previously mentioned the top part of the top chord of the frame in the middle suffered permanent deformation, which in turn lead to a substantial redistribution of the forces in the truss. This was especially true for the bottom chord. In Figure 84 the bottom chord is divided into five different members, which will be studied in more detail by calculating the degree of utilization for each member as a function of time, taking the axial force, bending moments and buckling into account according to Eurocode (26) and (4). For members in tension, the degree of utilization is presented as negative. The results at ambient temperature are basically not valid as the formulas for elevated temperatures were used. The method of calculation is presented in more detail in Annex B.

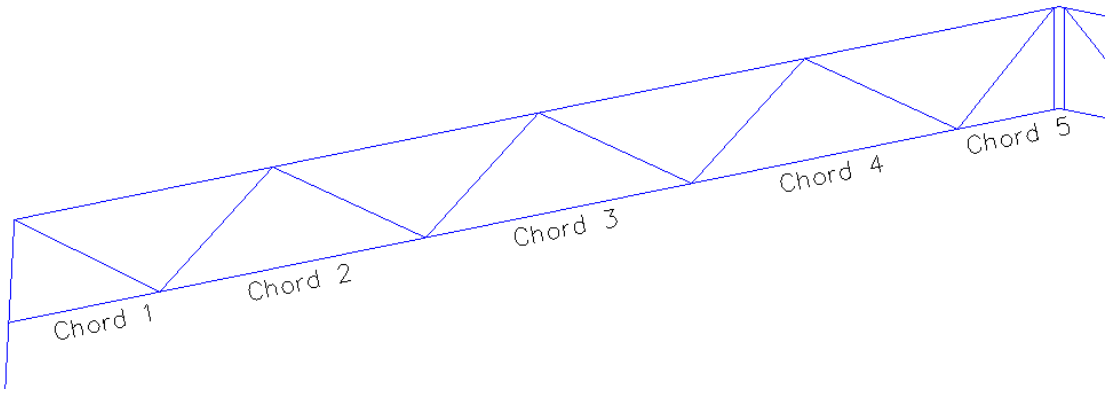

Figure 84 Final analysis, mid-span local fire; bottom chord members

The development of the axial forces of the five chord members is presented in Figure 85. It can clearly be noticed that the forces developed in the same way in all of the members. Initially the two members closest to the column, chords 1 and 2, were in compression as they pressed against the supporting column, whereas the rest of the members, chords 3-5, were in tension. In the heating phase the forces decreased somewhat at first, but started to increase rapidly at about 7 min when the behaviour of the truss started to change. At about 9 minutes all of the members were in compression, i.e. the behaviour of the truss had changed drastically so that the top chord exposed to the highest temperature of 800 °C did not carry any substantial load anymore. The axial forces reached a first maximum in the stationary phase, ranging from 10 to 15 minutes. At the beginning of the decay phase the forces decreased somewhat, but started to increase again from about 18 minutes onwards, reaching their maximum values at the end of the decay phase.

The degrees of utilization according to Eurocode for the five members of the bottom chord, calculated based on the sections and buckling lengths in Table 1, are presented in Figure 86. The buckling lengths were taken as the lengths between the diagonal connection points. For chords 1-4 the highest degree of utilization was reached at the end of the decay phase, whereas for the fifth chord the highest degree of utilization was reached in the stationary phase. For chords 2 and 5 the highest degree of utilization exceeded 100 %, i.e. exceeded the capacity according to Eurocode, but as Vulcan limit the compressive force to the Euler critical buckling load, giving a higher compressive capacity, the members were able to carry the load during the analysis and a stable solution could be found.

The results of the bottom chord are summarized in Table 1.

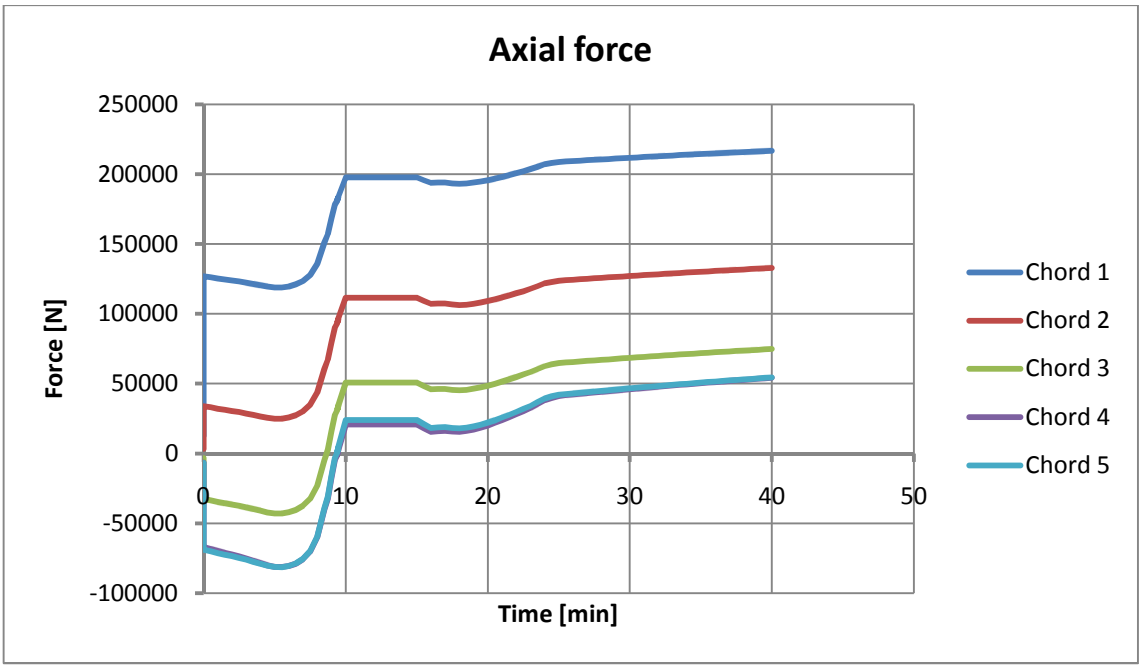

Figure 85 Final analysis, mid-span local fire; bottom chord axial forces

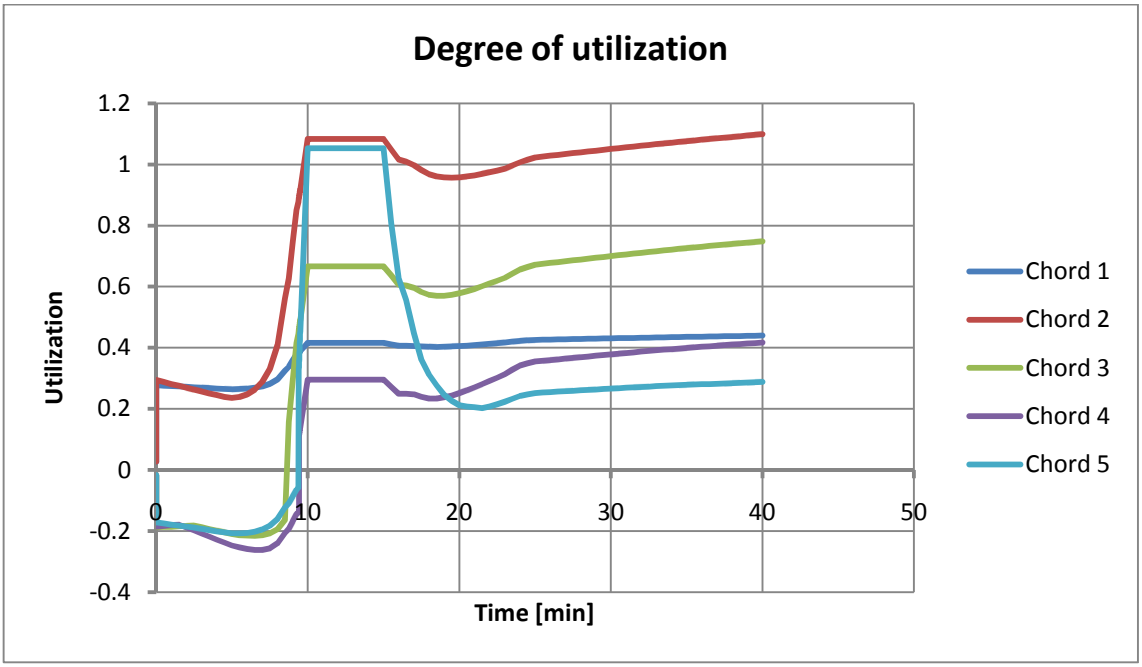

Figure 86 Final analysis, mid-span local fire; bottom chord degrees of utilization

Table 1 Final analysis, mid-span local fire; results for bottom chord

	Section	Length	Initial force	Ultimate compressive force	Ultimate degree of utilization / when reached
Chord 1	CFRHS120x120x6	1,7 m	126,9 kN	216,8 kN	44 % / end of decay
Chord 2	CFRHS80x80x4	3,0 m	33,9 kN	132,8 kN	110 % / end of decay
Chord 3	CFRHS80x80x4	3,0 m	-32,6 kN	74,8 kN	75 % / end of decay
Chord 4	CFRHS80x80x4	3,0 m	-67,0 kN	54,2 kN	42 % / end of decay
Chord 5	CFRHS80x80x4	1,1 m	-68,9 kN	54,5 kN	105 % / stationary phase

As the whole structure was subjected to both thermal expansion and contraction, and due to the fact that the mid-frame behaved differently than the two outer frames, axial forces were developed in the roof purlins. As the structure was bisymmetrical, it's only necessary to study the eight purlins marked in Figure 87.

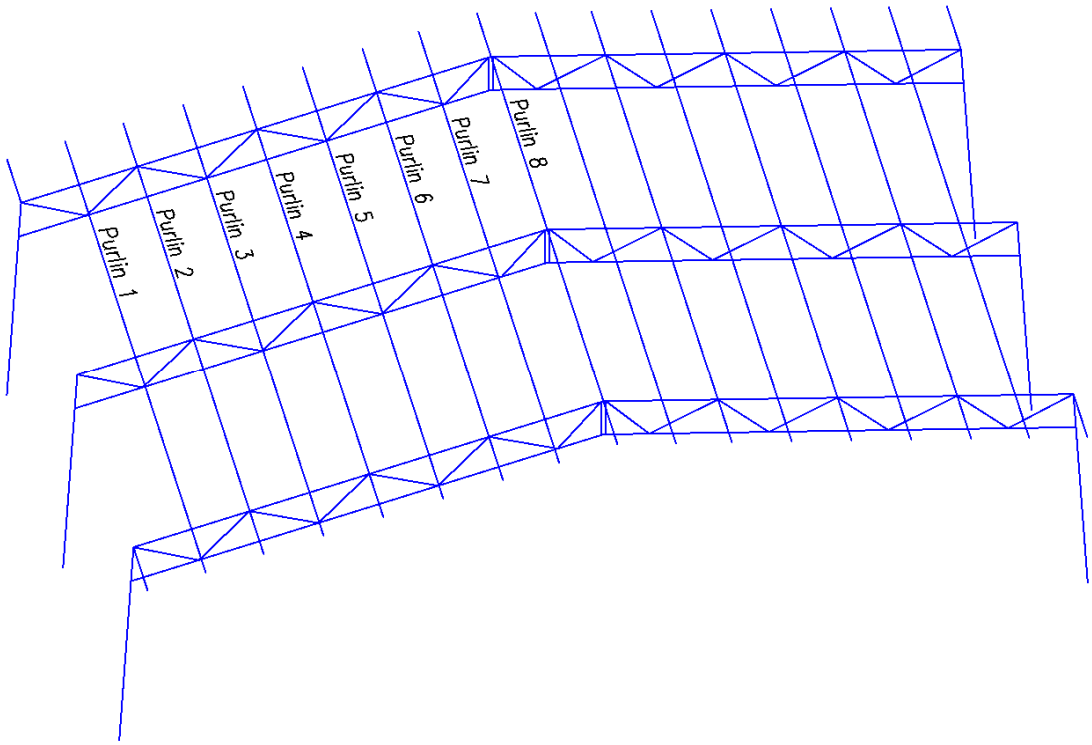

Figure 87 Final analysis, mid-span local fire; purlins

The maximum allowable axial force in pure compression for the purlins in Vulcan can be calculated as the Euler critical buckling load, based on the second moment of area about the weak axis:

$$N_{cr} = \frac{\pi^2 \cdot EI}{(KL_c)^2} = \frac{\pi^2 \cdot 210000\ MPa \cdot 3995000\ mm^4}{(1 \cdot 6000\ mm)^2} = 230\ kN$$

The development of the axial forces in the three outermost purlins included in the analysis, purlins 1-3, is presented in Figure 88. The development of the axial forces for the remaining purlins, purlins 4-8, is presented separately in Figure 89 as the forces in these purlins were much lower than for the three outermost purlins. The reason for the forces being significantly larger in the three outermost purlins is that the spring stiffness at the supports was much higher at the ends of the trusses than at the middle. This was especially true for the second purlin where the spring stiffness was the largest, meaning that also the axial force developed in the purlin was the largest. The general behaviour of all of the purlins was very much the same; the purlins were in tension in the initial loaded state, but developed into compression as soon as the thermal expansion began. The compressive axial forces of all purlins, except for purlins 5 and 7, reached their maxima in the stationary phase. For purlins 5 and 7 the maximum values were reached at the end of the heating phase at about 9 minutes. Especially purlin 7 was affected by the plastic deformations taking place in the part of the top chord of the mid-

frame heated to 800 °C. The axial forces decreased throughout the decay phase. All but purlins 5 and 7 were left with residual compressive forces at the end of the decay phase. Purlins 5 and 7 developed into tension during the decay phase and were left with residual tensile forces at the end of the analysis due to the deformed shape of the truss of the mid-frame.

The degrees of utilization according to Eurocode, calculated based on the profiles and buckling lengths in Table 2, are presented for purlins 1-3 in Figure 90 and for purlins 4-8 in Figure 91. For all but purlin 7 the highest degrees of utilization were reached in the stationary phase. For purlin 7 the highest degree of utilization was reached at the end of the analysis when the tensile force reached its maximum value. Only for purlin 2 the degree of utilization exceeded 100 % according to Eurocode, but as the axial compressive force remained well below the Euler critical buckling load, a stable solution could be reached in Vulcan.

The results are summarized in Table 2.

The sharp corner that can be observed in the figures at 25 minutes was caused by the change of rate of decrease of the temperature taking place at 25 minutes.

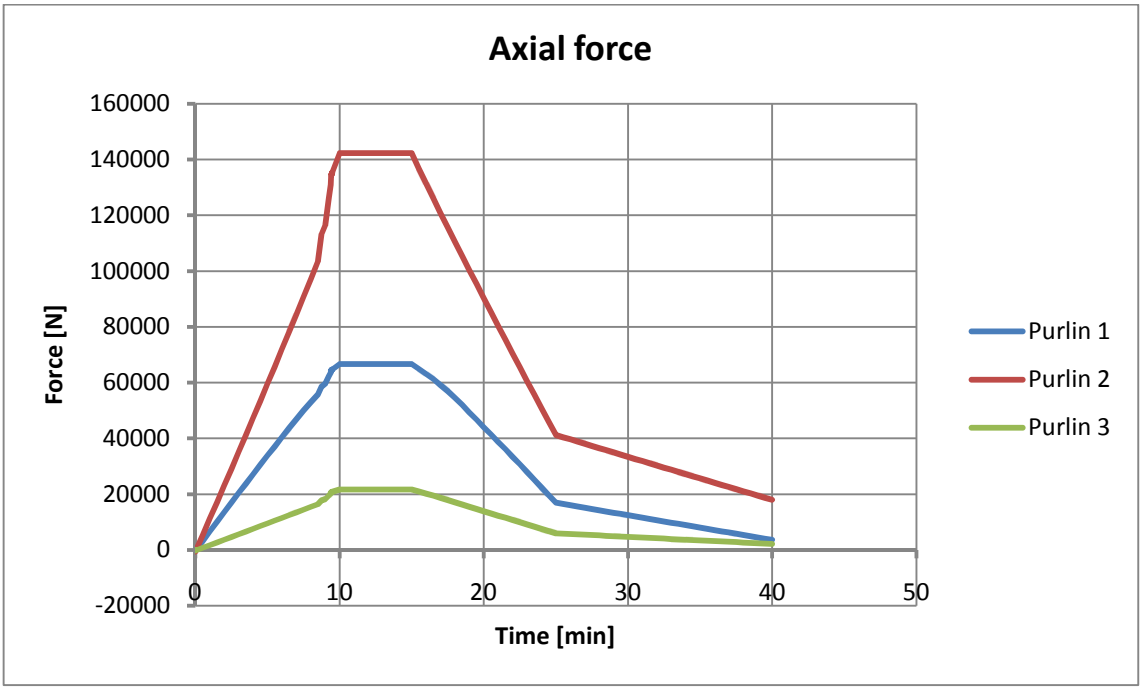

Figure 88 Final analysis, mid-span local fire; purlins 1-3 axial forces

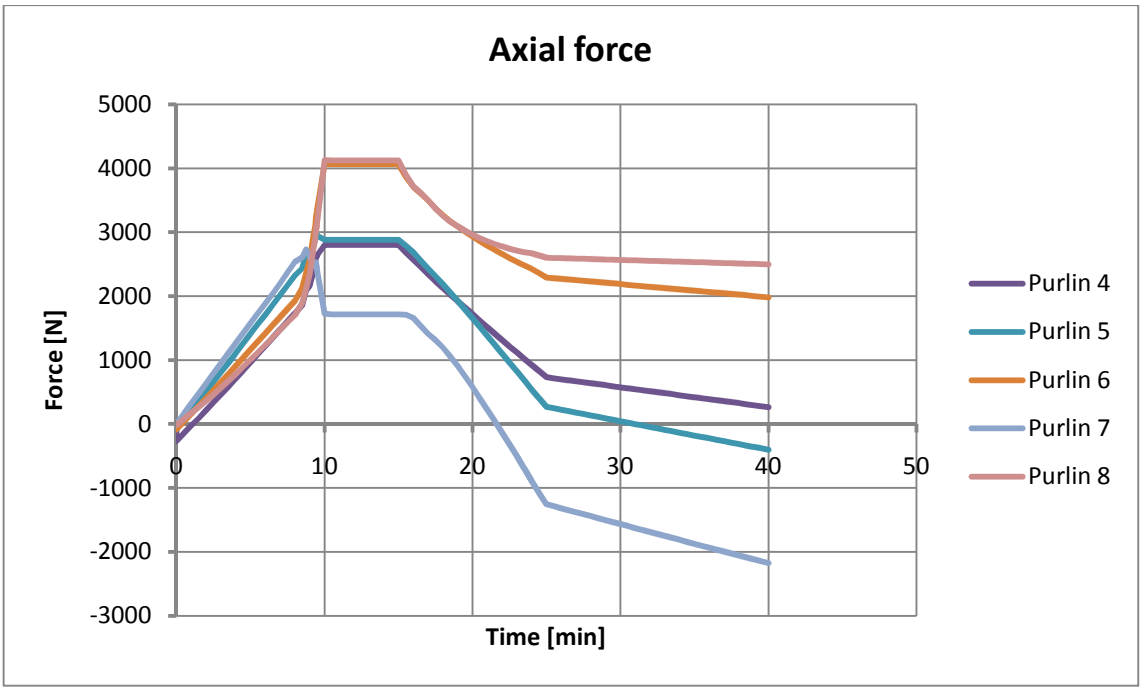

Figure 89 Final analysis, mid-span local fire; purlins 4-8 axial forces

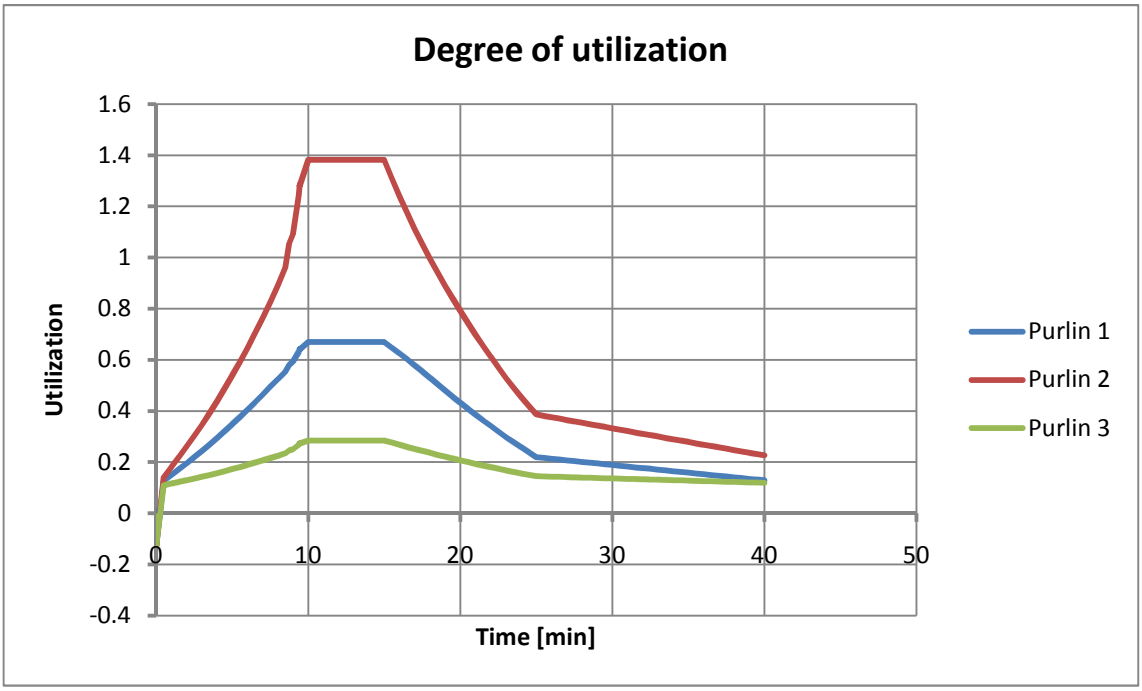

Figure 90 Final analysis, mid-span local fire; purlins 1-3 degrees of utilization

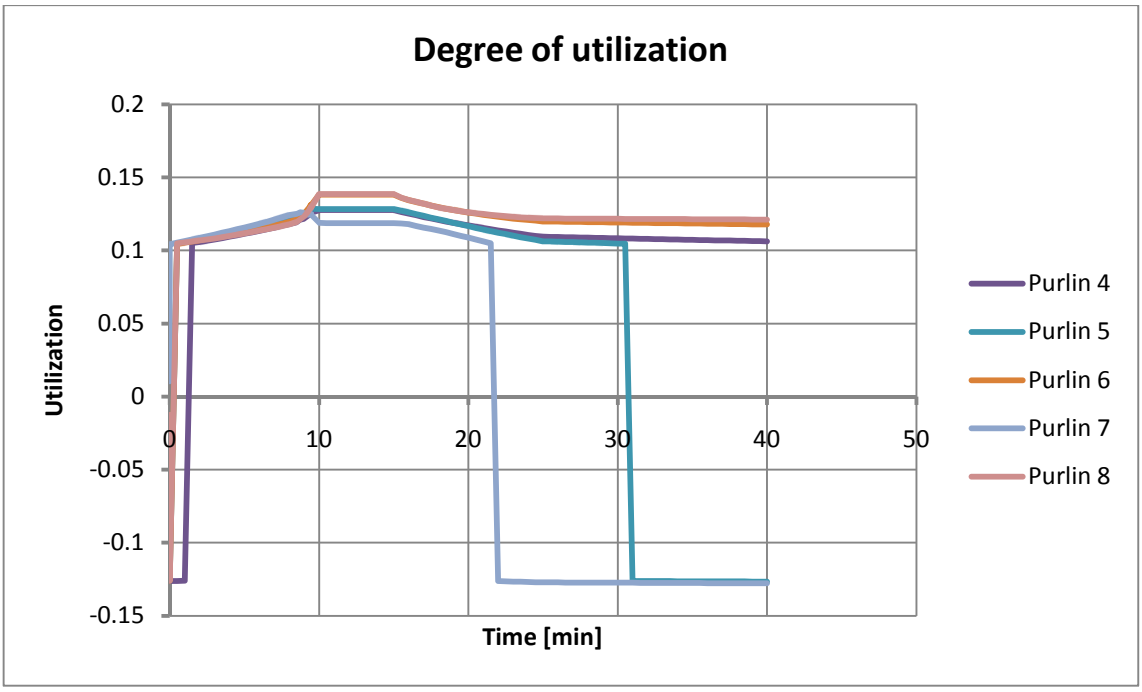

Figure 91 Final analysis, mid-span local fire; purlins 4-8 degrees of utilization

Table 2 Final analysis, mid-span local fire; results for purlins

	Section	Length	Initial force	Ultimate compressive force	Ultimate degree of utilization / when reached
Purlin 1	CFRHS150x100x5	6,0 m	-0,1 kN	66,6 kN	67 % / stationary phase
Purlin 2	CFRHS150x100x5	6,0 m	-0,6 kN	142,3 kN	138 % / stationary phase
Purlin 3	CFRHS150x100x5	6,0 m	-0,2 kN	21,7 kN	28 % /stationary phase
Purlin 4	CFRHS150x100x5	6,0 m	-0,3 kN	2,8 kN	13 % / stationary phase
Purlin 5	CFRHS150x100x5	6,0 m	-0,1 kN	3,0 kN	13 % / stationary phase
Purlin 6	CFRHS150x100x5	6,0 m	-0,1 kN	4,1 kN	14 % / stationary phase
Purlin 7	CFRHS150x100x5	6,0 m	0,0 kN	2,7 kN	-13 % / end of decay
Purlin 8	CFRHS150x100x5	6,0 m	0,0 kN	4,1 kN	14 % / stationary phase

The general behaviour of the mid-frame in this analysis, replicating the situation of a local fire at mid-span, was very similar to the corresponding frames in local fire 1 and local fire 5. This in fact verifies the observation made in local fire 5, that the behaviour of the mid-frame subjected to a local temperature exposure is not dependent on the adjacent frames or the purlins. Furthermore the analysis showed that significant compressive forces develop in the bottom chord, normally designed for tension, as the behaviour of the truss changes when it undergoes plastic deformations. The analysis also showed that large compressive forces develop in the purlins as they are heated, but that they don't affect the structural integrity.

4.3.2 Mid-span local fire, strengthened truss

A second analysis, in which the profile of the top chord of the trusses was changed from CFRHS100x100x5 to CFRHS120x120x8, was performed on the model in order to investigate the effect of strengthening the top chord.

The model performed in very much the same way as in the previous, original, analysis, but the permanent deformations were much smaller, which can be observed from Figure 92 showing a comparison of the vertical displacement of the top node in the mid-frame between the two models. From the figure it can be observed that the strengthened model underwent only small permanent deformations, with an increase in the final vertical deflection of only 5 mm compared to the 40,5 mm in the original model. Hence it could be expected that the overall behaviour of the strengthened model would not change at the same extent as the original model.

The horizontal support reaction at the base connection of the right column of the mid-frame is compared in Figure 93. From the figure it can be observed that the support reaction was only 2 kN bigger at the end of the analysis than in the initial loaded state for the strengthened model, compared to an increase of 15 kN in the original model.

The fact that the behaviour of the truss did not change significantly is confirmed by Figure 94, describing the development of the axial force in the top chord closest to the apex of the truss of the strengthened model. From the figure it can be observed that the member at the end of the analysis carried almost the same load as prior to the fire exposure, the decrease being 13 kN.

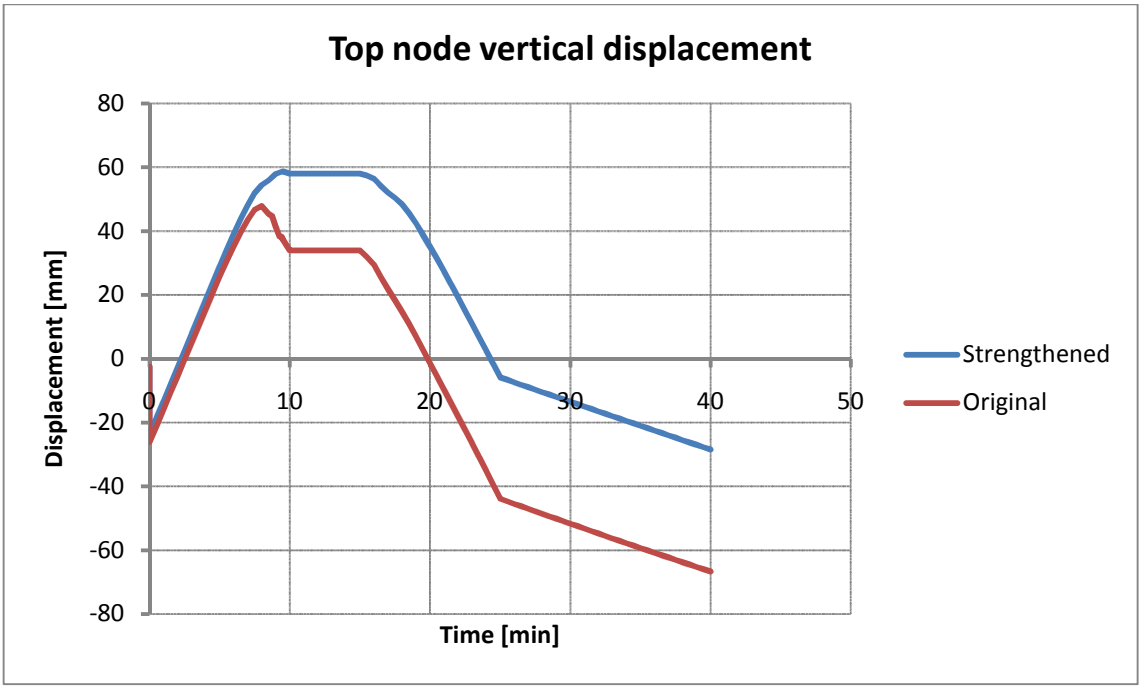

Figure 92 Final analysis, mid-span local fire, strengthened truss; comparison of top node vertical displacement between original and strengthened model

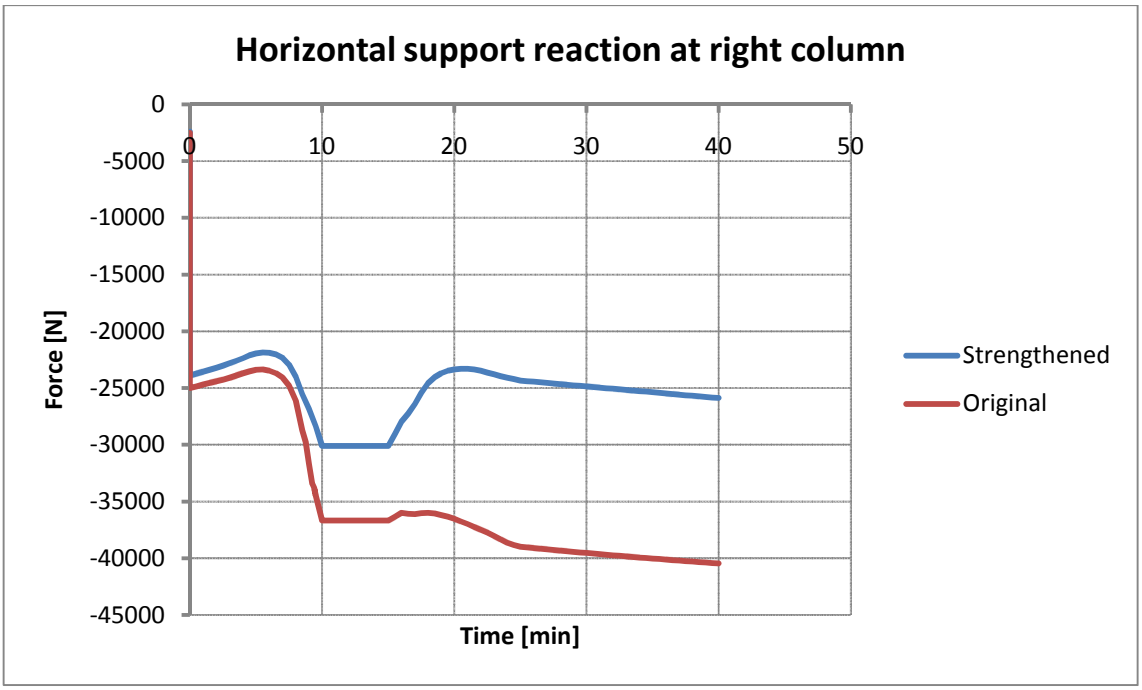

Figure 93 Final analysis, mid-span local fire, strengthened truss; comparison of horizontal support reaction at base connection between original and strengthened model

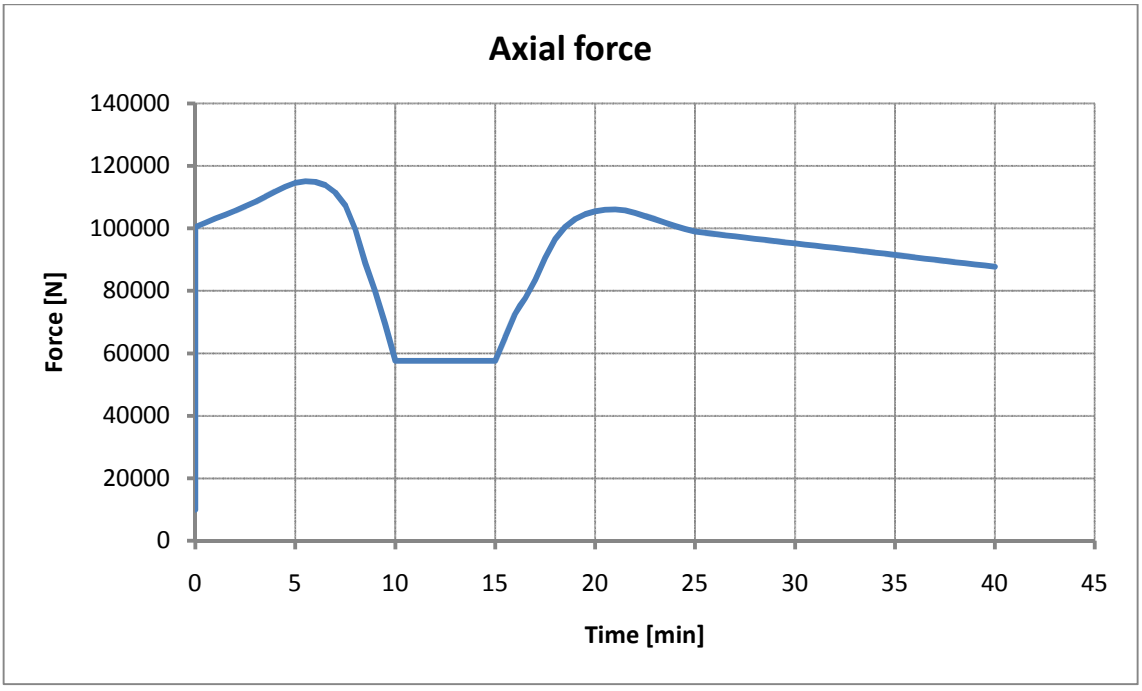

Figure 94 Final analysis, mid-span local fire, strengthened truss; top chord axial force

This analysis showed that by strengthening the top chord any significant change in the behaviour of the truss due to exposure to elevated temperatures could be avoided.

4.3.3 Mid-span local fire, Eurocode temperature development

An analysis on the same, original, model was also performed using the steel temperature development method for unprotected internal steelwork presented in Eurocode 3 part 1-2 (4) where the steel temperature is calculated based on the gas temperature. The gas tempera-

tures where however modified so that the maximum temperatures of the steel members equalled the maximum temperatures used in the two previous analyses. This approach was chosen to study if there were any substantial differences in the results when using a simplified steel temperature development compared to using a steel temperature development calculated with the Eurocode equations, but with equal maximum temperatures. In other words, the target was mainly to study the influence of the shape of the temperature curve. In reality the temperature of the columns would of course be somewhat lower than for the trusses as the section factor of the IPE profile of the columns is smaller than for the hollow sections of the trusses. The same loading and boundary conditions as in the previous analyses were used.

In the temperature development calculations the same section factor, A_m/V = 200/m of the CFRHS100x100x5 profile, was used for all the hollow sections in order to simply the analysis, whereas the section factor for the IPE500 columns was 150,9/m, which also was the case in (25). The coefficient of heat transfer by convection, α_c, was 25 W/m^{2}K. The correction factor for the shadow effect, k_{sh}, the emissivity of the fire, ε_f, and the configuration factor, Φ, were all taken as 1. The surface emissivity of the member, ε_m, was 0,7. The uniform temperature pattern was used in Vulcan also in this case as the steel temperature was calculated separately in Excel.

The mid part of the middle frame, indicated by red in Figure 95, was exposed to the steel temperature curve shown in Figure 96, which also shows the gas temperature curve based on which the steel temperature was calculated.

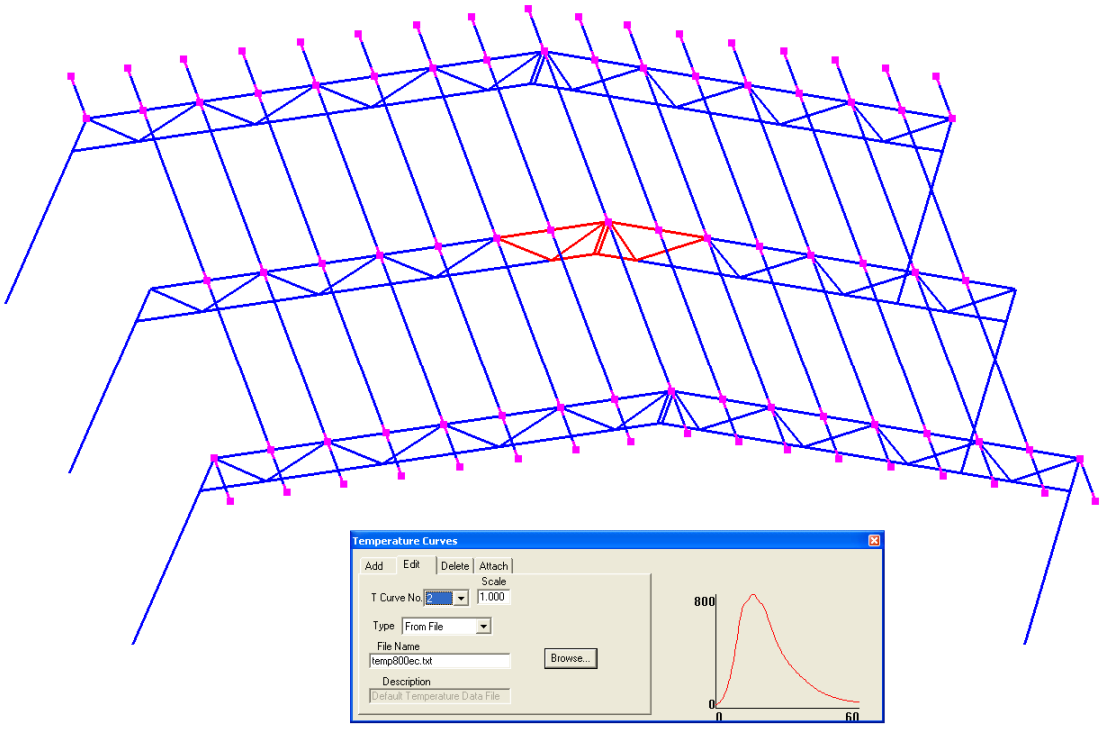

Figure 95 Final analysis, mid-span local fire, Eurocode temperature development; hollow section members exposed to 800 °C temperature curve

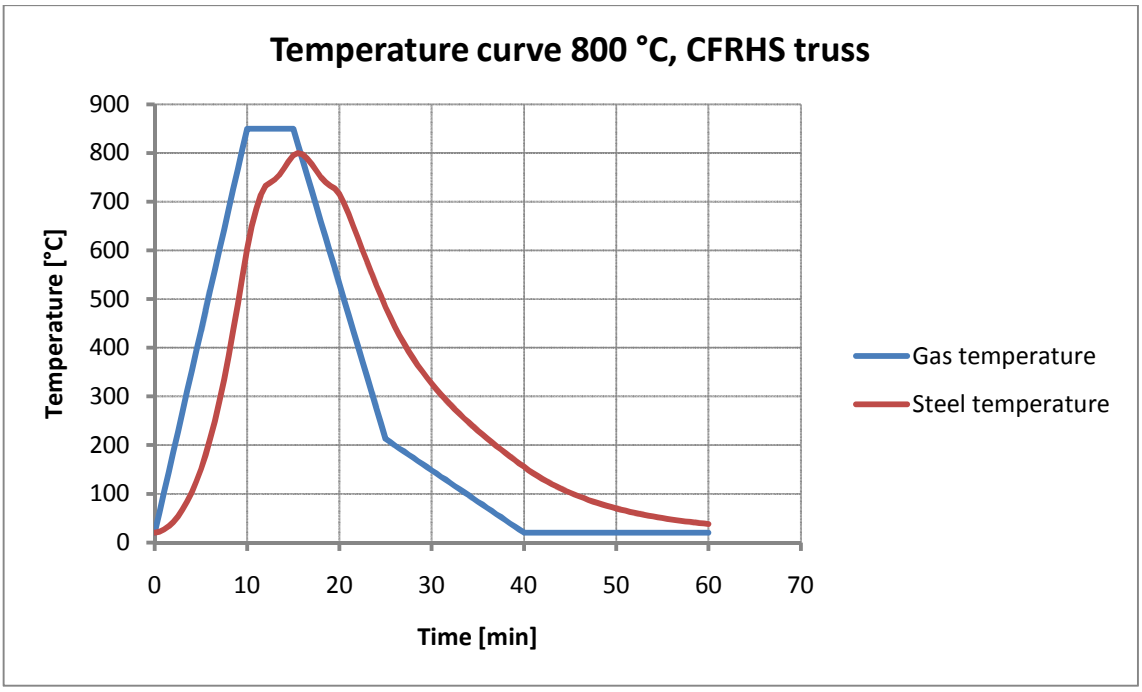

Figure 96 Final analysis, mid-span local fire, Eurocode temperature development; 800 °C temperature curve for CFRHS truss

All other hollow sections, indicated by red in Figure 97, was exposed to the steel temperature curve shown in Figure 98, which also shows the gas temperature curve based on which the steel temperature was calculated.

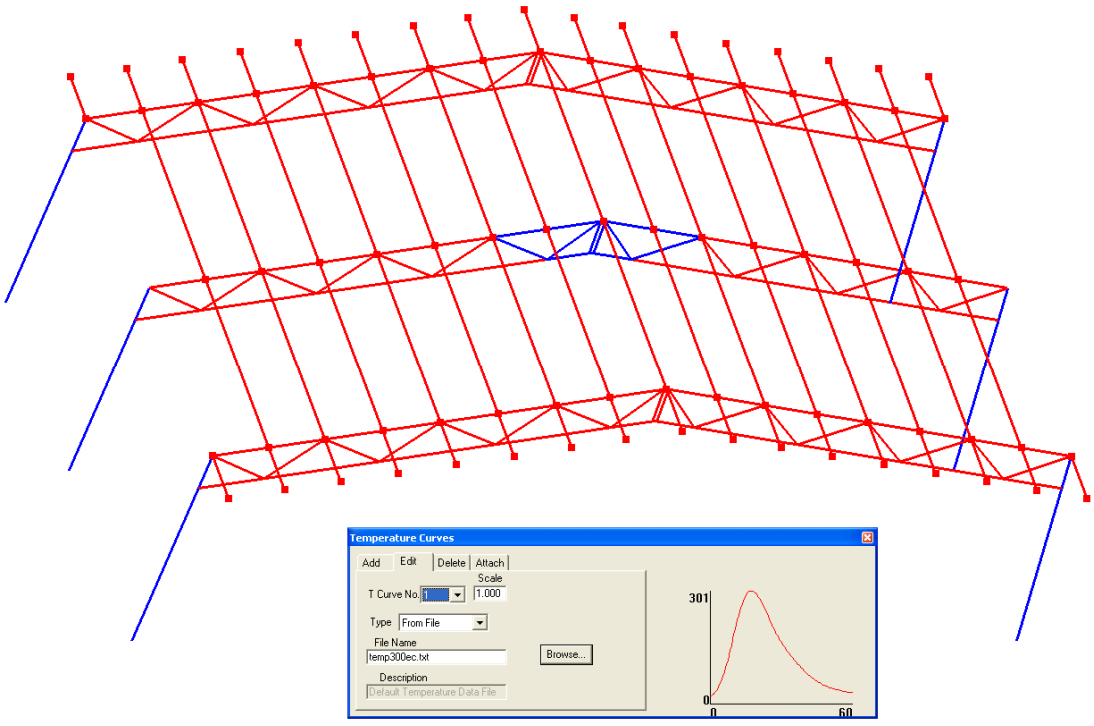

Figure 97 Final analysis, mid-span local fire, Eurocode temperature development; hollow section members exposed to 300 °C temperature curve

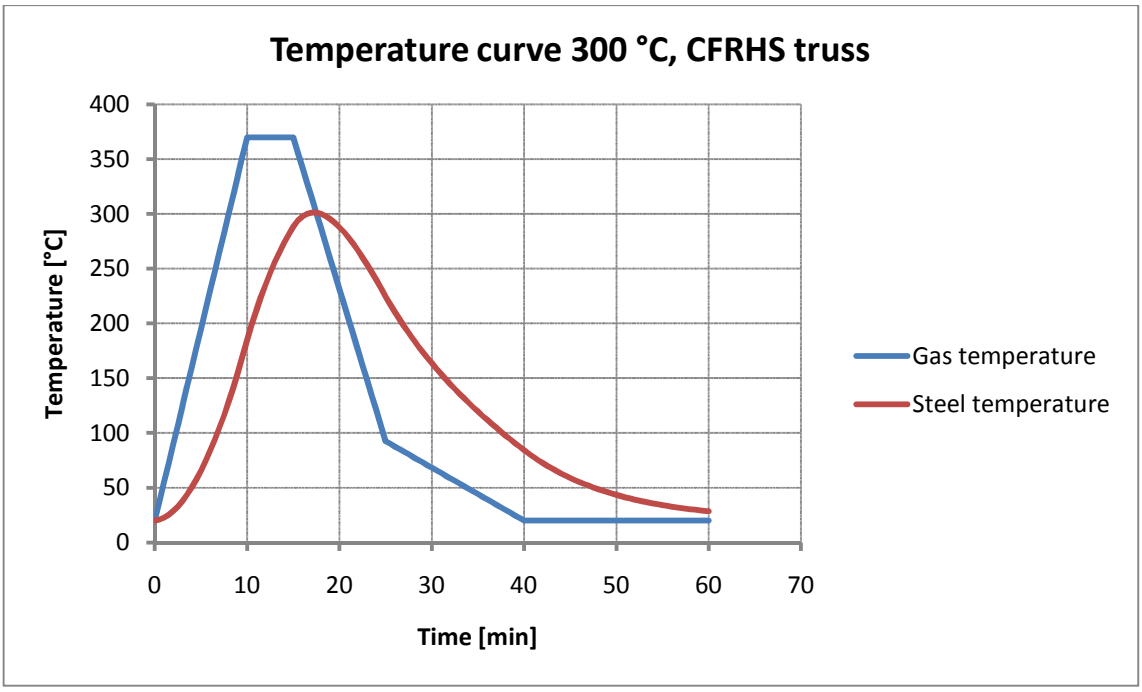

Figure 98 Final analysis, mid-span local fire, Eurocode temperature development; 300 °C temperature curve CFRHS truss

The IPE500 columns, indicated by red in Figure 99, was exposed to the steel temperature curve shown in Figure 100, also showing the gas temperature curve based on which the steel temperature was calculated.

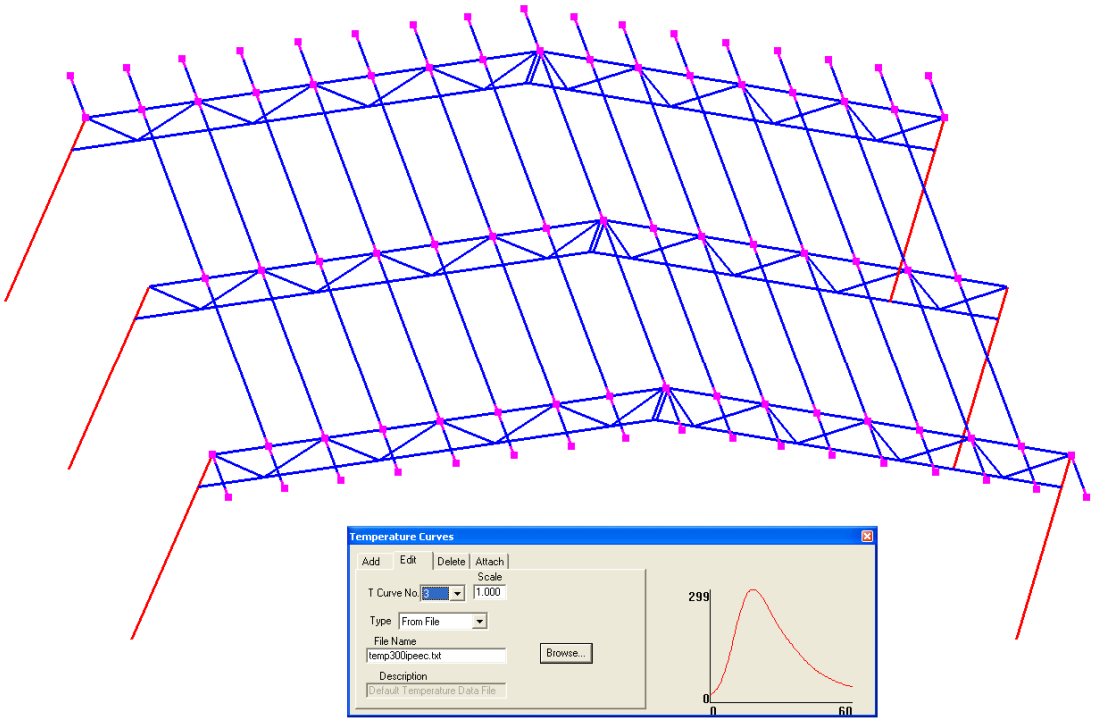

Figure 99 Final analysis, mid-span local fire, Eurocode temperature development; IPE columns exposed to 300 °C temperature curve

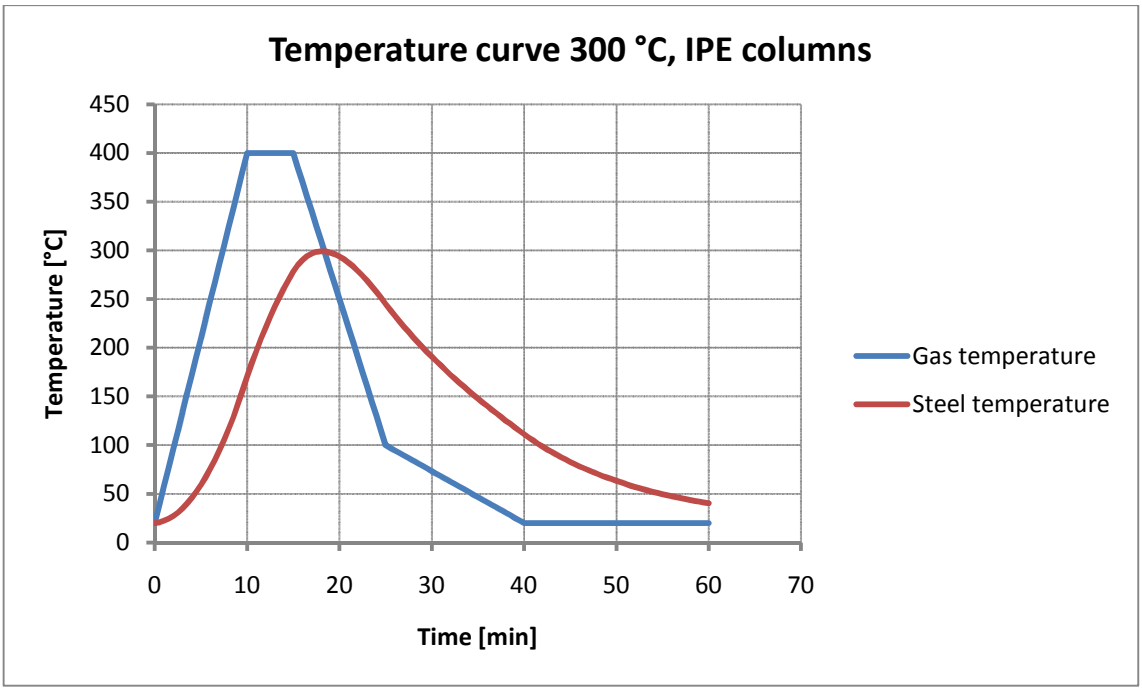

Figure 100 Final analysis, mid-span local fire, Eurocode temperature development; 300 °C temperature curve for IPE columns

The structure behaved very much in the same way as in the corresponding model where the steel temperature was set to directly follow the gas temperature curves. The main difference was that the structure response was slower as the temperature development also was slower, stretching the total analysis time to 60 minutes. This is verified by Figure 101, showing a comparison of the vertical displacement of the top node of the mid frame between the original model, with direct temperature development, and the model with the Eurocode temperature development, as well as by Figure 102, showing a comparison of the horizontal support reaction at the right column base of the mid frame between the two models. From the figures it can clearly be noticed that the general pattern of both the displacement and support reaction curves as well as the value of the displacements and support reactions essentially are similar in both models even though there is a clear shift in time, meaning that the linear simplification of the steel temperature development is acceptable in design. The linear simplification however of course has to be done based on the real temperature development of the steel, i.e. the development calculated according to Eurocode.

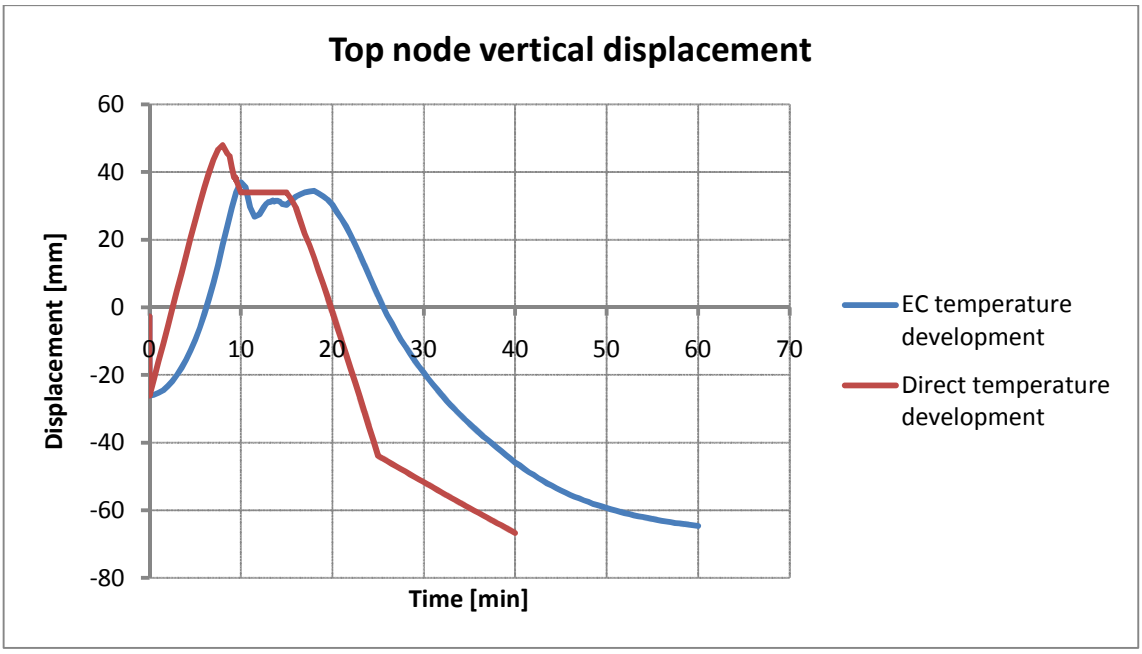

Figure 101 Final analysis, mid-span local fire, Eurocode temperature development; comparison of top node vertical displacement between original and Eurocode model

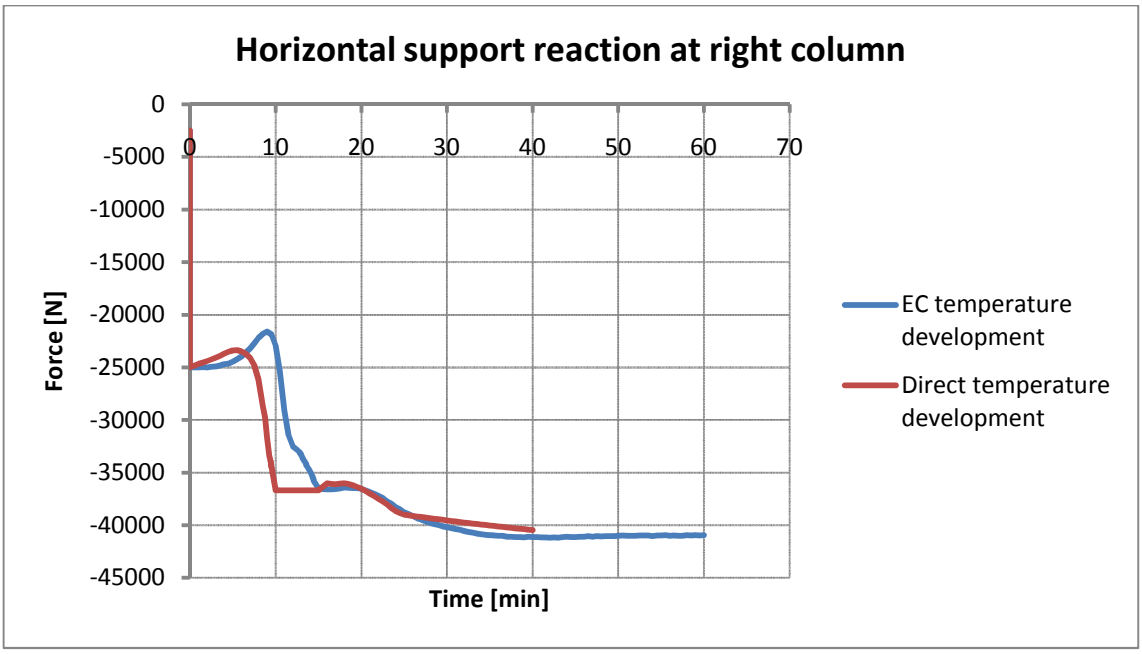

Figure 102 Final analysis, mid-span local fire, Eurocode temperature development; comparison of horizontal support reaction at base connection between original and Eurocode model

4.3.4 Quarter span local fire

The original model was also analysed subjected to a fire at one quarter of the span from one column. The part of the truss subjected to the most severe temperature curve in Figure 47, reaching 800 °C, is marked with red in Figure 103. The remaining parts of the structure were subjected to the temperature curve in Figure 48, reaching 300 °C. Otherwise the structure was analysed using the same loads and boundary conditions as in previous analyses, using the uniform temperature pattern in Vulcan, i.e. the temperature of the steel was assigned to directly follow the gas temperature curve.

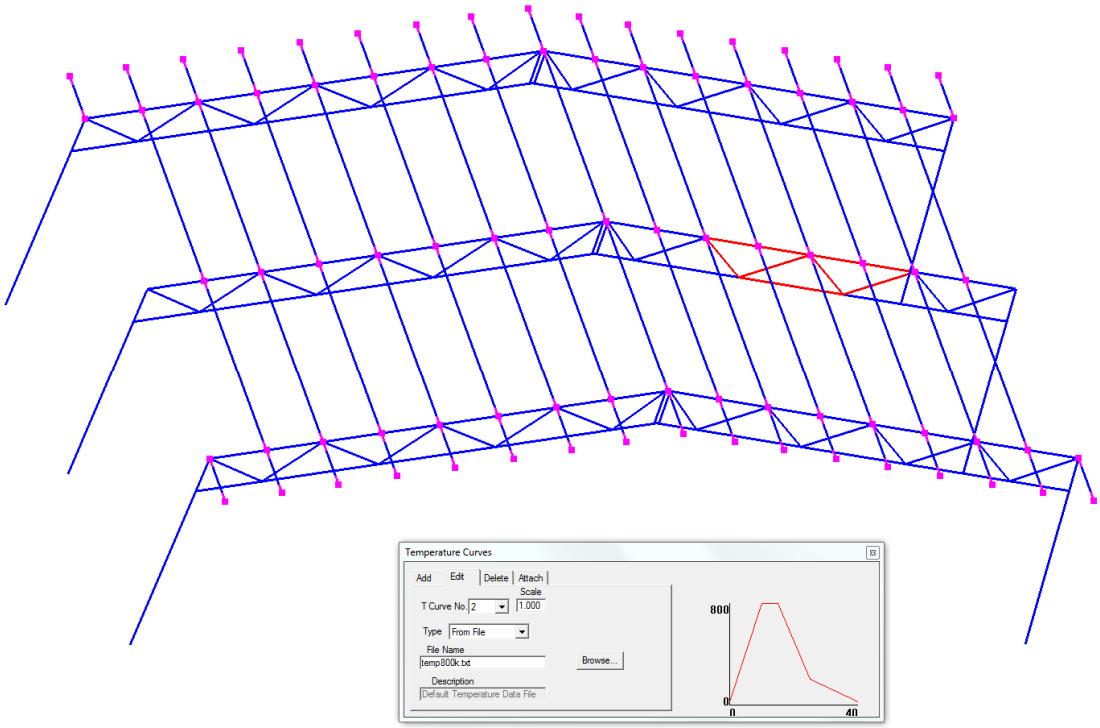

Figure 103 Final analysis, quarter span local fire; parts subjected to 800 °C temperature curve

The analysis ran for about 8 minutes when it failed prematurely due to numerical instability caused by buckling of one of the diagonals subjected to the temperature curve reaching 800 °C. The situation at 8 minutes, when the maximum temperature was about 644 °C, can be seen in Figure 104 for a section of the mid-frame, the failed member being the fourth diagonal from the right.

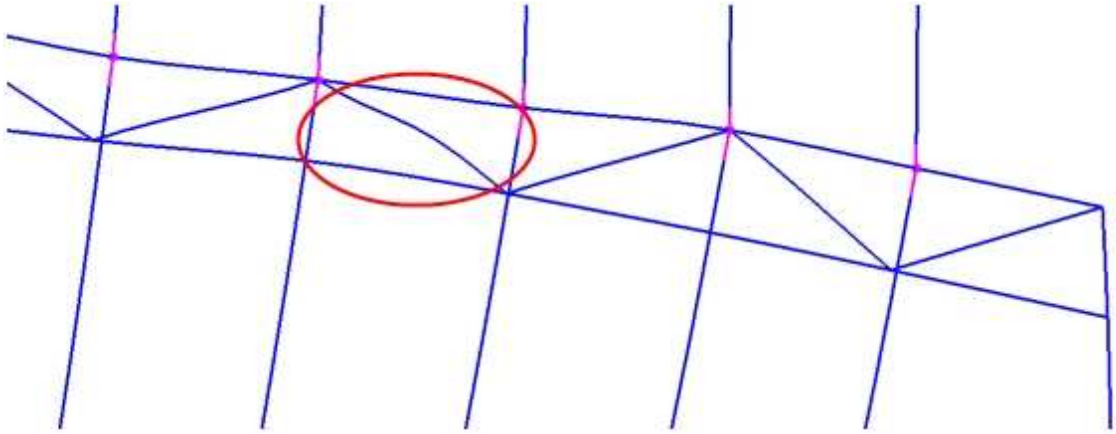

Figure 104 Final analysis, quarter span local fire; diagonal failing in buckling fourth from right

4.3.5 Quarter span local fire, strengthened model

The same quarter span local fire model was analysed once more, the only difference being that all the diagonals were strengthened by changing the cross-section from CFRHS60x60x4 and CFRHS50x50x4 to CFRHS120x120x6, i.e. the strengthening was very substantial but the target was only to prevent the diagonals from buckling. This analysis ran without failure through the whole 40 minutes of exposure to elevated temperatures.

The deformed shape of the structure at every 5 minutes, as well as at 9 minutes when the top chord start to deform rapidly, can be seen in Figure 105, scaled by a factor of 5.

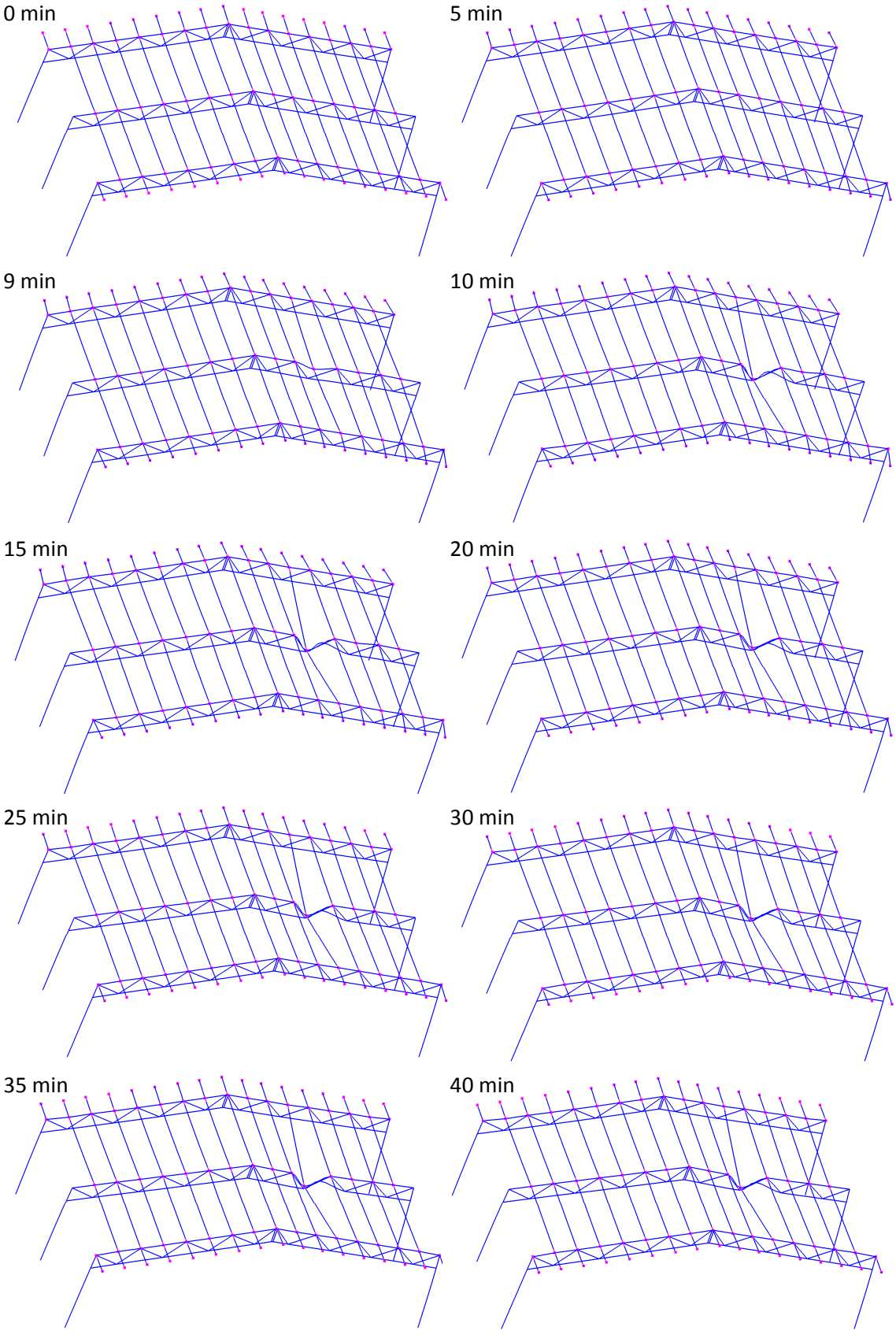

Figure 105 Final analysis, quarter span local fire, strengthened model; 0-40 min

From the previous figure it can be observed that the structure undergoes rather large plastic deformations; a part of the heated top chord deflects downward due to the load imposed from the roof purlins and a part of the bottom chord deflects out of plane due to the horizontal imperfection load applied at one quarter of the span from the column.

The vertical displacement of the top node of the mid frame is presented in Figure 106. The final deflection was 55,0 mm larger than the initial value before the temperature exposure, i.e. almost 15 mm larger than in the mid-span local fire.

The horizontal support reactions of the base connections at both columns of the mid frame are presented in Figure 107, which clearly shows that the behaviour is not symmetrical anymore. The largest horizontal support reaction at the left column, i.e. the one further away from the section of the truss exposed to the higher temperature, took place during the stationary phase, reaching a value of 36,1 kN. The largest horizontal support reaction at the right column took place at 9,5 minutes into the analysis, reaching 30,7 kN, but the same value was also reached at the end of the decaying phase.

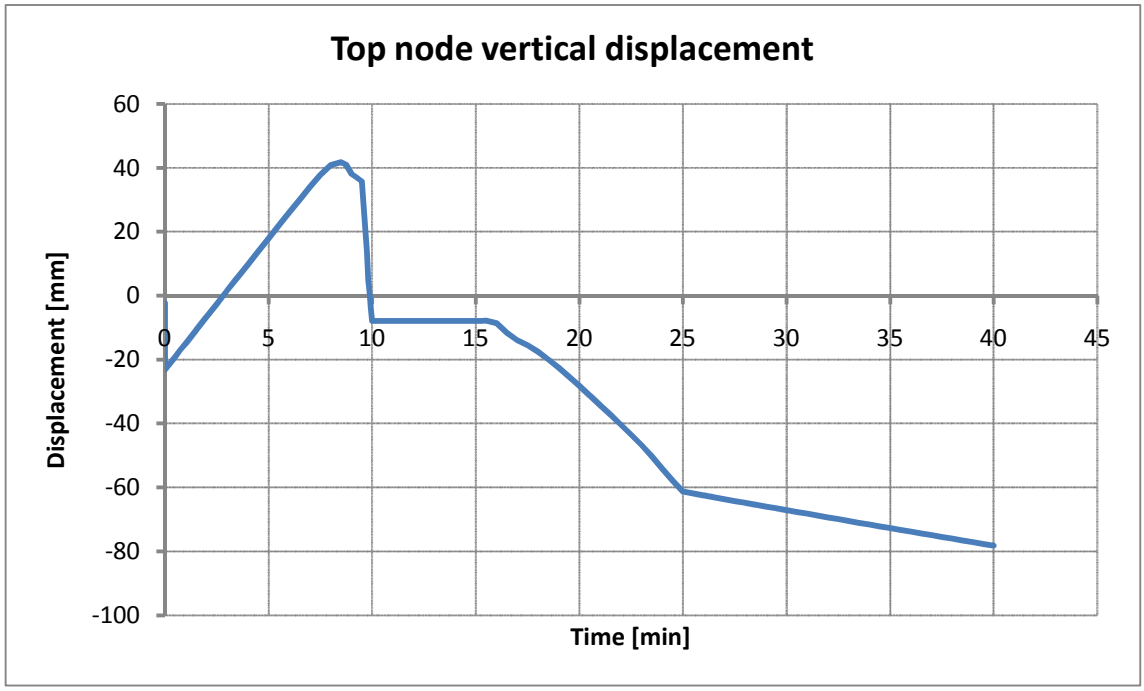

Figure 106 Final analysis, quarter span local fire, strengthened model; vertical displacement at top node

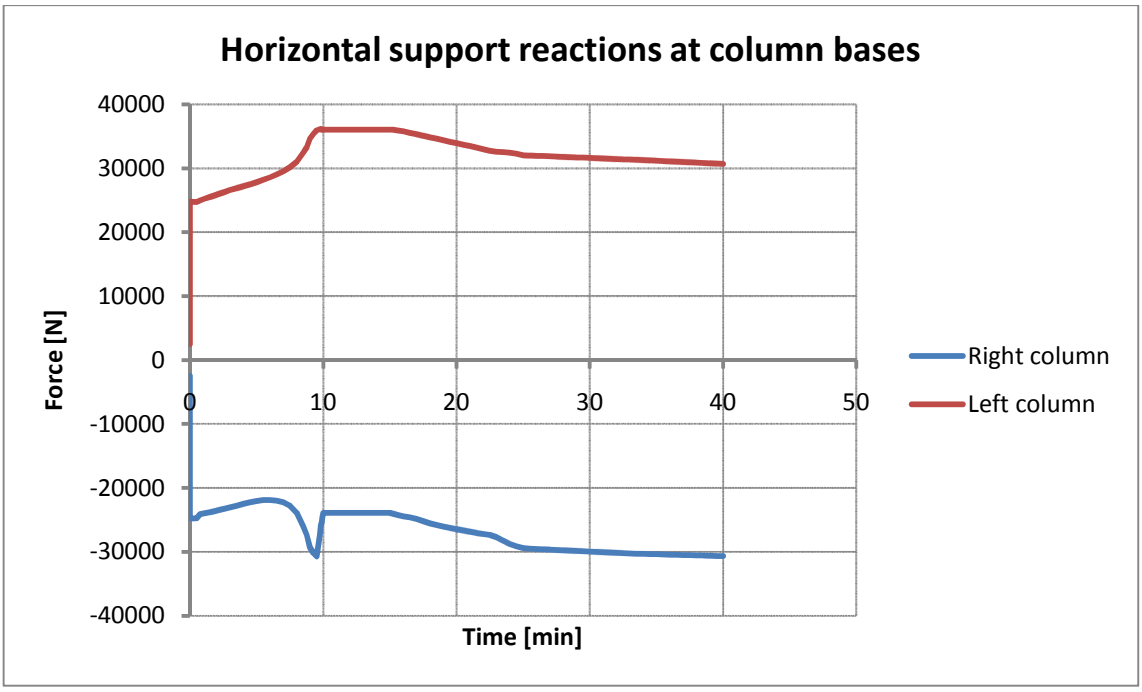

Figure 107 Final analysis, quarter span local fire, strengthened model; horizontal support reactions at base connections

As stated before, part of the upper chord, exposed to the temperature curve reaching 800 °C, underwent permanent deformation and would therefore not be able to carry load in the same way as before the fire exposure. This is confirmed by Figure 108, which describes the axial force in the part of the upper chord that underwent the large deformations as a function of time. Before the fire, the member was in compression, but as the member was heated and the deformation started to grow, the force decreased and was eventually developed into a tensile force in the decay phase, meaning that the truss behaved differently in the decay phase than before the fire exposure.

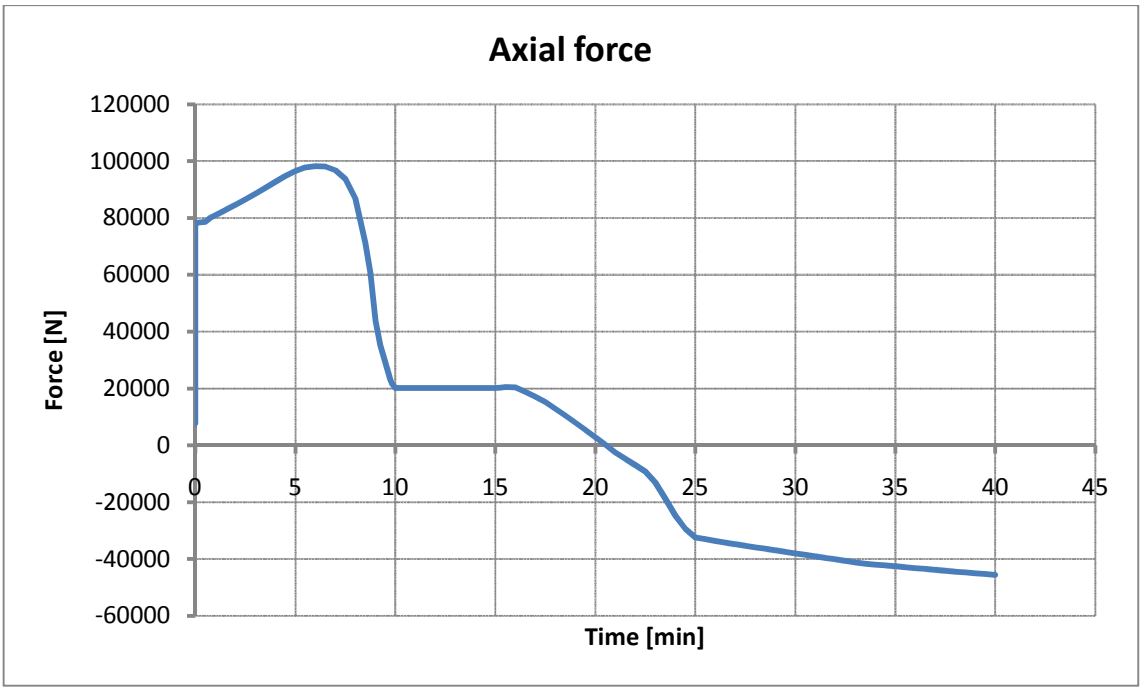

Figure 108 Final analysis, quarter span local fire, strengthened model; top chord axial force

The bottom chord of the truss was divided into ten members according to Figure 109. Each member was studied separately and the degrees of utilization calculated according to Eurocode (26) and (4), taking the axial force, bending moments and buckling into account.

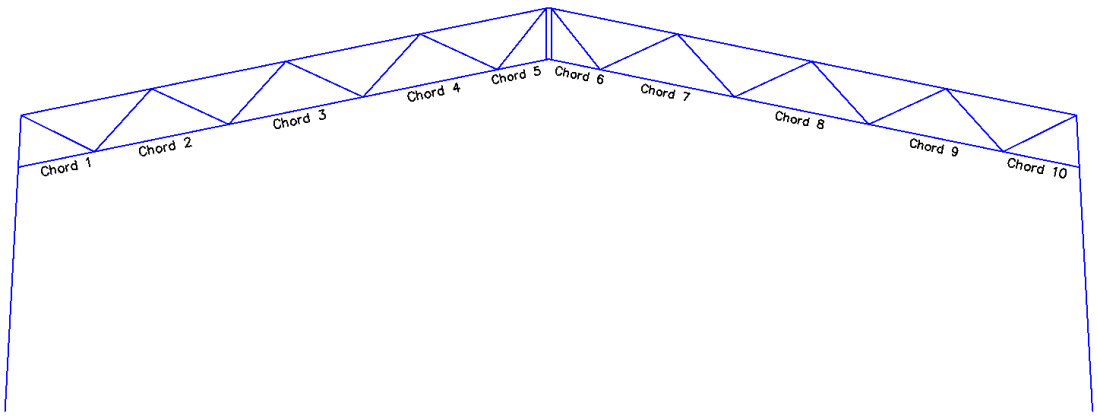

Figure 109 Final analysis, quarter span local fire, strengthened model; bottom chord members

The development of the axial forces for the members of the bottom chord on the left side, chords 1-5, is presented in Figure 110 and for the right side, chords 6-10, in Figure 111. The members on the left side of truss were not exposed to any temperatures that would have affected the strength of the steel, reaching a maximum of only 300 °C, as opposed to the right side where part of the structure was exposed to temperatures as high as 800 °C.

Chords 1 and 2 were initially in compression as they pressed against the supporting column. In the heating phase the axial forces of these chord members started to increase slowly due to thermal expansion until the truss started to undergo large deformations on the right side causing the axial forces to increase rapidly until reaching their maxima in the stationary phase. In

the decay phase the forces decreased slowly but remained in compression throughout the analysis. The residual forces in these two chord members were higher than the initial ones.

Chords 3-5 were initially in tension but the axial forces started to increase rapidly and were developed into compression as the right side of the truss started undergoing plastic deformations. In the decay phase the forces initially decreased somewhat but started increasing again at about 25 minutes when the rate of cooling changed and remained in compression to the end of the analysis at 40 minutes.

The development of the axial forces of the members of the bottom chord on the right side all followed the same pattern. Chords 6-8 were initially in tension whereas chords 9 and 10 initially were in compression as they pressed against the supporting column. In the heating phase the axial forces started to decrease slowly until about 7 minutes when the behaviour of the truss started to change causing the forces to increase rapidly. Between 9,5 and 10 minutes the forces decreased again as the shape of the truss changed drastically. In the stationary phase all but chord 7 were in compression. In the decay phase the forces started increasing in chord members 5, 8 and 9, whereas for chords 6 and 7 the forces initially decreased somewhat but started to increase at about 19 minutes. For all of the bottom chord members on the right side the maximum compressive forces were reached at the end of the analysis at 40 minutes.

The degrees of utilization according to Eurocode, calculated based on the profiles and buckling lengths presented in Table 3, are presented in Figure 112 for bottom chord members 1-5 and in Figure 113 for bottom chord members 6-10. For chords 1-3 the maximum degrees of utilization were reached in the stationary phase, none however exceeding the capacity according to Eurocode. Chords 4-6 reached their maximum degrees of utilization during the heating phase, still being at low levels throughout the analysis. Chord 7 reached its maximum degree of utilization at the end of the analysis at 40 minutes. The maximum value for chord 8 was as high as 401 % in the end of the heating phase and remained high during the stationary phase. This was due to the large deformations of the truss and the bending moments developed in it, however, Vulcan was still able to find a stable solution for the structure. Also for chords 9 and 10 the maximum values were reached in the heating phase, when the value for chord 9 was close to 100 %.

The results for the members of the bottom chord are summarized in Table 3.

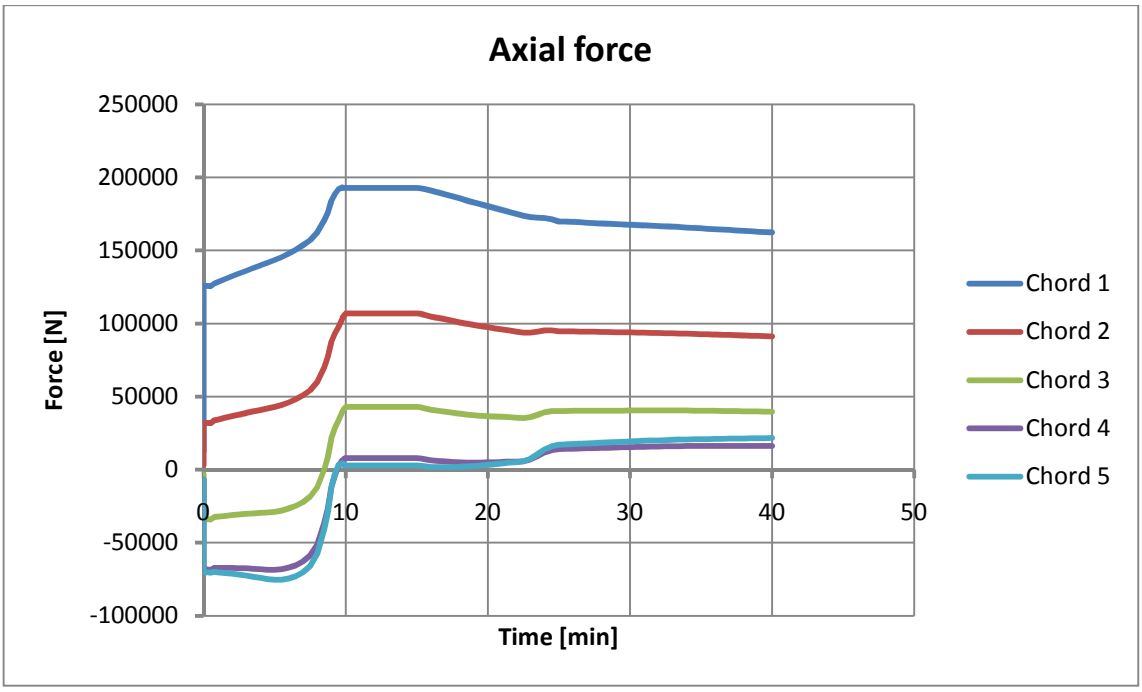

Figure 110 Final analysis, quarter span local fire, strengthened model; bottom chord members 1-5 axial forces

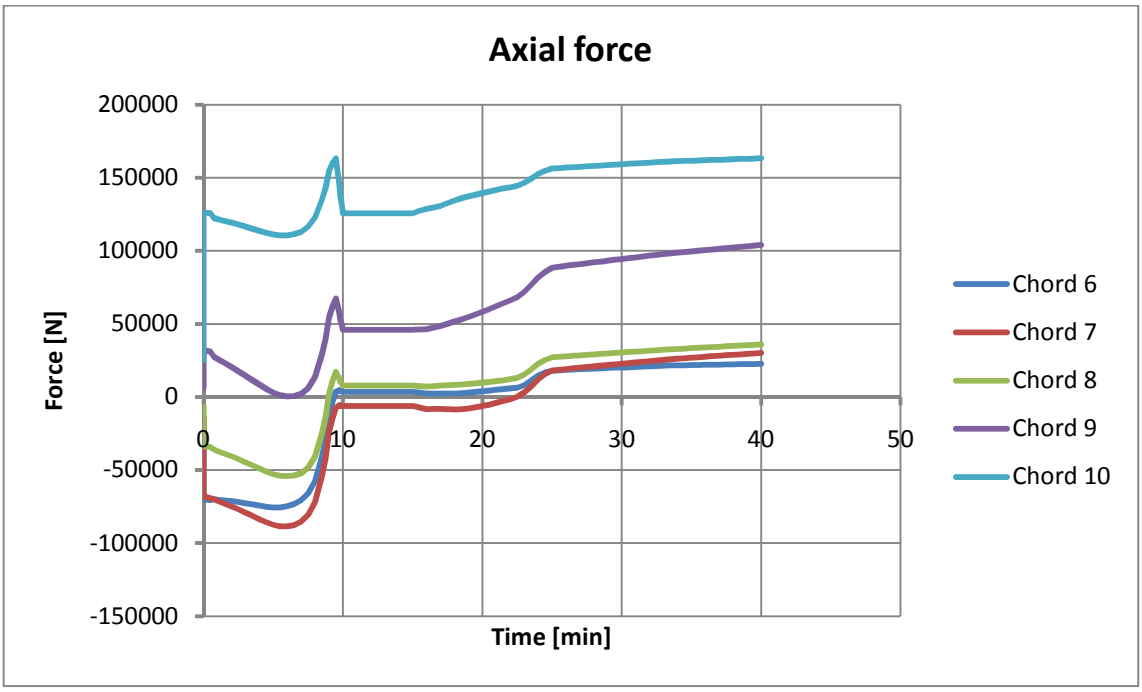

Figure 111 Final analysis, quarter span local fire, strengthened model; bottom chord members 6-10 axial forces

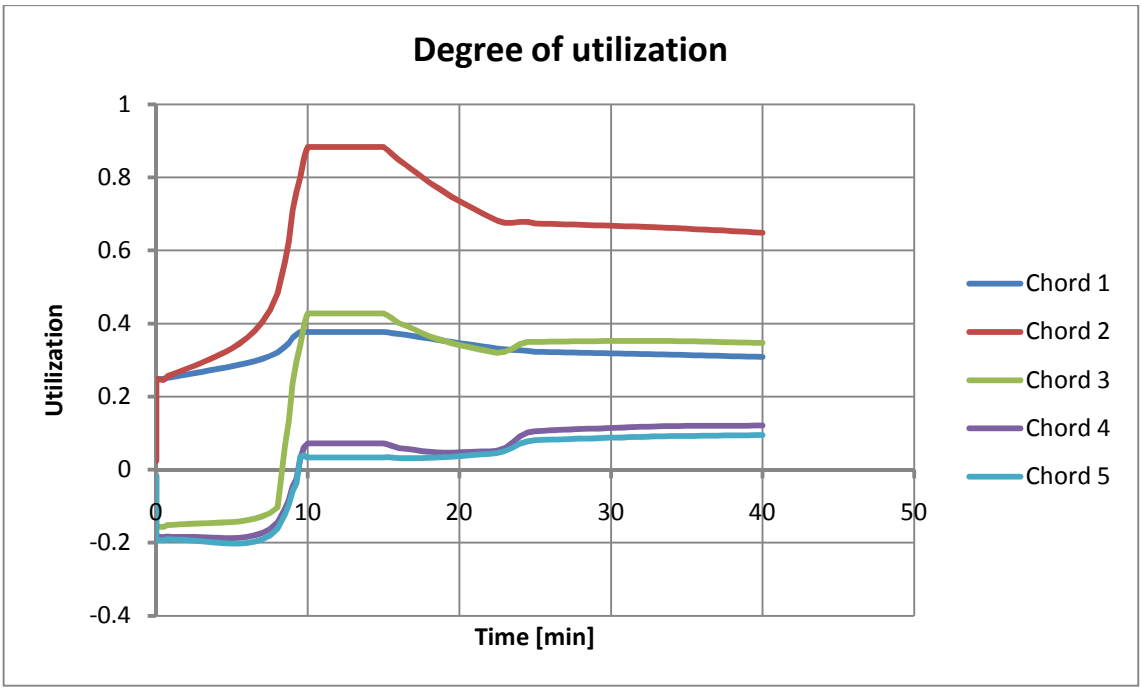

Figure 112 Final analysis, quarter span local fire, strengthened model; bottom chord members 1-5 degrees of utilization

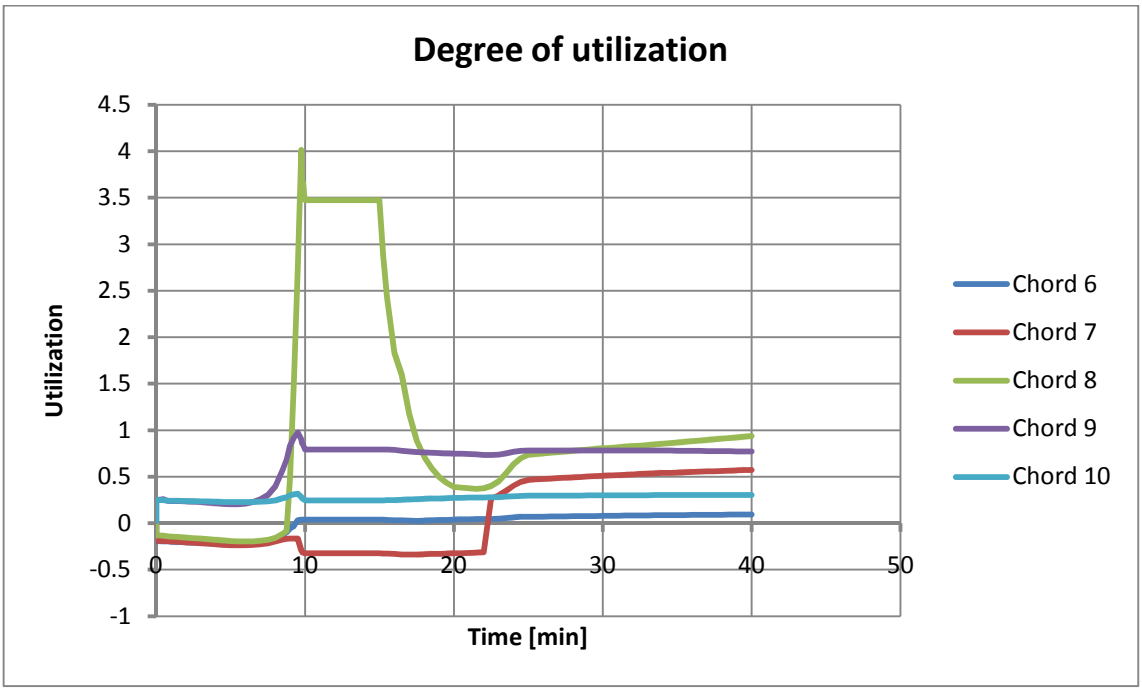

Figure 113 Final analysis, quarter span local fire, strengthened model; bottom chord members 6-10 degrees of utilization

Table 3 Final analysis, quarter span local fire, strengthened model; results for bottom chord

	Section	Length	Initial force	Ultimate compressive force	Ultimate degree of utilization / when reached
Chord 1	CFRHS120x120x6	1,7 m	126,1 kN	193,2 kN	38 % / stationary phase
Chord 2	CFRHS80x80x4	3,0 m	32,2 kN	107,0 kN	88 % / stationary phase
Chord 3	CFRHS80x80x4	3,0 m	-33,8 kN	43,0 kN	43 % / stationary phase
Chord 4	CFRHS80x80x4	3,0 m	-68,0 kN	16,3 kN	-19 % / heating phase
Chord 5	CFRHS80x80x4	1,1 m	-70,0 kN	21,6 kN	-20 % / heating phase
Chord 6	CFRHS80x80x4	1,1 m	-70,0 kN	22,7 kN	-23 % / heating phase
Chord 7	CFRHS80x80x4	3,0 m	-68,0 kN	30,1 kN	57 % / end of decay
Chord 8	CFRHS80x80x4	3,0 m	-33,8 kN	36,0 kN	401 % / heating phase
Chord 9	CFRHS80x80x4	3,0 m	32,2 kN	104,0 kN	98 % / heating phase
Chord 10	CFRHS120x120x6	1,7 m	126,1 kN	163,4 kN	32 % / heating phase

This analysis showed that by strengthening the diagonals and thereby preventing them from failing in buckling, the structure was able to sustain a local temperature exposure at quarter span. The behaviour of the truss changed in the same type of manner as in the mid-span local fire scenarios, i.e. large compressive forces were developed in the bottom chord. Furthermore tensile forces were developed in the top chord at the place of the highest temperature exposure.

5 CONCLUSIONS

In this licentiate thesis the behaviour of a typical single-bay all steel hall was studied throughout all the phases of a fire, focusing especially on the decay phase. This type of structure with steel roof trusses and columns has previously not been studied in the decay phase and the purpose was to find information to fill a part of this gap. This was done largely by using advanced non-linear FEM-software.

There are only a very few FEM-software available that are capable of doing this type of structural analysis and that at the same time at least at some level are suitable for everyday design work. Within the frames of this thesis two different FEM-software, Safir and Vulcan, were tried out and studied in more detail. Eventually Vulcan was chosen as the final tool as it proved to be both more user-friendly and better suited for solving the given problems.

In the development of the final analysis model, several different arrangements of boundary conditions and temperature exposures were studied in order to reach an understanding on how different factors influence the behaviour of the structure. Based on the initial development analyses and extensive testing, a model consisting of three mid frames of the CEE-hall was chosen for further in-depth study. The excluded part of the building was taken into account by modifying the boundary conditions using springs. In order to keep the analysis simple, only two temperature curves were used to study the structure, simulating a local fire placed at first at mid-span and then at one quarter of the span from one column.

5.1 Results

In structural fire engineering it's a well known fact that the behaviour of a structure exposed to fire is greatly influenced by the stiffness of the structures surrounding the fire affected area in all the phases of the fire. For a single-bay frame there is however no surrounding structures in the plane of the frame, so the influence of the stiffness of the frame itself need to be evaluated. In this study this was done by analysing different base connections and temperature distributions. The analyses clearly showed that for this type of frame rigid, or fixed, base connections induce substantially larger forces and permanent deformations in the structure than pinned base connections. The study also pointed out the importance of the massiveness of the columns; if the columns are substantially more massive than the members of the truss, hence having a much smaller section factor, they will both heat and cool down slower than the truss, leading to a higher degree of restraint on the truss at least in the heating phase. In a local fire naturally only a relatively small part of the structure will be exposed to high temperatures, whereas the adjacent parts will remain cooler and retain a greater deal of their stiffness, hence providing a higher degree of restraint on the members in the immediate vicinity of the fire, causing larger forces to be developed.

In the first final mid-span local fire analysis, where the mid-part of the frame in the middle was subjected to a temperature curve reaching a maximum of 800 °C, the structure was able to withstand the temperature exposure without collapsing. As a part of the top chords suffered from substantial permanent deformation, the behaviour of the truss changed and the loads were redistributed, so that the bottom chords went into compression and the structure basically started acting as a three-pin portal frame with hinges at the column base connections and

at mid-span. The compressive forces developed in all of the members of the bottom chords reached their maxima at the end of the decay phase and exceeded the capacity according to Eurocode, however the members were still able to carry the loads without failure. No substantial tensile forces were developed in the purlins, meaning that the mid-frame was not depending on the purlins or the adjacent frames in order to withstand the temperature exposure.

The same model was also modified by strengthening the top chords and analysed in the same way to show the importance of the behaviour of the top chords for the behaviour of the whole structure. As the top chords of the strengthened model suffered from hardly any permanent deformations, the behaviour of the structure did not change significantly and it performed in the same way after the temperature exposure as before.

Another analysis on the same model, where the temperatures of the steel members were calculated according to Eurocode, but so that the same maximum temperatures were reached, was also performed in order to study whether linear simplifications of the steel temperature curves can be justified or not. The analysis showed that the performance or general behaviour of the structure did not change much, meaning that linear simplifications can be used without losing accuracy. It's however essential to evaluate the steel temperatures of the different members properly according to Eurocode and first thereafter do the linear simplifications of the curves.

In the first analysis of the quarter-span local fire, the same model as in the first mid-span local fire analysis was used, changing it only by assigning the higher temperature curve to the members of the truss at one quarter-span from one column. The analysis however stopped prematurely at about 8 minutes due to buckling of a diagonal.

In order to overcome the problem with buckling of diagonals and to get to study the behaviour of the truss, the diagonals were strengthened and the model analysed again. This time the analysis ran without any problems, even though part of both the bottom- and top chords heated to 800 °C suffered from permanent deformations, causing the forces to redistribute and the behaviour of the truss to change. Essentially the behaviour changed in the same way as in the mid-span local fire, so that the bottom chords developed compressive forces, exceeding their capacity according to Eurocode. Opposed to the mid-span local fire, the maximum compressive forces were however not reached for all of the members of the bottom-chord at the end of the decay phase; for the part of the bottom chord furthest away from the fire the maximum compressive forces were reached in the stationary phase.

5.2 Design aspects

When designing an unprotected truss for a local fire scenario, it is not enough to study only the heating and stationary phase, but also the decay phase. As this study has shown, the largest and most critical forces may well be developed during the decay phase or even at its end when the structure has cooled down back to ambient temperature.

The part of the CEE-hall studied in the scope of this licentiate thesis was able to withstand both the mid-span local fire and, if strengthened, the quarter-span local fire without total failure. However, the behaviour of the structure changed significantly and high compressive forces, exceeding the capacity according to Eurocode, were developed in the bottom chords. Hence,

in the structural fire safety design of such a structure, the bottom chord, which normally is designed for tension, has to be designed to be able to carry the compressive forces that may develop in the case of fire and especially during the decay phase. This in turn means that it is necessary to provide not only the top chords but also the bottom chords with lateral supports. It may also be necessary to check the diagonals carefully, so that they don't fail in buckling when heated causing instability of the truss. In fact, according to this study it would be beneficial to design the top chord to be the weakest link in case of fire, as the forces then are allowed to be redistributed within the structure when the top chord starts to undergo permanent deformations.

Great attention especially need to be put on the evaluation of the stiffness of both the surrounding structures as well as frame itself, as it to a large extent will influence the behaviour of the structure. Special care should be put on avoiding an unintentional decrease of the stiffness, both in the boundary conditions and in the temperature distributions.

The horizontal support reactions at the base connections of the columns were in no case larger than the horizontal tie force calculated according to Eurocode. The support reactions measured during the final analyses were at most in the range of 40 kN, whereas the tie force according to Eurocode was 77 kN. In one of the initial development analysis, using fixed base connections for the columns, the horizontal support reaction however reached 93 kN, showing the importance of the restraints. In this study it was however decided that hinged base connections better resembled reality and were hence used in the final analyses. This in turn means that for this structure the tie force according to Eurocode gave a reliable, conservative, estimate on the horizontal support reaction, suitable for use at least in the initial design stage.

When using Vulcan as a design tool, it's advisable to simplify the model as much as possible, without losing any essential information, in order to enhance the possibilities of the model to converge and to save calculation time. The main problem with Vulcan is that it presents results only in the global coordinate system, leaving it to the user to calculate the internal forces in the local coordinate systems of the members. Otherwise the usability of Vulcan is good, with a clear graphical user interface. Even writing the input file manually imposes no greater difficulties. The usage of the smoothed Ramberg-Osgood material model for steel seems to be advisable as the model is continuous without any sharp edges in the stress-strain curves. Still, the usage of the Eurocode model is possible and this study showed no substantial difference in the results from the two material models.

When it comes to assigning the temperature curves to the different members in Vulcan it is advisable to keep it simple, using only a few different curves. However, it's important to remember that the stiffness of the structure, which is greatly influenced by the temperature development, plays a significant role on the behaviour and forces developed in the structure. Hence, assigning a too high temperature curve to restraining structures can in fact be very unconservative.

5.3 Limitations

This study focused on only one type of industrial hall, the CEE-hall by Ruukki Hungary, under certain local temperature exposures and the results are therefore directly applicable only for this structure. The intention with this study was to get an overall picture on how this type of

structure behaves when exposed to a local fire. Hence it was not possible to give any precise design rules but only to describe the general points that need attention when designing this type of structure for the case of fire. The results will vary depending on the structure configuration and the fire scenarios used.

5.4 Suggestions for future research

In order to improve the usability of Vulcan the most important point of future research and development would be to make it possible to get the results in the local coordinate system of the members. Further effort should also be put on studying the definition of the rotation of members as it at this point remains a bit unclear and makes it necessary to perform quite extensive testing to achieve the desired configuration. Research should also be done on how to enable the extraction of structural data from other modelling- or FEA-software to Vulcan.

In order to find clear design rules on how to take the decay phase of the fire into account in the design, extensive research on how different configurations of fire exposures and the structure itself affects the behaviour of the structure would be needed. Based on the findings from this licentiate thesis, the effect of the stiffness of the structure surrounding the fire affected area should be one of the main areas of focus. Other areas of great interest would be studying the different material models and their influence in more detail and how far the simplification of the temperature input can be taken without losing accuracy.

As the focus in this thesis was on the behaviour of the main frames only, the ends of the hall, including the main bracing system, were omitted from the analysis and their stiffness was taken into account in the boundary conditions of the analysed model. Hence the behaviour of the ends of the halls, including the essential bracing system, when subjected to a local fire was not studied in detail and remains an important area of focus for further studies.

6 BIBLIOGRAPHY

1. *A parametric natural fire model for the structural fire design of multi-storey buildings.* **Zehfuss, J. et al.** UK : Elsevier Ltd., 2007, Fire Safety Journal, Vol. 42. ISSN 0379-7112.

2. *Analyses of the Effects of Cooling and Fire Spread on Steel-framed Buildings.* **Bailey, C.G. et al.** UK : Elsevier Science Ltd., 1996, Fire Safety journal, Vol. 26. ISSN 0379-7112.

3. *The Treatment of Strain Reversal in Structural Members During the Cooling Phase of a Fire.* **El-Rimawi, J.A. et al.** UK : Elsevier Science Ltd., 1996, Journal of Constructional Steel Research, Vol. 37. ISSN 0143-947X.

4. *Eurocode 3: Design of steel structures. Part 1-2: General rules. Structural fire design.* Helsinki, Finland : Finnish Standards Association, 2005.

5. **Shepherd, P.** *The Performance in Fire of Restrained Columns in Steel-Framed Construction.* UK, Sheffield : University of Sheffield, 1999.

6. **Outinen, J.** *Mechanical Properties of Structural Steels at High Temperatures and after Cooling Down.* Espoo (Finland) : Helsinki University of Technology, 2007.

7. **Kirby, B.R. et al.** *The Reinstatement of Fire Damaged Steel and Iron Framed Structures.* United Kingdom : British Steel Corporation Swinden Laboratories, 1986. ISBN 0 900206 46 2.

8. *Nonlinear pre-fire and post-fire analysis of steel frames.* **Iu, C.K. et al.** UK : Elsevier Ltd, 2008, Engineering Structures, Vol. 27. ISSN 0141-0296.

9. *Effects of the cooling phase of a fire on steel structures.* **Wang, P. et al.** UK : Elsevier Ltd., 2008, Fire Safety Journal, Vol. 43. ISSN 0379-7112.

10. *Experiment on restrained steel beams subjected to heating and cooling.* **Li, G-Q et al.** UK : Elsevier Ltd., 2007, Journal of Constructional Steel Research, Vol. 64. ISSN 0143-974X.

11. *Experimental study of structural fire behaviour of steel beam of concrete filled tubular column assemblies with different types of joints.* **Wang, Y.C. et al.** UK : Elsevier Ltd., 2007, Engineering Structures, Vol. 29. ISSN 0141-0296.

12. *Numerical modelling of Structural fire behaviour of restrained steel beam-column assemblies using typical joint types.* **Wang, Y.C. et al.** UK : Elsevier Ltd., 2010, Vol. 32. ISSN 0141-0296.

13. *Numerical study of a steel sub-frame in fire.* **Santiago, A. et al.** 15-16, UK : Elsevier Ltd., 2008, Computers and Structures, Vol. 86. ISSN 0045-7949.

14. *Design of steel portal fram buildings for fire safety.* **Moss, P.J. et al.** 5, UK : Elsevier Ltd., 2009, Journal of Constructional Steel Research, Vol. 65. ISSN 0143-974X.

15. **Bong, M.W.** *Structural Fire Performance of Steel Portal Frame Buildings.* Christchurch, New Zealand : University of Canterbury, 2005.

16. *Numerical investigation of cold-formed steel purlin in fire.* **Lu, Wei et al.** 1, Espoo, Finland : Rakenteiden mekaniikan seura r.y., 2010, Journal of Structural Mechanics, Vol. 43. ISSN 0783-6104.

17. *Eurocode 1: Actions on structures. Part 1-7: General actions. Accidental actions.* Helsinki, Finland : Finnish Standards Association, 2006.

18. *Horizontal forces in steel structures tested in fire.* **Wald, F. et al.** UK : Elsevier Ltd., 2009, Journal of Constructional Steel Research, Vol. 65. ISSN 0143-974X.

19. *Fire Safety of Industrial Hall.* s.l. : Arcelor Mittal et al., 2007.

20. **Franssen, J.M.** *Users's Manual For Safir 2007a.* Liege (Belgium) : University of Liege, 2008.

21. SAFIR - Software for the simulation of building structures subject to fire. [Online] University of Liege. [Cited: 11 February 2010.] http://www.argenco.ulg.ac.be/logiciels/SAFIR/index.html.

22. *3D simulation of Industrial Hall in case of fire. Benchmark between ABAQUS, ANSYS and SAFIR.* **Vassart, O. et al.** London, UK : Interscience Communications Limited, 2004. Interflam 2004. Proceedings of the 10th international conference, vol. 2.

23. Vulcan Solutions Limited (VSL). [Online] [Cited: 11 May 2010.] http://www.vulcan-solutions.com.

24. Buckling. *Wikipedia, the free encyclopedia.* [Online] [Cited: 20 October 2010.] http://en.wikipedia.org/wiki/Buckling.

25. **Heinisuo, M. et al.** *Natruel Fire Design (NFD), Work Package 4 (WP4). Case Study, CEE-Hungary Hall by Ruukki.* Tampere, Finland : Tampere University of Technology, 2008.

26. *Eurocode 3: Design of steel structures. Part 1-1: General rules and rules for buildings.* Helsinki, Finland : Finnish Standards Association, 2005.

27. *STAAD.Pro 2007, Technical Reference Manual.* United States : Bentley Systems, Incorporated, 2008.

APPENDIX A VULCAN INSTRUCTIONS

A.1 Creating the input file

The creation of the Vulcan model is usually done with the help of the graphical user interface of Vulcan. However, if there already is some kind of model, e.g. a Tekla model, and it is to be converted to a Vulcan model, it's first necessary to study how the input file is made. Unfortunately the help files for Vulcan does not tell much about this, neither is there any manual for this. When a Vulcan input file is created using the graphical user interface, the software itself adds short descriptions of all the information needed to the input file. The units used by Vulcan are always N, mm, °C, rad and minutes, unless otherwise stated below. The input file will be presented hereafter in the same order and using the same terminology as when Vulcan itself creates the input file.

A.1.1 Title

First of all the input file is given a title, which the user himself/herself is free to choose, and does not have to be the same as the file name. In the graphical user interface this is given under Analysis/Analysis Parameters in the Project Description box.

A.1.2 Version

This section only deals with the version number of the file format. The current number is 10.12.0. This is specified automatically when using the graphical user interface.

A.1.3 View

This section specifies what view is saved to the file, i.e. view angles, panning, zoom ratio, which parts of the model are visible and which labels of the parts are visible. These values do not affect the analysis. When using the graphical user interface these values are given automatically based on the view at the point of saving.

A.1.4 Analysis parameters

The first line in this section specifies the output parameters such as at which points the results are stored and whether or not the stiffness matrix is to be reordered in order to optimize the calculation. These can nearly always be taken as the default values.

The second line specifies at which point in time the analysis is to be started and at what time it is to be ended, as well as the maximum time step used in the analysis, all given in minutes.

The third line specifies which solution procedure is used (basically Newton-Raphson), what thermal strain models are used for concrete (several available, including Eurocode) and steel (Eurocode or Ramberg), what layer procedure is used for concrete, whether or not geometrical nonlinearity is to the included in the analysis, the iteration limit as well as the tolerances for the displacements, forces, moments and time to be used.

In the graphical user interface all these are chosen in the Analysis/Analysis Parameters window, even though some values cannot be changed.

A.1.5 Nodal geometry

This section defines the geometry of the nodes used in the model.

On the first line of this section the total number of nodes in the model is given.

On the next lines the nodes are given, one node per line, by four values: the number of the node (running from 1), the X coordinate, the Y coordinate and the Z coordinate.

In the graphical user interface the nodes are given, edited and deleted in the Geometry/Nodes window.

Here it can also be worth mentioning that Y should be defined as the vertical direction, X as the direction of the frame and Z at a right angle to the frame, otherwise the analysis can run into difficulties.

A.1.6 Fixity

This section defines the boundary conditions at nodes used in the model.

The first line specifies the total number of fixities used in the model.

The next lines define the fixities of the model, one node per line, by three values: the number of the node, the translational and rotational fixities according to the global coordinate system.

The translational and rotational fixities are given as numbers according to Table A. 1 and Table A. 2.

Table A. 1 Translational fixities

Number	X	Y	Z
0	free	free	free
1	fixed	free	free
2	free	fixed	free
3	fixed	fixed	free
4	free	free	fixed
5	fixed	free	fixed
6	free	fixed	fixed
7	fixed	fixed	fixed

Table A. 2 Rotational fixities

Number	RX	RY	RZ
0	free	free	free
1	fixed	free	free
2	free	fixed	free
3	fixed	fixed	free
4	free	free	fixed
5	fixed	free	fixed
6	free	fixed	fixed
7	fixed	fixed	fixed

In the graphical user interface the boundary conditions are given in the Properties/Boundary Conditions window.

A.1.7 Steel materials

In this section the properties of the different steel materials used in the model are defined.

The first line specifies the total number of different steel materials used in the model.

The next lines define the steel materials, one material per line, by four values: the number of the material (running from 1), the yield stress (MPa), Young's modulus (MPa) and Poisson's ratio.

In the graphical user interface the steel materials are given in the Properties/Steel Materials window.

A.1.8 Costing (fire protection)

This section defines the properties of different fire protection materials, or costing types, used in the model.

The first line specifies the total number of different costing types used in the model.

The next lines define the costing types, one type per line, by ten values: the number of the type (running from 1), protection type (0 – none, 1 – on-site intumescent painting, 2 – off-site intumescent painting, 3 – lightweight board, 4 – dense board, 5 – spray), protection period (0 – none, 1 – 30 minutes, 2 – 60 minutes, 3 – 90 minutes, 4 – 120 minutes), exposed sides (2-4), unknown (default 0), composite (0 – no, 1 – yes), thickness of material (mm), density of material (kg/m^3), specific heat of material (1050 J/kgK) and thermal conductivity of material (W/mK).

In the graphical user interface these values are given in the Properties/Fire Protection window.

A.1.9 Temperature curves

This section defines the temperature curves used in the model.

The first line specifies the total number of different temperature curves used in the model.

On the next lines the different temperature curves are defined by several values. The different types available are Standard (ISO 834/BS 476), Eurocode (EC1: Part 1-2), Linear, BiLinear and From File.

The Standard temperature curve is defined on two lines. The first line is made up of the number of the temperature curve (running from 1) and the word "STANDARD". The second line defines if there is a cooling phase (0 – no, 1 – yes), the length of heating period in minutes (0 if no cooling) and the cooling period in minutes (60 if no cooling).

The Eurocode temperature curve, meaning the parametric temperature curve according to Eurocode, is defined on two lines. The first line is made up of the number of the temperature curve (running from 1) and the expression "EC_____". The second line defines the opening area (m^2), the total area (m^2), the average opening height (m), the B factor (J/m^{2}s^{0,5}K), the fire load density (MJ/m^2), the floor area (m^2) and the limiting time (minutes).

The Linear temperature curve is defined on two lines. The first line is made up of the number of the temperature curve (running from 1) and the word "LINEAR__". The second line defines

the time (minutes) at the first point of the line, the temperature (°C) at the first point of the temperature line, the time (minutes) at the second point of the line and the temperature (°C) at the second point of the temperature line.

The BiLinear temperature curve is defined on two lines. The first line is made up of the number of the temperature curve (running from 1) and the word “BILINEAR”. The second line defines the time (minutes) at the first point of the curve, the temperature (°C) at the first point of the curve, the time (minutes) at the second point of the curve, the temperature (°C) at the second point of the curve, the time (minutes) at the third point of the curve and the temperature (°C) at the third point of the curve.

The From File temperature curve is defined on six lines. The first line is made up of the number of the temperature curve (running from 1) and the word “FROMFILE”. The second line defines the scale which is to be used (default 1), i.e. the temperature curve can be scaled by a factor. The third line gives the whole path from where the temperature file can be found. The fourth line is empty. The fifth line gives the name of the temperature file, including the file extension (.txt). The sixth line is the title from the temperature file. An example of how the From File temperature curve is specified in the input file can be seen in the following section.

```
//  First line is Number of Temperature Curves
//  Then Number, Type (Standard, EC, Linear, BiLinear, FromFile)
//  Then temperature data in whatever format dependant on Type
<TEMPERATURE CURVES>
1

1    FROMFILE
1.000
D:\Example\Vulcan\Model

Temp1.txt
temp1
</TEMPERATURE CURVES>
```

The temperature file consists of a title, which can be chosen freely by the user and the actual temperature curve data. The first line of the temperature curve data section specifies the number of points, between which the curve is made up by straight lines. This is followed by an empty line. The next lines give the points, one point per line, as the time (minutes) and the temperature (°C). The temperature file should be saved in txt-format. An example of a temperature file can be seen in the following section.

```
<TITLE>
temp1
</TITLE>
// First line is number of data lines to read
// Then each line is a Time and a Temperature
<TEMPERATURE CURVE DATA>
5
```

```
0.0     20.00
10      630
15      630
25      200
40      20
</TEMPERATURE CURVE DATA>

</END OF FILE>

.
```

All of this, except for making the temperature files, can be given in the Properties/Temperature Curves window in the graphical user interface.

A.1.10 Temperature patterns

The temperature pattern describes how the temperature of the steel is calculated based on the temperature curve. There are seven different types of temperature patterns available in Vulcan, these are: Uniform, FlangeWebFlange, Linear 1D, Linear 2D, BiLinear, From File and Eurocode (EC3: Part 1.2).

The first line in the temperature patterns section specifies the total number of temperature patterns used in the model. On the next lines the different temperature patterns are defined.

The Uniform temperature pattern is defined on two lines. The first line is made up of the number of the temperature pattern (running from 1) and the number of the type (0). The second line is a scale factor, which just scales the temperature relative to the temperature curve.

The FlangeWebFlange temperature pattern is defined on two lines. The first line is made up of the number of the temperature pattern (running from 1) and the number of the type (1). The second line consists of three numbers; multipliers, or scale factors, for the top, web and bottom of the section. These multipliers scale the temperature relative to the temperature curve.

The Linear 1D temperature pattern is defined on two lines. The first line is made up of the number of the temperature pattern (running from 1) and the number of the type (2). The second line consists of two numbers; multipliers, or scale factors, for the top and bottom, in between a 1D linear interpolation of the temperature relative to the temperature curve is made.

The Linear 2D temperature pattern is defined on two lines. The first line is made up of the number of the temperature pattern (running from 1) and the number of the type (3). The second line consists of four numbers; multipliers for the top, bottom, left and right of the section, in between a 2D linear interpolation of the temperature relative to the temperature curve is made.

The BiLinear temperature pattern is defined on two lines. The first line is made up of the number of the temperature pattern (running from 1) and the number of the type (4). The second line consists of four numbers; multipliers for the top, bottom and middle as well as the relative

position of the middle from the bottom (0-1), scaling the temperature relative to the temperature curve.

The From File temperature pattern is defined on 6 lines. The first line is made up of the number of the temperature pattern (running from 1) and the number of the type (5). The second line consists of the number of width divisions and the number of depth divisions of the section. The third line gives the whole path from where the temperature pattern file can be found. The fourth line is empty. The fifth line gives the name of the file, including the file extension (.txt). The sixth line is the title from temperature pattern file.

The temperature pattern file consists of three sections. The first section is the title, which the user is free to choose. This is followed by the temperature pattern section, consisting of two lines. The first line is made up of two numbers; the number of width divisions and number of depth divisions of the section. The second line is a description, which the user can choose. The third section is the actual temperature pattern data. The first line of this section is the number of time steps. The next lines then define the pattern, one line per time step, given by the time step and then the scale factors (number of width divisions x number of depth divisions) for each part of the section.

The Eurocode temperature pattern is defined on just one line, made up of the number of the temperature pattern (running from 1) and the number of the type (6). The Eurocode temperature pattern calculates the temperature of the section according to the section factor.

In the graphical user interface the temperature patterns are defined and edited in the Properties/Temperature Patterns window.

A.1.11 Rebar properties

This section defines the properties of the different reinforcement bar properties used in the model.

On the first line the total number of different reinforcement bar properties is given.

On the next lines the material properties, one per line, are defined by four numbers: the number of the reinforcement bar properties (running from 1), the yield stress (MPa), Young's modulus (MPa) and type of bar (0 – cold worked, 1 – hot rolled).

In the graphical user interface the rebar properties are defined in the Properties/Reinforcement Bars window.

A.1.12 Concrete materials

This section defines the properties of the different concrete materials used in the model.

On the first line the total number of different concrete materials is given.

The next lines, one material per line, consists of nine numbers: the number of the concrete material (running from 1), the compressive strength (MPa), the cracked shear factor, Poisson's ratio, the parallel stiffness, the perpendicular stiffness, weight type (0 – normal, 1 – lightweight), moisture content (%) and the density (kg/m^3).

In the graphical user interface the concrete materials are defined in the Properties/Concrete Materials window.

A.1.13 Beam sections

The beam sections describe the geometry and properties of the different sections used in the model. In Vulcan several profile families are built in and the geometry is recognized based on the name and a few parameters, these are I-profiles (custom, HE, IPE, UB and UC) and ASB-profiles (custom and ASB). Other profiles, such as hollow sections, need to have the geometry defined with the help of matrixes.

On the first line of the beam sections section the total number of different beam sections used in the model is defined. This is then followed by the different beam sections.

The first line of the beam section always consists of the following numbers: the number of the beam section (running from 1), number of width divisions (number of elements in the horizontal direction), number of depth divisions (number of elements in the vertical direction), depth (mm), top width (mm), bottom width (mm), top flange thickness (mm), bottom flange thickness (mm), web thickness (mm) (if there are two webs the total web thickness can be used), section factor (1/m) and type (0 – non standard, 1 – I-profile, 2 – ASB). The second line is the name of the family (e.g. HE or if using non standard the name can be chosen freely) and the third line is the exact section (e.g. HE1000B or if using non standard the name can be chosen freely). From this point on the definition of the profile is different when using standard profiles (I or ASB) and non standard profiles.

When specifying a standard profile the fourth line defines the number of the steel material being used.

When specifying a non standard profile the fourth line defines the width (mm) of each of the elements. The fifth line defines the depth (mm) of each of the elements. This is then followed by the material matrix where each element is assigned its material (0 – air, 1 – steel, 2 – concrete and 3 – reinforcement bar). The material matrix is then followed by the property matrix where each element is assigned its type of steel/concrete/reinforcement bar material. E.g. if all of the elements of the profile have been defined to be steel in the material matrix, then the number of which steel material to be used is chosen in the property matrix.

In the graphical user interface the sections are specified in the Properties/Beam Sections window.

A.1.14 Beams

In this section the beam elements used in the model are defined.

The first line of the section defines the total number of beam elements used in the model.

The next lines define the beam elements, one per line, by thirteen numbers: the number of the beam element (running from 1), start node, mid node, end node, web offset (mm) (vertical direction), flange offset (mm) (horizontal direction), X-twist (0-1), Y-twist (0-1), Z-twist (0-1), section number, costing number, temperature curve number and temperature pattern number.

The twists mean that the strong direction of the section is aligned according to the twist values, e.g. if the Z-twist is 1 and X- and Y-twists are 0, then the strong direction of the section is aligned with the global Z-axis. In case of non standard sections that are equally strong in both directions, the twist giving the highest capacity in Vulcan is the one to be used.

In the graphical user interface the beams are defined and edited in the Geometry/Beams window.

A.1.15 Spring stiffness

In this section the spring types used in the model are defined.

On the first line of this section the total number of different spring types is given.

On the next lines the different spring types, one per line, are defined by 7 numbers: the number of the spring type (running from 1), the X-axial stiffness (N/mm), the Y-axial stiffness (N/mm), the Z-axial stiffness (N/mm), the RX-rotational stiffness (N/rad), the RY-rotational stiffness (N/rad) and the RZ-rotational stiffness (N/rad).

Even though Vulcan mostly uses the global coordinate system, the spring stiffness properties are not completely defined according to the global coordinate system but depend on the twist of the beams. If e.g. rotation around the global Z-axis needs to be fixed at the end of a beam parallel to the X-axis and the twist of the beam is Z, then the RZ-rotational stiffness should be assigned a large value (default $1{,}0*10^{12}$ N/Rad), however, if the twist of the beam is Y, then the RY-rotational stiffness should be assigned a large value. If the rotation around the global Y-axis needs to be fixed for the same beam parallel to the X-axis and the twist of the beam is Z, then the RY-rotational stiffness should be assigned a large value and if the twist of the beam is Y, then the RZ-rotational stiffness should be assigned a large value. The same also goes for the axial stiffness. The logic behind the system remains a bit unclear, and a trial-and-error approach seems to be the most reliable way of getting the correct solution. The results of the beams are however presented in the global coordinate system.

In the graphical user interface the spring types are defined in the Properties/Springs window.

A.1.16 Springs

In this section the springs used in the model are defined. In order to define a spring in Vulcan there need to be two nodes at the point of the spring. The first one is the regular node used to form the geometry of the structure, the second one is the spring node, which has the same coordinate as the first one, but is not used to define the geometry of the structure.

On the first line of this section the total number of springs used in the model is given.

On the next lines the springs, one per line, are defined by seven numbers: the number of the spring (running from 1), the start node (which is the geometrical node), the spring node, the number of spring stiffness, offset (mm) (should be the same as the offset of the beam) and the number of the temperature curve.

In the graphical user interface springs are defined in the Geometry/Springs window.

A.1.17 Shear connector properties

In this section the different shear connector properties used in the model are defined. There are four different interaction models available: none, partial, full and user. The stiffness of the connector depends on which interaction model is used.

The first line of the section defines the total number of different shear connector properties used in the model.

The next lines defines the different shear connector properties, one per line, by ten numbers: the number of the shear connector properties (running from 1), the diameter of the connector (mm), the ultimate shear strength (MPa), number of connectors per meter, interaction model (0 – none, 1 – partial, 2 – full, 3 – user), X-axial stiffness (N/mm) (none – $1x10^2$, partial – 0, full – $1x10^{15}$, user – chosen by user), Y-axial stiffness (N/mm) (none – $1x10^2$, partial – 0, full – $1x10^{15}$, user – chosen by user), Z-axial stiffness (N/mm) (none – $1x10^{15}$, partial – $1x10^{15}$, full – $1x10^{15}$, user – chosen by user), RX-rotational stiffness (N/rad) (none – $1x10^{15}$, partial – $1x10^{15}$, full – $1x10^{15}$, user – chosen by user) and RY-rotational stiffness (N/rad) (none – $1x10^{15}$, partial – $1x10^{15}$, full – $1x10^{15}$, user – chosen by user).

In the graphical user interface the shear connector properties are defined in the Properties/Shear Connectors window.

A.1.18 Shear connectors

In this section the shear connectors used in the model are defined. In order to define shear connectors in Vulcan between a slab and a beam, there needs to be separate nodes for the beam and the slab, even though they have the same coordinates.

On the first line in this section the total number of shear connectors used in the model is given.

On the next lines the shear connectors are defined, one connector per line, by four numbers: the number of the shear connector (running from 1), the number of the slab node, the number of the beam node and the number of the shear connector properties.

In the graphical user interface the shear connectors are defined in the Geometry/Shear Connectors window.

A.1.19 Concrete sections

In this section the concrete sections used in the model are defined. In Vulcan the concrete sections are made up of layers of concrete and reinforcement bars at different angles.

On the first line of this section the total number of concrete sections used in the model is given.

Each concrete section is then defined separately on three or more lines, depending on how many reinforcement bar layers there is. On the first line the number of the concrete section (running from 1), number of layers, number of rebar layers and the rib angle (rad) are given. On the second line the thickness coordinates for the layers are given (mm from the middle of the section). On the next lines the rebar layer list is presented, one layer per line, by: the layer number, angle (rad) and the rebar properties number.

The concrete sections are defined in the Properties/Concrete Sections window in the graphical user interface.

A.1.20 Slabs

In this section the concrete slabs used in the model are defined. The slabs in Vulcan are 9-noded, so that the first four nodes are in each corner, the second four nodes in the middle of each side (in the same order as the corner nodes) and one node in the middle of the slab.

On the first line the total number of concrete slabs used in the model is given.

On the next lines the slabs are defined, one slab per line, by 15 numbers: the number of the slab (running from 1), node 1, node 2, node 3, node 4, node 5, node 6, node 7, node 8, node 9, number of concrete section, number of concrete material, number of temperature curve, number of temperature pattern and the offset distance (mm).

In the graphical user interface the concrete slabs are defined in the Geometry/Slabs window.

A.1.21 Display temperatures

In this section the temperatures which are to be displayed and registered to be displayed as graphs during the analysis are given.

On the first line the total number of temperatures to be displayed is given.

On the next lines the temperatures to be displayed are defined, one per line, by four numbers: the temperature curve number, the temperature pattern number, the X- and Y-positions of the point at which the temperature is registered (relative from the middle of the pattern).

In the graphical user interface this is defined in the Analysis/Output Specification window.

A.1.22 Display nodal displacements

In this section the nodal displacements which are to be displayed as graphs during the analysis are given.

On the first line the total number of nodes at which the displacements are to be displayed is given.

On the next lines the nodal displacements to be displayed are defined, one per line, by seven numbers: the number of the node, X-displacement (0 – no, 1 – yes), Y- displacement (0 – no, 1 – yes), Z- displacement (0 – no, 1 – yes), RX-rotation (0 – no, 1 – yes), RY-rotation (0 – no, 1 – yes) and RZ-rotation (0 – no, 1 – yes), according to the global coordinate system.

In the graphical user interface this is defined in the Analysis/Output Specification window.

A.1.23 Display beam force

In this section the beam forces which are to be displayed as graphs during the analysis are given.

On the first line the total number of beams which forces are to be displayed is given.

On the next lines the beam forces to be displayed are defined, one per line, by seven numbers: the number of the beam, X-force (0 – no, 1 – yes), Y- force (0 – no, 1 – yes), Z- force (0 – no, 1 – yes), RX-moment (0 – no, 1 – yes), RY-moment (0 – no, 1 – yes) and RZ-moment (0 – no, 1 – yes), according to the global coordinate system.

In the graphical user interface this is defined in the Analysis/Output Specification window.

A.1.24 Display slab force

In this section the slab forces which are to be displayed as graphs during the analysis are given.

On the first line the total number of slabs which' forces are to be displayed is given.

On the next lines the slab forces to be displayed are defined, one per line, by three numbers: the number of the slab, PStress1 (0 – no, 1 – yes) and PStress2 (0 – no, 1 – yes).

In the graphical user interface this is defined in the Analysis/Output Specification window.

A.1.25 Point loads

In this section the point loads used in the model are given.

On the first line the total number of point loads is given.

On the next lines the point loads are defined, one load per line, by four numbers: the number of the node, the load in X-direction (N), the load in Y-direction (N) and the load in Z-direction (N).

In the graphical user interface the point loads are defined in the Properties/Loading window.

A.1.26 Rotation loads

In this section the rotational loads used in the model are given.

On the first line the total number of rotational loads is given.

On the next lines the rotational loads are defined, one load per line, by four numbers: the number of the node, the load in RX-direction (Nmm), the load in RY-direction (Nmm) and the load in RZ-direction (Nmm).

In the graphical user interface the rotational loads are defined in the Properties/Loading window.

A.1.27 Line loads

In this section the line loads used in the model are given.

On the first line the total number of line loads is given.

On the next lines the line loads are defined, one load per line, by three numbers: the number of the beam, the load in the direction of the web (N/mm) and the load in the direction of the flange (N/mm).

In the graphical user interface the line loads are defined in the Properties/Loading window.

A.1.28 Area loads

In this section the area loads used in the model are given.

On the first line the total number of area loads is given.

On the next lines the area loads are defined, one load per line, by two numbers: the number of the slab and the uniformly distributed load (N/mm^2).

In the graphical user interface the area loads are defined in the Properties/Loading window.

A.1.29 Results

The results of the Vulcan analysis are quite easy to interpret and to use. When the analysis has finished and the model is saved, the results are written to the end of the input file, which hence also becomes the output file. This is important to remember as the results are deleted from the input file if the model is altered after analysis and saved with the same name. It is also possible to get the results directly from Vulcan as Excel tables and graphs. All results are presented according to the global coordinate system, even though the texts in the Excel graphs suggest otherwise.

A.2 Exporting the structural information from Tekla Structures

Tekla Structures is very often used to model steel structures. By using this model as a basis for other FEA models, considerable time and effort can be saved as each model does not need to be created from scratch. The question is only how to get the needed information extracted from Tekla in a usable format.

In order of the extracted information to be truly valuable, the Tekla model needs to be properly made putting great attention on the positioning of the elements and nodes. The ideal would be that the centrelines, or their extensions, of the elements coincide at the connections so that the creation of large amounts of small elements, representing the eccentricity, effectively is avoided. Also the profiles used should be easily recognizable and of standard profile families, preferably European standard, making the conversion simple. Furthermore the extracted information should not contain any unnecessary information such as bolts, holes and small parts without structural significance.

As Tekla, as well as most regular ambient temperature FEM softwares, use single continuous elements between connections, any extracted model will also be made up of single continuous elements between the connections or nodes. In Vulcan, however, the elements need to be split into smaller finite elements. This can either be done manually in Vulcan or in some way in the conversion process. Either way, a renumbering of both elements and nodes is necessary as the Vulcan model will contain more elements and nodes than the Tekla model.

A point where the conversion from Tekla to Vulcan might be facing problems is the rotation of non-standard profiles (meaning non-standard from Vulcan's point of view). This is due to the fact that it is not always clear which rotation is to be used for non-standard profiles, which are equally strong about both axes, in Vulcan. The correct rotation should be found by testing in Vulcan, if no consequent rule can be found.

The most easily interpreted way of getting the information extracted from Tekla seems to be converting the model to a Staad model, as its input file is written in a similar way to the Fortran style Vulcan input file. When the information is extracted from Tekla only the parts should be chosen and connections should in the first place be forced to be centric.

In the following paragraphs the main parts of the Staad input file will be explained in more detail, based on (27), and compared to the information needed for the Vulcan input file.

A.2.1 Coordinate system

In Staad the vertical axis of the default global coordinate system is the Y axis, i.e. the same as in Vulcan, and when extracting a model from Tekla the model is automatically created according to this global coordinate system.

For a member the local X axis is in the direction of the member, from start to end. The local Y axis coincides with the weak axis of the profile and the Z axis coincides with the strong axis of the profile. Vulcan, however, does not use any local coordinate systems.

A.2.2 Units

The general units used in Staad are defined at the beginning of the input file. It is however also possible to define other units to be used within separate commands, e.g. it's possible, and often also simpler, to define cross-sections using centimetres or millimetres instead of meters in the user tables for cross-sections. Even so, in order to simply transfer the information to Vulcan and to avoid mistakes it would be desirable to use the same units throughout the Staad input file and preferably the same units as in Vulcan, i.e. N and mm.

A.2.3 Joint coordinates

The joint coordinates, or nodes, are in the Staad input file given in a very simple way by four numbers: the number of the coordinate (node) and the X Y Z coordinates. Hence the main nodes are very easy to transfer to Vulcan, only the rotation of the coordinate system may need to be changed, but that is done very easily only by swapping the coordinates between each others.

To these main nodes that are extracted from Tekla to Staad, nodes in between these need to be added in order to split the members in Vulcan and to add the mid nodes of each finite element.

A.2.4 Member incidence

The members are defined by three numbers: the number of the member and the numbers of the start- and end nodes. Staad does not define any mid nodes. Also the members are hence easy to transfer to Vulcan only by adding the mid nodes.

A.2.5 Group definition

The start group definition command can be used in Staad to specify different groups of members that have the same properties, hence simplifying the compilation of the Staad input file. The Staad input file extracted from Tekla may contain these groups, but they are not used later on in the generated input file, hence they may be excluded from the file. Furthermore, they will not be applicable in Vulcan where no group definition is in use.

A.2.6 User tables for cross-sections

Staad has several profile libraries built into it, but if the profile identifications used in Tekla don't coincide with these libraries, even though they actually are of the same standard profile families, the profiles will be exported as user tables defining customized steel sections. Staad supports several different types of customized sections, but the three most common will be "wide flange", "tube" and "i-section" for common industrial buildings. All of these different types require several properties to be specified in order to define the actual section. When converting the input file to Vulcan it may actually be more convenient that the sections are defined with the help of these customized sections, at least for non I-sections, as these are basically the only standard profiles in Vulcan. This way the properties of the sections will then be easily found from the Staad input file and can be used to specify the sections in Vulcan and to make the section matrixes needed for non-standard profiles.

A.2.7 Material definition

The different steel materials used in Tekla are exported to the Staad input file as isotropic materials defined by a name, Young's modulus, the shear modulus (if not specified the shear modulus is calculated as G=0,5*E/(1+Poisson)), Poisson's ratio, the density, the coefficient of thermal expansion and the damping ratio for computing the modal damping. In reality when converting to Vulcan none of this information needs to be gathered from the Staad input file as these are known constants for most common steel grades. The actual steel strength properties are specified later on in the Staad input file extracted from Tekla. If the complete structure is of only one steel grade, the easiest way seems to be defining the material separately in the Vulcan input file, not using the information in the Staad input file at all.

A.2.8 Member properties

Whether standard or customized profiles are used, the members are assigned their profiles in the member property specification section.

If standard profiles, i.e. profiles specified in the built-in libraries of Staad, are used, the properties are assigned by making a list of the members in question and referring to the name of the profile family as well as specifying the size. Customized profiles are assigned to members in the same manner, the only difference being that reference is made to the user table defined above.

With the help of these lists it should be fairly easy to take extract the information to Vulcan.

A.2.9 Constants

In the constants command the materials defined above are assigned to the different members by listing the members in question. If no materials have been defined, all the properties can also be specified explicitly in the constants command. Again, if only one steel material is used, it seems easier to define the material properties separately in Vulcan.

In this command the member rotation angle can also be specified. This is done by giving an angle, α, which rotates the section through the angle 90° - α, where α then is the angle between the local principal axis system and the global axis system.

A.2.10 Member releases

The member end releases, force- and moment releases as well as partial moment releases for all axes, are specified in the local coordinate system in the member releases command. As the end releases in Vulcan must be specified with the help of springs, a direct conversion from Staad to Vulcan may be quite difficult. However, the necessity of even using end releases in a fire situation is in many cases questionable. For a beam it may be necessary to specify the end releases, but e.g. for a welded truss it is usually not essential.

The end releases can be specified for all members in Tekla. However, if it is necessary to use the end releases, it's essential to investigate how they are extracted, and if correctly, from Tekla when making the Staad input file and if it is possible to get the end releases transferred from Tekla to Vulcan. Otherwise the end releases, or springs, should be defined separately in Vulcan.

A.2.11 Supports

The supports can in the Staad input file be specified either parallel or inclined to the global coordinate system. As Vulcan only uses the global coordinate system for the supports, or fixities, it is desirable that the supports are defined parallel to the global coordinate system in Staad. In Staad the supports are either pinned, fixed or "fixed but". The "fixed but" supports can be released in any of the global directions and can also be assigned spring constants. Aside from the spring constants, the supports are easily converted to Vulcan.

For a sample export from Tekla to Staad (CEE-hall), all the base connections of the columns were automatically assigned to be fixed. The supports can be specified in Tekla, but attention should be put on whether the information is exported correctly or not in all situations.

A.2.12 Loads

Staad supports several different types of loads, the most important ones within the scope of this study are joint- and member loads. In Tekla loads can be given both at points and as line loads and they are indeed extracted to the Staad input file and are quite easily interpreted. This information could also most probably be quite easily transferred to Vulcan, even though attention should be put on the units and that the information is transferred correctly.

Also the self-weight can be automatically created from Tekla to Staad. However, for the conversion to Vulcan there is basically no need for this as Vulcan does not support self-weight, but all loads need to be defined as either point or line loads for members.

As Vulcan uses no load combinations all loads need to be combined in the applied loads, i.e. the total loads need to be applied directly to the nodes and members.

A.2.13 Parameters

The last part in the Staad input file extracted from Tekla is the design parameters. This part contains information such as which code the analysis is to follow (e.g. Eurocode), the steel strength, member lengths and several other parameters necessary in the Staad analysis. For Vulcan the only part of interest in this section is the steel strength.

A.2.14 Summary

In order to be able to take advantage of a Tekla model when making the Vulcan model there are a few points that need attention and that need to be taken into account already when making the Tekla model. The main geometry of the structure is fairly easy to export from Tekla to Staad, but in order of it to be usable great attention should be put on ensuring that the members are connected as desired in the FEA, otherwise the model will contain lots of small elements and the geometry will not necessarily be correct. Attention also needs to be put on the numbering of elements and nodes as the Vulcan model will inevitably contain many more nodes and elements than the Tekla and Staad models. One of the most important points to check is that the units match between the different software.

The properties of the members, such as profiles and materials, can be exported from Tekla but also this part needs some attention, especially the profiles, as the profile libraries and methods of specifying non-standard profiles are a bit different in all software.

The supports seem to be quite easy to transfer from Tekla to Vulcan via Staad, as their definition is quite simple and similar in all software.

The member releases are defined quite similarly in Tekla and Staad, whereas Vulcan uses springs, so the extraction of this information may need a lot attention if needed.

The loads are fairly easy to apply in all of the software, and they should be quite easy to transfer from Tekla to Vulcan, as long as the units and directions are correct.

A.3 Exporting the temperature data from FDS

As the temperature data is introduced in Vulcan as a simple text file, there is in theory no need at all to modify the data gathered from FDS. In reality it will however be necessary to simplify and smooth the results in order to save calculation time in Vulcan. It also seems advisable that the steel temperatures are calculated separately and assigned to groups of members, so that the data can be used directly as input in the Vulcan model. Another concern is how to assign the correct temperature curves to the correct members.

APPENDIX B EUROCODE FORMULAS

B.1 Steel temperature development

For unprotected internal steelwork the temperature development of the steel is calculated stepwise, so that the increase of temperature $\Delta\vartheta_{a,t}$ during a time interval Δt is:

$$\Delta\theta_{a,t} = k_{sh}\frac{A_m/V}{c_a\rho_a}\dot{h}_{net}\Delta t$$

where

$\Delta\vartheta_{a,t}$	increase of temperature [°C]
k_{sh}	correction factor for shadow effect (can be taken as 1) [-]
A_m/V	section factor for unprotected steel members [1/m]
V	volume of the member per unit length [m^3/m]
c_a	specific heat of steel [J/kgK]
h_{net}	design value of the net heat flux per unit area [W/m^2]
Δt	time interval [s]
ρ_a	unit mass of steel (can be taken as 7850 kg/m^3) [kg/m^3]

The specific heat of the steel c_a is determined by the following equations:

- for 20 °C ≤ ϑ_a < 600 °C

$$c_a = 425 + 7{,}73 * 10^{-1}\theta_a - 1{,}69 * 10^{-3}{\theta_a}^2 + 2{,}22 * 10^{-6}{\theta_a}^3 \ J/kgK$$

- for 600 °C ≤ ϑ_a < 735 °C

$$c_a = 666 + \frac{13002}{738 - \theta_a} \ J/kgK$$

- for 735 °C ≤ ϑ_a < 900 °C

$$c_a = 545 + \frac{17820}{\theta_a - 731} \ J/kgK$$

- for 900 °C ≤ ϑ_a ≤ 1200 °C

$$c_a = 650 \ J/kgK$$

where

ϑ_a	steel temperature [°C]

The net heat flux h_{net} is made up of two parts considering the heat transfer by convection and radiation by the following equation:

$$\dot{h}_{net} = \dot{h}_{net,c} + \dot{h}_{net,r}$$

where

h_{net}	net heat flux [W/m^2]
$h_{net,c}$	heat transfer by convection [W/m^2]
$h_{net,r}$	heat transfer by radiation [W/m^2]

The net convective heat flux component $h_{net,c}$ is calculated as follows:

$$\dot{h}_{net,c} = \alpha_c(\Theta_g - \Theta_m)$$

where

α_c	coefficient of heat transfer by convection (often taken as 25 W/m^{2}K) [W/m^{2}K]
Θ_g	gas temperature in the vicinity of the exposed member [°C]
Θ_m	surface temperature of the member [°C]

The net radiative heat flux component $h_{net,r}$ is calculated as follows:

$$\dot{h}_{net,r} = \Phi \cdot \varepsilon_m \cdot \varepsilon_f \cdot \sigma \cdot [(\Theta_r + 273)^4 - (\Theta_m + 273)^4]$$

where

Φ	configuration factor (often taken as 1) [-]
ε_m	surface emissivity of member (often taken as 0,7) [-]
ε_f	emissivity of fire (often taken as 1) [-]
σ	Stephan Boltzmann constant, 5,67*10^{-8} W/m^{2}K^4
Θ_r	effective radiation temperature of the fire environment [°C]
Θ_m	surface temperature of the member [°C]

B.2 Structural fire design of steel members

B.2.1 Mechanical properties

The reduction factors for the stress-strain relationship of steel at elevated temperatures are given in Table B. 1.

Table B. 1 Reduction factors

Steel temperature ϑ_a	Reduction factors at temperature ϑ_a relative to the value of f_y or E_a at 20 °C		
	Reduction factor (relative to f_y) for effective yield strength	Reduction factor (relative to f_y) for proportional limit	Reduction factor (relative to E_a) for the slope of the linear elastic range
	$k_{y,\vartheta}=f_{y,\vartheta}/f_y$	$k_{p,\vartheta}=f_{p,\vartheta}/f_y$	$k_{E,\vartheta}=E_{a,\vartheta}/f_y$
20 °C	1.000	1.000	1.000
100 °C	1.000	1.000	1.000
200 °C	1.000	0.807	0.900
300 °C	1.000	0.613	0.800
400 °C	1.000	0.420	0.700
500 °C	0.780	0.360	0.600
600 °C	0.470	0.180	0.310
700 °C	0.230	0.075	0.130
800 °C	0.110	0.050	0.090
900 °C	0.060	0.038	0.068
1000 °C	0.040	0.025	0.045
1100 °C	0.020	0.013	0.023
1200 °C	0.000	0.000	0.000
NOTE: For intermediate values of the steel temperature, linear interpolation may be used.			

B.2.2 Resistance of tension members

For a tension member with a uniform temperature ϑ_a the design resistance is calculated by the following equation:

$$N_{fi,\theta,Rd} = k_{y,\theta} N_{Rd} [\gamma_{M,0}/\gamma_{M,fi}]$$

where

$N_{fi,\vartheta,Rd}$	design tensile resistance [N]
$k_{y,\vartheta}$	reduction factor for the yield strength at temperature ϑ_a [-]
N_{Rd}	design resistance of the cross-section $N_{pl,Rd}$ at ambient temperature according to SFS-EN 1993-1-1 [N]
$\gamma_{M,0}$	partial factor at normal temperature (taken as 1) [-]
$\gamma_{M,fi}$	partial factor at elevated temperature (taken as 1) [-]

B.2.3 Resistance of members with class 1 or 2 cross-sections subjected to combined bending and axial compression

For a member with class 1 or 2 cross-section, subjected to combined bending and axial compression, the resistance is calculated by two equations, of which the second one takes lateral torsional buckling into account. Here only the first one will be presented as the calculations in this thesis deal only with tubular hollow sections that generally do not undergo lateral torsional buckling. The equation for calculating the resistance is hence:

$$\frac{N_{fi,Ed}}{\chi_{min,fi} A k_{y,\theta} \frac{f_y}{\gamma_{M,fi}}} + \frac{k_y M_{y,fi,Ed}}{W_{pl,y} k_{y,\theta} \frac{f_y}{\gamma_{M,fi}}} + \frac{k_z M_{z,fi,Ed}}{W_{pl,z} k_{y,\theta} \frac{f_y}{\gamma_{M,fi}}} \leq 1$$

where

$N_{fi,Ed}$	design axial compressive load [N]
$\chi_{min,fi}$	minimum value of reduction factors for flexural buckling $\chi_{y,fi}$ and $\chi_{z,fi}$ [-]
A	cross sectional area [mm^2]
$k_{y,\vartheta}$	reduction factor for the yield strength at temperature ϑ_a [-]
f_y	yield strength [N/mm^2]
$\gamma_{M,fi}$	partial factor at elevated temperature (taken as 1) [-]
k_y	interaction factor for y-axis [-]
$M_{y,fi,Ed}$	design bending moment about y-axis [Nmm]
$W_{pl,y}$	plastic bending moment resistance about y-axis [mm^3]
k_z	interaction factor for z-axis [-]
$M_{z,fi,Ed}$	design bending moment about z-axis [Nmm]
$W_{pl,z}$	plastic bending moment resistance about z-axis [mm^3]

The reduction factors for flexural buckling in the fire design $\chi_{y,fi}$ and $\chi_{z,fi}$ are calculated for both axes of the cross-section as:

$$\chi_{fi} = \frac{1}{\varphi_\theta + \sqrt{\varphi_\theta{}^2 - \bar{\lambda}_\theta{}^2}}$$

where

$$\varphi_\theta = \frac{1}{2}[1 + \alpha\bar{\lambda}_\theta + \bar{\lambda}_\theta{}^2]$$

and

$$\alpha = 0{,}65\sqrt{235/f_y}$$

The non-dimensional slenderness $\bar{\lambda}_\theta$ for both axes of the cross-section for the temperature ϑ_a is calculated as:

$$\bar{\lambda}_\theta = \bar{\lambda}[k_{y,\theta}/k_{E,\theta}]^{0,5}$$

where

$\bar{\lambda}$	non dimensional slenderness for the relevant axis at ambient temperature [-]
$k_{y,\vartheta}$	reduction factor for the yield strength at temperature ϑ_a reached at time t [-]
$k_{y,E}$	reduction factor for the slope of the linear elastic range at temperature ϑ_a reached at time t [-]

The non-dimensional slenderness $\bar{\lambda}$ for both axes of the cross-section at ambient temperature for class 1, 2 and 3 cross-sections is calculated as:

$$\bar{\lambda} = \sqrt{\frac{Af_y}{N_{cr}}} = \frac{L_{cr}}{i}\frac{1}{\lambda_1}$$

where

$$\lambda_1 = \pi\sqrt{\frac{E}{f_y}}$$

and

A	cross sectional area [mm^2]
f_y	yield strength [N/mm^2]
N_{cr}	elastic critical force for the relevant buckling mode based on the gross cross sectional properties [N]
L_{cr}	buckling length in the buckling plane considered [mm]
i	radius of gyration about the relevant axis [mm]
E	modulus of elasticity [N/mm^2]

The interaction factors k_y and k_z are calculated as:

$$k_y = 1 - \frac{\mu_y N_{fi,Ed}}{\chi_{y,fi} A k_{y,\theta}\frac{f_y}{\gamma_{M,fi}}} \leq 3$$

with

$$\mu_y = \left(1{,}2\beta_{M,y} - 3\right)\bar{\lambda}_{y,\theta} + 0{,}44\beta_{M,y} - 0{,}29 \leq 0{,}8$$

and

$$k_z = 1 - \frac{\mu_z N_{fi,Ed}}{\chi_{z,fi} A k_{y,\theta}\frac{f_y}{\gamma_{M,fi}}} \leq 3$$

with

$$\mu_z = \left(2\beta_{M,z} - 5\right)\bar{\lambda}_{z,\theta} + 0{,}44\beta_{M,z} - 0{,}29 \leq 0{,}8 \; and \; \bar{\lambda}_{z,\theta} \leq 1{,}1$$

where

$\beta_{M,y}$	equivalent uniform moment factors for the y-axis [-]
$\beta_{M,z}$	equivalent uniform moment factors for the z-axis [-]

The equivalent uniform moment factors $\beta_{M,y}$ and $\beta_{M,z}$ are determined with the help of Figure B. 1. In order to simplify the calculations in this thesis, the equivalent uniform moment factors were assumed to be 1,3 in all cases. This was quite well in range with the real situation for the

bottom chord of the truss. The purlins on the other hand behaved as simply supported beams, also giving equivalent uniform moment factors of 1,3.

Moment diagram	Equivalent uniform moment factor β_M
End moments 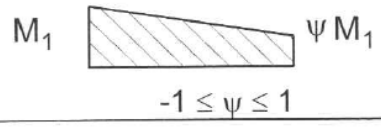 	$\beta_{M,\psi} = 1,8 - 0,7\ \psi$
Moments due to in-plane lateral loads 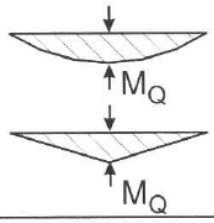 	$\beta_{M,Q} = 1,3$ $\beta_{M,Q} = 1,4$
Moments due to in-plane lateral loads plus end moments 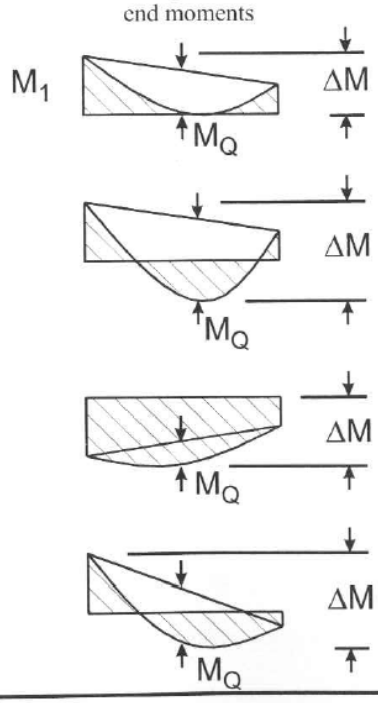 	$\beta_M = \beta_{M,\psi} + \frac{M_Q}{\Delta M}(\beta_{M,Q} - \beta_{M,\psi})$ $M_Q = \lvert \max M \rvert$ due to lateral load only ΔM = $\lvert \max M \rvert$ for moment diagram without change of sign $\lvert \max M \rvert + \lvert \min M \rvert$ for moment diagram with change of sign

Figure B. 1 Equivalent uniform moment factors